ANALYZING THE IMPACTS OF URBAN MORPHOLOGY ON LAND SURFACE TEMPERATURE IN EUROPEAN CITIES

SNIGDHA DEV ROY
July, 2024

SUPERVISORS:
prof. dr. Monika Kuffer
dr. Jiong Wang

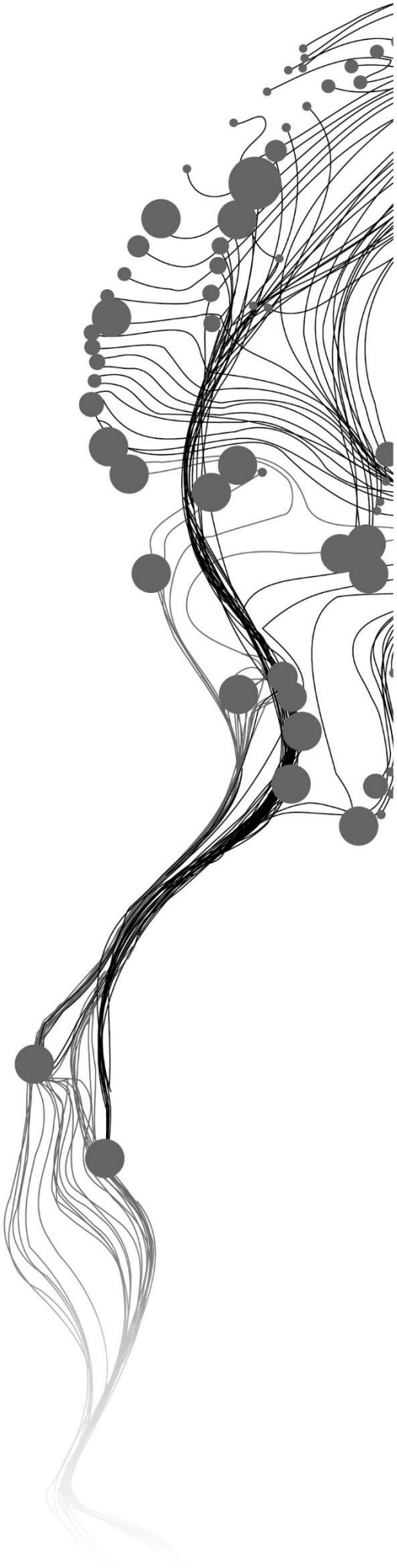

ANALYZING THE IMPACTS OF URBAN MORPHOLOGY ON LAND SURFACE TEMPERATURE IN EUROPEAN CITIES

SNIGDHA DEV ROY
Enschede, The Netherlands, July, 2024

Thesis submitted to the Faculty of Geo-Information Science and Earth Observation of the University of Twente in partial fulfilment of the requirements for the degree of Master of Science in Geo-information Science and Earth Observation.

Specialization: Urban Planning and Management

SUPERVISORS:
prof. dr. Monika Kuffer
dr. Jiong Wang

THESIS ASSESSMENT BOARD:
dr. rer. nat. Diana Reckien (Chair)
Ángela Abascal (External Examiner, University of Brussels)

Abstract

With projections indicating that nearly 70% of the global population will reside in urban areas by 2050, rapid urbanization is profoundly modifying land cover with built surfaces, along with the transformation of the urban morphology (UM) and exacerbating the thermal environment of cities. UM constantly evolves in response to people's needs and local contexts, leading to diverse building structures and materials. These changes significantly impact the thermal environment, making especially cities hotter than their surrounding areas. Given the growing risks, it is essential to study the relationship between UM and land surface temperature (LST). This study focuses on LST over air temperature because LST directly affects near-surface air temperatures and offers broader spatial coverage as it can be mapped using thermal infrared (TIR) data. It is more consistently available across diverse urban environments compared to sparse and unevenly distributed air temperature data measured by sensors on ground. Previous research has mainly focused on landscape metrics, spectral indices, and surface attributes' impacts on LST. They have often neglected finer-scale building-level analyses which are the most important urban elements having influence on heat patterns. Although some studies have considered 3D aspects, comprehensive 2D analyses are scarce due to the underutilization of building data, particularly in European cities, despite better data availability. This research addresses this gap by investigating the impacts of UM on daytime LST during the summer period in Paris, Rotterdam, Milan, and Vienna, chosen as illustrative examples. Utilizing NASA's high-resolution ECOSTRESS data, the research conducts a hotspot analysis to identify areas with significant temperature anomalies and understand their relationship with specific land uses. A comprehensive set of thirty urban morphometrics (UMMs) is measured using momepy, an open-source python toolkit, to study the UM patterns of these cities at the building level. Afterwards, a Random Forest Regression (RFR) model is applied at a grid level of 70 by 70 meters (the spatial resolution of ECOSTRESS) to explore the relationship between the UMMs and LST. The hotspot analysis reveals that most of the hotspots across all these cities are mainly business parks, industrial estates and manufacturing units. While the coldspots are predominantly low-density residential areas. The RFR model effectively captures the underlying patterns and relationships between UMMs and LST, explaining over 80% of the variability in LST across all cities. Key findings of the model highlight that mean height, orientation, alignment, building adjacency, and interbuilding-distance are the most influential UMMs across all cities. However, differences between cities also exist. For example, LST shows a positive correlation with mean building height in all cities except Paris. The patterns between orientation and LST varies, where Rotterdam and Milan exhibit a negative relationship, while Paris displays a contrasting pattern. Building adjacency and alignment demonstrated non-linear cooling effects on the urban environment across all cities. Lastly, the qualitative validation confirms that the variety of UMMs used in this study is both informative and crucial in this research field. The study outlines several implications for improving thermal comfort in existing as well as new urban developments across European cities. The limitation of the study encompasses the fact that the influence of UMMs do not demonstrate direct causality with LST and depend on various other factors such as building materials and wind patterns. Further research should aim to explore and deepen the understanding of the relatively novel UMMs used in this study, particularly regarding their influence on LST, as they have not been extensively explored in existing literature.

Keywords: urban morphometrics, momepy, building morphology, land surface temperature

Acknowledgements

It has been a significant journey, filled with both personal and scientific experiences that have deeply enriched my life. This path has had its share of highs and lows—moments of satisfaction and happiness, as well as times of frustration and despair. Beyond scientific investigation, it has been a journey of self-discovery, where I have identified my strengths, weaknesses, and learned to find peace within myself. I am grateful to this journey for granting me the opportunity to explore the vast ocean of knowledge and discover incredible scientific innovations. Every research project, no matter the scale, owes its success to the contributions of many remarkable individuals who have generously offered their wisdom, assistance, and encouragement. I am deeply grateful for the inspiration, support, and guidance provided by all those who played a crucial role in the completion of this research.

I am highly grateful to my supervisors, Prof. Dr. Monika Kuffer and Dr. Jiong Wang, who, with their enthusiasm, have continuously strived to get the best out of me. They have guided me throughout this year-long journey and helped me finalize my MSc research. A special thanks to my internship supervisor, Dr. Tobias Leichtle, for his encouragement and the invaluable lessons he provided, which I was able to apply in this research. I express my sincere gratitude to my chair, Dr. Diana Reckien, for her support, encouragement, and advice during the proposal defence and mid-term presentation, which were crucial to the completion of this research. I would also like to acknowledge the three city experts from Rotterdam, Milan, and Vienna who generously contributed their time and insights during the interviews. Their willingness to share their expertise was invaluable, adding significant depth and context to the analysis and greatly enriching the overall findings of this study.

Finally, I would thank my parents and my brother who supported me through this journey and any other individual, who, in different ways, supported this research. It is with great pleasure and profound gratitude that I acknowledge the help of these individuals.

Table of contents

List of figures

List of tables

Abbreviations

AρρEEARS	Application for Extracting and Exploring Analysis Ready Samples
ASTER	Advanced Spaceborne Thermal Emission and Reflection Radiometer
CRIB	Center of Expertise in Big Geodata Science
CSR	Complete Spatial Randomness
ECOSTRESS	ECOsystem Spaceborne Thermal Radiometer Experiment on Space Station
ERI	Equivalent Rectangular Index
EU	European Union
FDR	False Discovery Rate
ISS	International Space Station
LM	Landscape Metrics
LST	Land Surface Temperature
MID	Mean-Interbuilding Distance
ML	Machine Learning
MODIS	Moderate Resolution Imaging Spectroradiometer
MT	Morphological Tessellation
NbS	Nature-based Solutions
NOAA	National Oceanic and Atmospheric Administration
PDP	Partial Dependence Plot
RFR	Random Forest Regression
RI	Relative Importance
SLSTR	Sea and Land Surface Temperature Radiometer
SUHI	Surface Urban Heat Island
TIR	Thermal Infrared
UM	Urban Morphology
UMM	Urban Morphometric

1 Introduction

1.1 Background

According to the United Nations' revised World Urbanization Prospects, 68% of the world's population is predicted to live in urban areas by 2050 (United Nations, 2018). In the context of Europe, even though some regions are experiencing a decrease in population, cities have become highly urbanized compared to other parts of the world, with large concentrations of people living in urban areas (European Commission et al., 2019). By 2050, it is projected that Europe's urbanization rate will surge to around 83.7% (United Nations, 2018). Between 2015 and 2030, built-up areas are expected to grow by over 3%, covering approximately 7% of the EU's territory by 2030 (European Commission, 2019). This may be attributed to factors such as rural-urban migration, economic growth, higher quality of life and better access to facilities (World Health Organisation, 2021).

However, this urban expansion is not without consequences, particularly rising temperatures. The unprecedented intensification of heatwaves in urban areas of the European region has become a growing concern (World Health Organisation, 2021). Given the current trend of global warming, extreme heat patterns are going to continue unabated in near future (Guerreiro et al., 2018). According to Chrysanthou et al. (2014), urbanisation is responsible for a 0.0026 °C/decade increase out of the 0.179 °C/decade overall temperature rise in Europe. Moreover, Smid et al. (2019) estimates that the probability of heatwaves for 31 European capitals has increased, while in the coming decades all metropolitan cities in Europe will be more susceptible to higher temperatures.

Thus, monitoring and understanding these temperature variations are crucial for effective climate adaptation strategies. Land surface temperature (LST) and air temperature are the two main indicators typically used to assess heat in urban areas. Meteorological monitoring stations usually measure the air temperature, which are few and often dispersed. They can only offer an incomplete scenario of the temperature differences within diverse urban areas and their surrounding regions (Huang & Wang, 2019). LST has the capacity to influence the near-surface air temperature within an urban atmosphere (Mutiibwa et al., 2015), and moderate the internal climate of the buildings (Voogt & Oke, 2003). Moreover, as compared to the standard air temperature measurements, daytime LST exhibits a closer relationship with the radiative and thermodynamic properties of the Earth's surface (Hulley et al., 2019). Thus, most of the urban heat studies have relied on remotely sensed LST as a substitute for air temperature.

The high urbanisation rate has profound impacts on the built environment, along with the transformation of the urban morphology (Zhang et al., 2019). Urban morphology (UM) provides a quantitative representation of a city's physical shape, internal arrangements, and spatial structure (Liu et al., 2023). Depending on the people's demands and local context (diverse building structures, materials, human activities), their form keeps changing, which is evident in various spatial organization patterns of urban

areas throughout the world (Fleischmann, et al., 2021). This constant modification of urban vertical landscapes, coupled with surface geometrical and physical features (Huang & Wang, 2019), largely undermines the thermal environment of urban areas (Geletič et al., 2019; Zhou et al., 2022).

Heat-absorbing surfaces such as roads, roofs, and pavements, exhibit higher solar absorption and thermal retention compared to natural landscapes, leading to increased surface temperatures (Ayanlade, 2016; Senanayake et al., 2013). Limited vegetation cover and restricted ventilation between densely packed buildings can further exacerbate this effect (Huang & Wang, 2019; Mohajerani et al., 2017). Such urban characteristics can disturb the equilibrium of natural surface energy and radiation and make the urban areas relatively warmer (Kabano et al., 2021). Thus, urban heat fluctuations are observed near the city surfaces and approximately reach up to the average height of the buildings. These alterations in the UM impact the moisture, thermal, radiative, and aerodynamic attributes of the surroundings, resulting in the retention of heat in urban areas (Ayanlade, 2016). As a result, LST in cities is usually higher than their surrounding areas, which poses major sustainability challenges, especially in urbans areas (Portela et al., 2020). Thus, the intertwining factors of rapid urbanization and changing UM can contribute to rising temperatures and increased heat stress in urban environments.

This phenomenon has been linked to a variety of adverse effects, including growing energy demand in cities (Santamouris et al., 2015), urban climatic problems like untimely rainfall (Liu & Niyogi, 2020), increased pollution (Ulpiani, 2021), air and water quality degradation (Sabrin et al., 2020; Wang et al., 2021), exacerbating heat stress and ozone generation in the lower atmosphere (Gabriel & Endlicher, 2011; Kong et al., 2021), development of several health issues in vulnerable populations (Tan et al., 2010; Zander et al., 2018), and biodiversity disturbances (McGlynn et al., 2019).

About 27% of cities and 65% of the total urban population have been experiencing the Surface Urban Heat Island (SUHI) effect that could have drastic impacts on the economic sector leading to 5.6% GDP losses by 2100 (Estrada et al., 2017). The SUHI is measured by differencing the LST values of urban and rural areas (Voogt & Oke, 2003). The European Environment Agency (EEA) estimates that roughly half of hospitals and schools in European cities are situated on heat islands (at least 2 °C warmer than the regional average), which are a result of roads, pavements, and buildings absorbing solar heat and pushing up temperatures in built-up areas (Chamberlain & Merritt, 2023).

It is evident how the European cities built over the years have largely contributed to the increasing temperatures in the region. As Europe's level of urbanization continues to rise, there is a growing need to address the adverse effects of increasing temperatures. Given the increasing risks to different aspects discussed above, it becomes essential to have knowledge of three-dimensional (3D) and 2D urban forms, which are recognized as major factors in influencing LST (Ward et al., 2016). These factors are multifaceted and complex (Sandu, 2016), necessitating a comprehensive study. Moreover, it is imperative to explore various approaches to optimize these urban forms for mitigating future risks and implementing effective climate adaptation strategies (Guo et al., 2022; Peng et al., 2021).

This research primarily focuses on exploring the relationships between UM and LST using Urban Morphometrics (UMMs) and Machine Learning (ML) techniques. By examining a diverse sample of four European cities—Paris, Rotterdam, Milan, and Vienna—this study aims to uncover the underlying factors and potential relationships that contribute to variations in LST within and across these cities. Understanding these relationships is crucial for identifying the key urban morphological elements that influence thermal environments. Findings of this study will provide valuable insights to urban planners, architects, and other concerned actors on how different UM configurations contribute to variations in

LST within and across cities and how they could be optimized strategically for the improvement of the thermal environment in those cities. It is also expected that the methods used in this research could be replicated in diverse urban settings for similar types of LST studies.

1.2 Research gap

Firstly, there is increased interest in understanding the influence of UM of cities on the LSTs in the European region. However, these types of studies have been mainly limited to study areas of Chinese cities (refer to Annexure I). They have more homogeneous urban layouts, with extensive high-rise developments and large-scale urban expansion. In contrast, European cities often exhibit a mix of historic cores and modern urban forms, characterized by compact city centres, intricate street layouts, and diverse architectural styles (European Environment Agency, 2008). These differences in UM can lead to distinct temperature variations within cities. This highlights the need for research tailored towards European cities where such studies are notably scarce. Understanding how different UM influence LST is essential for informed urban planning, design, and policy interventions aimed at enhancing the thermal comfort and sustainability of European cities.

Secondly, majority of these studies have mainly concentrated on Landscape Metrics (LMs), spectral indices and surface attributes, but it is also important to recognize the significance of UM in the context of LST at a building level (Zheng et al., 2018). UM can be measured across various scales, but studies done at a finer scale can add more scientific insights into analysing cities (Wang et al., 2022). A more comprehensive understanding of UM can be achieved by analysing the specific features of buildings, plots and roads (Dibble et al., 2019). Among them, buildings are the most important urban elements which exert the greatest influence on heat patterns (Kong et al., 2022). Various studies have reviewed that building density and building height are a fundamental part of the UM (Labetski et al., 2023), that largely influences the LST (Futcher et al., 2017; Guan et al., 2021; Yang et al., 2019). They can significantly enhance solar radiation absorption and reduce the natural ventilation of urban areas, as a result, trapping in a substantial amount of heat within an urban environment. Although building morphology has been studied as a part of the 3D aspect in some of the past studies, including building height and volume, sky view factor, shape coefficient, frontal area index, and building shadow (see Table 2.1), a thorough analysis of the 2D characteristics account for a negligible number of studies. The primary reason for this is the underutilization of building data (Labetski et al., 2023; Yang et al., 2018). Moreover, a multitude of datasets is available, and users often encounter challenges in selecting the most suitable one for their analyses (Gonzales, 2023). There is still considerable scope for further research on the influence of the 2D and 3D aspect of UM on LST in European cities. Hence, this research uses an open-source morphometrics toolkit called *momepy* to measure UM across multiple European cities. It is relatively a newer method in this area of research. The toolkit includes a wide range of 2D and 3D morphometric characters to detect patterns of urban form. It distinguishes itself from the metrics or factors typically used in previous UM related-studies and based on basic urban elements such as building and streets, introduces a comprehensive set of spatial metrics (Fleischmann, 2019).

Lastly, most of these studies have analyzed LSTs using low or medium-resolution imageries (see Annexure I), derived from polar-orbiting satellites such as Landsat with a resolution of 100 meters, resampled to 30 meters, Moderate Resolution Imaging Spectroradiometer (MODIS) with a resolution of 1 kilometre and (ASTER) with a resolution of 90 meters. Some studies (Sobrino & Irakulis, 2020) have even used the Sea and Land Surface Temperature Radiometer (SLSTR) thermal bands of Sentinel-3A to extract LST which also has a resolution of 1 kilometre. At present, only a limited number of studies have utilized high-resolution remote sensing imagery to study the relationship between UM and LST (Elmes et al., 2017;

Huang & Wang, 2019). This research utilizes NASA's spaceborne thermal radiometer, ECOsystem Spaceborne Thermal Radiometer Experiment on Space Station (ECOSTRESS) LST data which has a spatial resolution of 70 m. It has a revisit time of 1 to 5 days, which is significantly shorter compared to other satellites (Xiao et al., 2021), that allowed for an acquisition of larger number of images during the study period.

1.3 Objectives and research questions

The overall aim of this research is to analyze the impacts of UM on the LST on a selected diverse sample of four European cities using Urban Morphometrics (UMMs) and Machine Learning (ML) techniques. To achieve this aim, the following specific objectives have been defined.

Objective 1: To analyze the spatial patterns of LST across these cities such as local extremes or hotspots during the summer period (June-August) of 2023.

RQ1.1: What is the variance of daytime LSTs during the study period across the cities?

RQ1.2: What are the locations and sizes of hot or coldspots with high or low LST values, identifiable through metrics such as the Getis Ord Gi*, across these four European cities during the summer of 2023?

Objective 2: To assess the UM of these cities at a building level.

RQ2.1: How are the UM of cities in different geographic regions distinct or consistent in terms of morphological types and metric variations?

RQ2.2: What spatial patterns and relationships exist between the distribution of hotspots, land uses and the UM characteristics observed across the cities?

Objective 3: To examine the relationship between UM and LST using Random Forest Regression (RFR) modelling and compare the results across the cities.

RQ3.1: How well does the regression model perform in predicting LST based on UM in each city?

RQ3.2: What are the specific urban morphological features that contribute most significantly to LST variations and how does it vary across the selected cities?

RQ3.3: Do expert insights through interviews contribute to a deeper understanding and contextual interpretation of the observed relationships between UM and LST?

1.4 Thesis structure

This thesis comprises of six chapters, excluding the introductory chapter. The subsequent chapters include 'Literature Review' (Chapter 2) which provides a review of existing literature on the influence of UM on LSTs, and different methodologies adopted for those studies. 'Study area and datasets' (Chapter 3) introduces the study area and the datasets utilized. 'Methodology' (Chapter 4) outlines the methodological approach adopted for this research. 'Results' (Chapter 5) presents the experimental results obtained from the methodology described in Chapter 4. The discussion of these results is presented in Chapter 6, which summarizes the findings and implications of the research. Finally, 'Conclusion' (Chapter 7) serves as the conclusion of this research.

2 Literature review

This chapter provides a review of existing literature and is divided into four main sections. 2.1 ('Importance of air and surface temperatures in urban planning') discusses the significance of studying air and surface temperatures in the context of urban planning and the study's focus on LST. Section 2.2 ('Studying LST using thermal remote sensing') explores the role of thermal remote sensing in examining LST and highlights their pros and cons. Section 2.3 ('Factors influencing LST") focuses on various indicators associated with UM that have been investigated in the past to understand their influence on LST. Section 2.4 ('Methods to assess factors influencing LST) discusses the past methodologies employed in these types of studies, and their shortcomings.

2.1 Importance of air and surface temperatures in urban planning

The study of air and surface temperatures hold immense significance across various domains such as climate change, health, infrastructure, agriculture, biodiversity, urban planning and design and many more. For instance, temperature monitoring is crucial for maintaining the health of vegetation, optimizing crop yields, and managing water resources effectively. Fluctuations in temperature can directly impact plant growth, pest populations, and soil moisture levels, which are vital for food security and sustainable farming practices (Akpenpuun et al., 2023). Studying temperatures in the infrastructure sector ensures material durability, enhances energy efficiency, and mitigates risks from extreme weather. This knowledge helps design safer, more sustainable, and adaptable infrastructure, especially in the face of climate change (European Commission, n.d.). In the field of urban planning and design, understanding these temperatures is pivotal for creating sustainable and resilient cities. Urban areas are particularly susceptible to the UHI effect, where densely built environments and human activities lead to higher temperatures compared to surrounding rural areas. As urban areas continue to expand and face the challenges of climate change, temperature considerations play a critical role in shaping the fabric of our communities. Incorporating temperature analysis into urban planning allows for the development of adaptation strategies to mitigate heat island effects and enhance the overall liveability of cities (Visvanathan et al., 2024). Moreover, understanding temperature patterns enable planners to address disparities in heat exposure across different scales, ensuring that vulnerable communities have access to adequate cooling resources and green spaces (Chen, 2024).

It is well established that escalating temperatures attributed to climate change pose significant risks to both human health and ecological systems. Understanding the spatial variations in heat exposure can be effectively studied using both air temperature and LST. Air temperature is primarily used for assessing atmospheric conditions and human comfort levels, while LST plays an important role in the near-surface energy balance and is typically employed in analysing surface heat patterns (Martilli et al., 2020). Due to significant variations in air temperature over time and space in urban areas, comprehensive data is required to study urban air temperatures (Kloog et al., 2014). The ability to provide detailed spatial information

needed to mitigate the adverse effects of urban heat is limited by the insufficient number of monitoring stations (Baranka et al., 2016). On the other hand, availability of LST data for such studies is quite consistent (Zhou et al., 2019). Satellite-based LST, known for its high spatial resolution and ease of use, is one of the simplest methods to analyze urban thermal environments (Han, 2023; Jothimani et al., 2021). Hence, understanding LST becomes particularly relevant for this study as it focuses on building morphology, which directly influences surface attributes affecting heat absorption and retention.

2.2 Studying LST using thermal remote sensing

A plethora of research has been conducted in the past investigating the causes, effects, and modelling of LST. Numerous advanced mathematical and physical models have been used to derive LST. These include Surface Energy Balance (SEB) models (Bhattacharya et al., 2022; Hu et al., 2023), Temperature-Emmisivity Separation (TES) algorithms (Rokugawa et al., 1999; Ru et al., 2023), and Gaussian models (Guo et al., 2022). Moreover, various statistical and machine learning models play an important role in linking LST with surface attributes, which will be discussed further in Section 2.4. With the advancement of remote sensing technology, assessment of LST using broad detection ranges and extensive spatial information has become possible and more cost-efficient (Halder et al., 2021). Thermal infrared (TIR) imagery offers the advantage of providing a spatially continuous and time-synchronized dense grid of temperature data over entire cities (Steininger, 1996). This capability allows researchers to study the effects of both natural and human-caused alterations on surface temperatures (Jin & Dickinson, 2010). It has been a powerful tool used by planners and decision makers for investigating thermal challenges and monitor the urban environment (Shawabkeh et al., 2023; Derdouri et al., 2021; Hu & Brunsell, 2013).

The utilization of thermal remote sensing to determine LST has been extensively reviewed in scholarly literature (Qin & Karnieli, 1999; Voogt & Oke, 2003; Weng, 2009). Rao (1972) was the pioneer in examining the potential of thermal footprint detection generated by urban areas. Since then, TIR data obtained through remote sensing have been extensively employed for the retrieval of LST (Quattrochi & Luvall, 1999; Weng et al., 2004). Various combinations of sensors and platforms (including satellites, aircraft, and ground-based systems) have been designed to collect TIR data from the Earth's surface, specifically retrieving urban surface temperatures.

Many TIR instruments operating within the 8-14 μm atmospheric window wavelength region have been deployed on various satellites since the 1960s. These instruments have been extensively utilized to produce a variety of LST products, spanning different spatial resolutions from regional to global scales. These include the National Oceanic and Atmospheric Administration (NOAA), Landsat series, MODIS and ASTER operating on Earth Observing System's Terra and Aqua satellites, respectively and the SLSTR operating on Sentinel 3 satellite (Li et al., 2023). ASTER and MODIS can scan specific geographic locations twice a day, capturing temperature variations during both daytime and nighttime, facilitating various studies to understand diurnal patterns of LST. The ECOSTRESS instrument, launched most recently and currently operational aboard the International Space Station (ISS), has garnered significant attention due to its higher spatial resolution and lower temporal resolution compared to all the previously mentioned instruments (Xiao et al., 2021).

Annexure I lists down several studies that have examined the spatial patterns of LST and their relation to various LMs, spectral indices and surface attributes in urban areas using thermal remote sensing. High-resolution imagery, primarily acquired through airborne remote sensing, has been employed to analyse the thermal dynamics of urban surfaces, particularly concerning surface attributes like sky view factor (Heldens et al., 2013; Scarano & Mancini, 2017), or building morphological attributes (Berger et al., 2017).

Landsat's TIR data has also been extensively utilized to derive LSTs in most of these studies. Li et al. (2011) used Landsat-7 Enhanced Thematic Mapper Plus (ETM+) images, with a spatial resolution of 60 meters, to retrieve LST in the Shanghai metropolitan region in China. Estoque et al. (2017) carried out a similar study in Bangkok, Manila and Jakarta, while Scarano & Mancini (2017) focused in Bari, Italy, both using Landsat-8 Operational Land Imager (OLI) and Thermal Infrared Sensor (TIRS) which has a resampled spatial resolution of 30 meters. Apart from these studies, Heldens et al. (2013), Huang & Wang (2019), Chen et al. (2020), Guo et al. (2020) and numerous others have utilized various missions of Landsat (7-9) to retrieve LST in their research. Scarano & Mancini (2017) also used ASTER data (spatial resolution of 90 meters) to conduct a comparative analysis of LST patterns, examining the impact of different spatial resolutions. Yang et al. (2017) utilised version 5 of EOS-Aqua-MODIS 8-day composite product (1 kilometre spatial resolution) to analyse the relationship between SUHI and various LMs across 332 cities situated in various climatic zones throughout China.

While thermal remote sensing offers numerous benefits for retrieving LST, it also comes with some shortcomings. A significant limitation arises from the 3D structure of urban surfaces, which impacts the effective radiometric source of the remotely sensed area. This limitation leads to incomplete coverage of the urban surface within the sensor's instantaneous field of view, influenced by both sensor viewing geometry and surface roughness (Voogt & Oke, 2003). Consequently, a considerable portion of the urban surface may not be observed, impacting the accuracy of LST retrievals. Furthermore, TIR data are susceptible to cloud cover, which diminishes their effectiveness in areas with frequent cloud presence (Mo et al., 2021).

Despite its limitations, thermal remote sensing remains indispensable for urban climate and environmental studies. Without it, assessing factors like LST and understanding urban heat dynamics would be significantly challenging (Weng, 2009).

2.3 Factors influencing LST

Previous research has associated LST with various biophysical and meteorological factors such as built-up areas, urban and street layouts, land use and land cover, vegetation, population, and the level of human activities (Weng, 2009). However, the relationship between LMs, various spectral indices or surface attributes and LSTs under different scenarios have been most extensively studied in the past. Table 2.1 shows a comprehensive list of factors that have been used by various authors to analyse the impacts of UM on LST.

LMs are a widely studied field closely associated with UM that quantifies the spatial characteristics and patterns of the urban landscape (Bhatti et al., 2018). This area of research underscores the significance of alterations in land use, the presence of impermeable surfaces, the presence of vegetation, and the influence of water bodies in contributing to higher LSTs. Estoque et al. (2017) used LMs such as shape and aggregation of patches to study the relationship between impervious surfaces and green spaces with mean LST in three Southeast Asian megacities. The study revealed that impervious surfaces had an LST of approximately 3 ºC higher as compared to green spaces. Yang et al. (2017) analysed the SUHI effect and its correlation with the corresponding differences in urban landscape patterns using five most common LMs, namely, i) Percentage of landscape (PLAND), ii) Patch Density (PD), iii) Mean Shape Index (MSI), iv) Shannon's Diversity Index (SHDI), v) Contagion Index (CONTAG), and vi) Clumpiness Index (CI). The results showed that the correlation between the metrics and SUHI is distinct and strongly influenced by daily variations, seasonal fluctuations, and climatic factors. Similarly, Zhang et al. (2022) employed a

five class-level and four landscape-level metrics to analyse the spatial patterns of different levels of impervious surface density on the UHI effect using Moran's I analysis in a Chinese city.

Table 2.1 Summary of 2D/3D metrics used by various authors to analyse the impacts of UM on LST (Source: Author, 2023)

AUTHORS	2D METRICS																									3D METRICS								
	Vegetation Index - NDVI	Modified Water Index - MNDWI	Built-up Index - NDBI	Soil Brightness Index - NDSI	Impervious Surface Index - NDISI	Night Lighting (NL)	Albedo	Plot/Building Area	Vegetation Fraction (Fv)	Impervious Surface Area (ISA)	Mean Patch Size (AREA_MN)	Mean Shape Index (SHAPE_MN)	Aggregation index (AI)	Green Space Density	Percentage of Landscape (PLAND)	Shannon's Diversity Index (SHDI)	Patch Density (PD)	Clumpiness Index (CI)	Contagion Index (CONTAG)	Edge Density (ED)	Landscape Shape Index (LSI)	Patch Cohesion Index	Largest Patch Index (LPI)	Shannon's Evenness Index (SHEI)	Sky View Factor (SVF)	Shape Coefficient (SC)	Building/Block Density (BD)	Building/Block Height (BH)	Height Variance (HV)	Frontal Area Index (FAI)	Building Shadow (BS)	Floor Area Ration (FAR)	Mean Compactness Factor	Building Surface Fraction (%)
Li et al., 2011	■								■	■					■	■	■	■	■	■	■			■									
Heldens et al., 2013																									■								
Estoque et al., 2017		■								■	■	■	■																				
Yang et al., 2017												■			■	■	■	■	■														
Scarano & Mancini, 2017																									■								
Huang & Wang, 2019															■		■			■	■	■			■	■		■	■				
Chen et al., 2020	■							■																				■					
Guo et al., 2020	■		■	■		■							■	■			■							■									
Li et al., 2020	■		■												■	■					■						■	■					
Logan et al., 2020	■	■	■				■			■															■								
Li et al., 2021																									■		■	■		■	■	■		
Cilek & Cilek, 2021										■																		■					■
Yang et al., 2021	■	■		■				■																			■	■			■		
Yin et al., 2022														■													■	■					
Zhang et al., 2022										■					■	■	■	■			■		■	■									
Molina-Gómez et al., 2022	■	■	■		■																												
Yao et al., 2022	■	■	■			■								■											■		■	■			■		
Puche et al., 2023										■																	■	■					
He et al., 2023																									■		■	■				■	
Zhu et al., 2023	■	■	■																						■		■	■	■			■	
Han, 2023																											■	■	■			■	■

Few studies (Logan et al., 2020; Molina-Gómez et al., 2022; Yao et al., 2022) have also used spectral indices such as Normalized Difference Vegetation or Built-up Index (NDV/BI) and Normalized Difference Impervious Surface Index (NDISI) to study how configurations and patterns of landscape can influence the SUHI effect. These studies have incorporated various statistical methods such as Principal Component Analysis (PCA) and Random Forest Regression (RFR) modelling to examine their relationship. There are some studies (Li et al., 2011; Li et al., 2020) which have used both landscape patterns and spectral indices to study the influence of urban characteristics on LST for different Urban Functional Zones (UFZs). Guo et al. (2020) investigated the spatial variability of LST in a Chinese city using Moran's I analysis and correlated it with similar landscape characteristics using the Geographically

Mean Regression (GWR) model. Another study (Chen et al., 2020) used the same statistical approach to assess the interactions between urban morphological indicators (plot area and NDVI) and LST in a Dutch city.

Cilek & Cilek (2021) established a statistical relationship between the Local Climate Zones (LCZs) and LST during the hot and arid summer period in Adana City, Turkey. The concept of LCZ was coined by Stewart & Oke (2012), which is characterized as regions of uniform surface cover (sky view factor, aspect ratio), structure (building height/density), thermal properties (surface albedo), and human activity (space heating/cooling) that span hundreds of meters to several kilometres in horizontal scale. The LCZ system offers a structured framework for conducting research on SUHI and provides a standardized approach for comparing temperature data across different urban areas worldwide. Yang et al. (2021) studied the LST patterns of LCZs in Shenyang, China and constructed statistical models to examine the key driver of LST within each LCZ. Similarly, Puche et al. (2023) have analysed the LST and air temperature patterns for different LCZs in the city of Milan using ANOVA.

Most of these studies have determined that the primary cause of intensified LSTs in urban areas, can be associated with variations in land cover and structural patterns when compared to rural areas. Recently few studies such as Han (2023), He et al. (2023), Zhu et al. (2023), have also taken into account the influence of building morphology such as sky view factor, building height/density on LST, Floor Area Ratio (FAR). This thesis makes an effort to advance this field of research by exploring a broader range of building metrics, thereby contributing to a deeper understanding of the relationship between UM and LST patterns.

2.4 Methods to assess factors influencing LST

Researchers have utilized correlations, regressions, ML and various other analytical methods to examine the relationship between UM and LST. Providing an exhaustive overview of all the techniques is neither feasible nor practical. Therefore, only the most commonly used techniques have been shown in Annexure I. The following sections provide concise discussions of some of these methods.

2.4.1 Simple linear regression and correlation

Pearson's and Spearman's rank correlations have been used by various authors (Berger et al., 2017; Huang & Wang, 2019; Li et al., 2020; Scarano & Mancini, 2017; Yang et al., 2021; Yao et al., 2022) to study the relation between different UM factors and LST. Pearson's correlation measures the linear association between two continuous variables (Mujtaba et al., 2019). While Spearman's rank correlation assesses the monotonic relationship between two ranked variables. It works by ranking the data and then calculating the correlation using these ranks (Schober & Schwarte, 2018). Both correlation coefficients are scaled to range from -1 to +1. A value of 0 indicates no linear or monotonic association. As the coefficient approaches 1 or -1, the relationship between the variables becomes stronger and indicates a near-perfect linear relationship for Pearson's correlation and a near-perfect monotonic relationship for Spearman's correlation, where the data points form a constantly increasing or decreasing pattern. Pearson's correlation is advantageous for its simplicity and clear measure of linear relationships, making it widely recognized and easy to compare across studies. However, it assumes linearity and normality, capturing only linear associations and being highly sensitive to outliers. In contrast, Spearman's rank correlation is more robust, as it does not assume a specific distribution and is less affected by outliers, effectively capturing monotonic relationships, suitable for non-linear data. However, it is less informative about the magnitude of relationships and can lose information when data is ranked, particularly in small datasets. Additionally, the ranking process can be computationally intensive for large datasets (Winter et al., 2016).

Studies such as Chen et al. (2020) and Guo et al. (2020) used Ordinary Least Squares (OLS) regression to analyse the impact of UM on LST. It is a statistical method used for estimating the relationship between a dependent variable and one or more independent variables. It aims to find the best-fitting linear regression model by minimizing the sum of squared differences between the observed data points and the predicted values. This method is easy to interpret and widely used for inferential statistics and prediction (Burton, 2021). However, OLS regression is sensitive to outliers, violates assumptions such as normality and homoscedasticity, and may overfit data, especially when dealing with complex, non-linear patterns. Its limited flexibility in capturing non-linear relationships and assumption of independence among observations also pose challenges.

Geographically Mean Regression (GWR) is a spatial analysis technique that extends traditional regression models by allowing the relationships between variables to vary over space (Wu et al., 2022). Unlike OLS regression, which assumes that the relationship between independent and dependent variables is constant across the study area, GWR provides localized estimates of the parameters by incorporating the geographical coordinates of the data points (Fotheringham & Brunsdon, 1999). This approach recognizes and incorporates nonstationarity in the data, providing more accurate and context-specific insights (Wu et al., 2022). GWR modelling can suffer from multicollinearity if the predictor variables are highly correlated, making it difficult to distinguish their individual effects on the response variable. Moreover, this method can be computationally demanding, especially with large datasets, as it requires fitting a separate regression model for each location in the dataset (Wheeler & Tiefelsdorf, 2005).

2.4.2 Simple and advanced ML methods

Principal Component Analysis (PCA) used by Molina-Gómez et al. (2022) is a dimensionality reduction technique that transforms a large set of variables into a smaller one that still contains most of the information. It does this by identifying the principal components, which are orthogonal directions of maximum variance in the data. PCA helps in visualizing high-dimensional data and reducing noise. The main advantage is its ability to reduce complexity while preserving data structure. However, PCA assumes linear relationships between variables and may not perform well if this assumption is violated (Jollife & Cadima, 2016).

Random Forests (RF) is a commonly used ensemble ML algorithm. Developed by Breiman (2001), this algorithm can solve both classification and regression problems. Many studies (Han, 2023; Li et al., 2021; Yao et al., 2022; Zhu et al., 2023) have adopted this method for analysing the driving factors of both LST and air temperature. RF regression (RFR) is an example of non-linear and non-parametric algorithm that is based on random decision trees (Abdel-Rahman et al., 2014; Li et al., 2021). It combines the predictions of multiple individual decision trees, where each tree is trained on a random subset of the data (called bagging) and makes independent predictions (Breiman, 2001). These predictions are averaged to produce a final prediction, which often results in a more generalizable model and also avoids overfitting (Liaw & Wiener, 2002). This method is robust to multivariate collinearity among the independent variables (Li et al., 2021). RF is also capable of assigning importance score and calculating the impurity of each variable, which can indicate how much influence each variable has on the dependent variable (Greenwell et al., 2018). Logan et al. (2020) tested several linear and non-linear regression models to understand how urban characteristics relate to LST. RFR stood out as the most effective model with the highest accuracy.

3 Study area and datasets

This chapter provides a comprehensive overview of the study area, datasets utilized in the research. Section 3.1 ('Study area') outlines the geographical scope and characteristics of the study area, offering insights into its climatic conditions, urban morphologies, and spatial organizations. Section 3.2 ('Datasets') provides a detailed information of various datasets employed in the research.

3.1 Study area

The cities of Paris, Rotterdam, Milan, and Vienna have been selected as the testbed for this research (as shown in Figure 3.1). Despite their distinct morphological characteristics and spatial organizations, as outlined in Table 3.1, these cities share a common trait: they are among the hottest in Europe. They have been experiencing notable heatwaves in the past, underscoring their vulnerability to extreme temperatures—a critical concern in urban environments characterized by high population densities and extensive built-up areas.

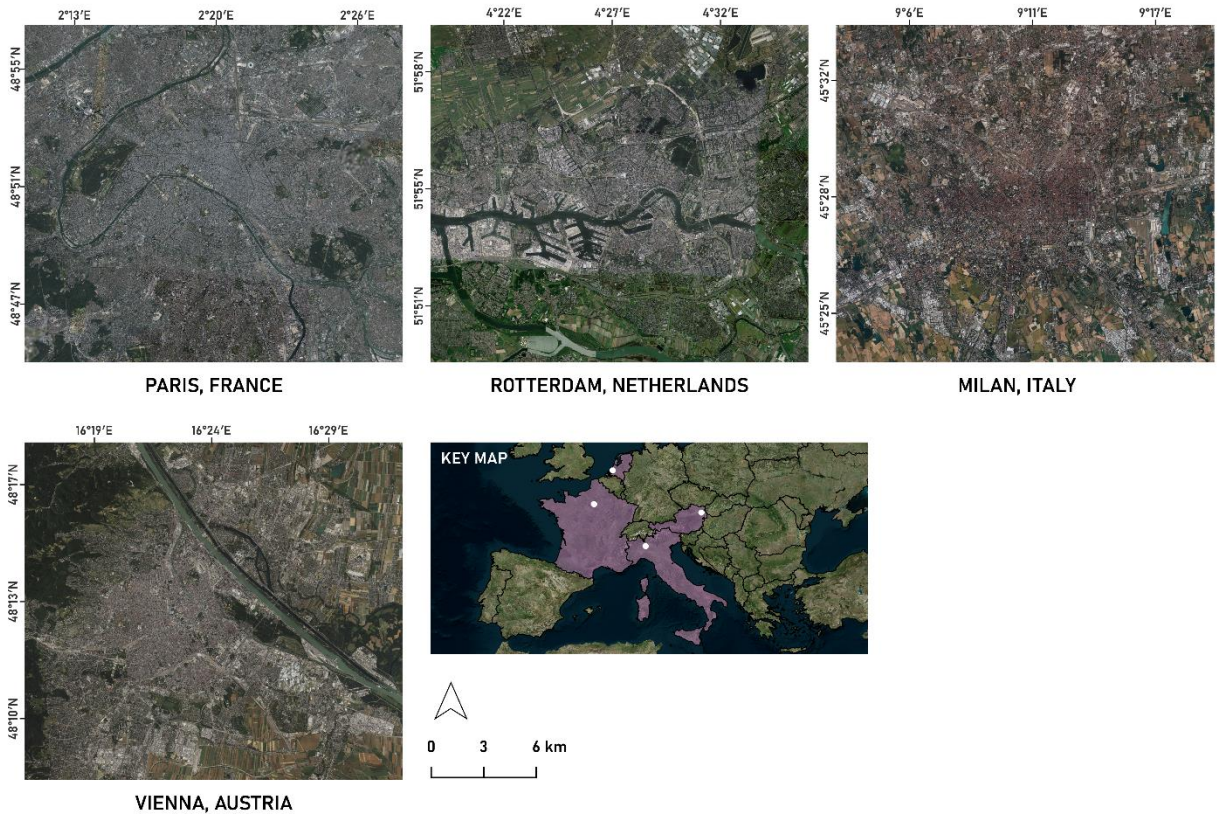

Figure 3.1 Selected case study cities with an arbitrary rectangle of 440 km² from the urban centres

They have been drawn from various climatic zones identified by the Köppen-Geiger Classification (Annexure II), spanning across different regions of Europe, each characterized by its unique environmental conditions. According to Eurostat, the population density of the city of Paris ranks the highest with 21,044 inhabitants/km² in the entire European Union (Kokkinidis, 2022). Around 60% and 41% of Paris and Milan Metropolitan area, respectively, is covered by built-up areas (NYU & UN-Habitat, 2014; Telespazio, 2020), making the SUHI phenomenon prevalent in this region. Moreover, Rotterdam faced an unprecedented heatwave in 2023, with temperatures reaching record highs since temperature monitoring began in the Netherlands over a century ago (NL Times, 2023). In the second quarter of 2023, more than 39,000 people died in the Netherlands, which was 5% higher than what was expected for that time. Moreover, Milan experienced its hottest day in centuries, with temperatures surpassing 33 °C (Reuters, 2023). These cities exhibit UHI summer intensities exceeding 1.5 °C above the 90th percentile of summer temperatures when compared to other urban areas, as depicted in the Climate-ADAPT heat map (Annexure III). Lastly and most importantly, the selection of these cities was based on the availability and consistency of building and LST data.

Table 3.1 European cities selected for this study and their baseline information

COUNTRY	CITY	CLIMATE ZONE	BUILT FORM
France	Paris	Temperate – No Dry Season (Warm Summer)	Mix of grid, axial & radial pattern, polycentric, densely populated historic centre (mostly low rise), extensive boulevard networks linked to landmarks by roundabouts
Netherlands	Rotterdam	Temperate – No Dry Season (Warm Summer)	Post-industrial port city, modern core, compact city, with mixed land-use and taller buildings
Italy	Milan	Temperate – No Dry Season (Hot Summer)	Radial pattern, compact & irregular structure
Austria	Vienna	Cold – No Dry Season (Warm Summer)	Roman-medieval street grid pattern, ring road connected to major institutions, well networked tourist space system, abundant green spaces outside urban borders

Due to the inconsistencies in the administrative boundary areas across cities, an arbitrary rectangle of 440 km² was delineated from the main urban centre. To interpret the heat patterns and UM within the cities, the defined study area covered a diverse range of urban gradients. This included the most densely built-up areas in the urban centre and gradually decreasing densities reaching to the suburbs.

3.2 Datasets

In this research, two primary datasets have been used, i) ECOSTRESS images, to study the LST variations across the cities and, ii) building data from EUBUCCO, which served as the base input for the UM analysis. They have been discussed in detail in the Sections 3.2.1 and 3.2.2.

3.2.1 LST data

The ECOSTRESS instrument was installed on the ISS on July 3, 2018, equipped with five TIR bands ranging from 8 to 12.5 μm (Hulley et al., 2022). Owing to the orbit of the ISS, it can record LST measurements at a high spatial resolution of 70 meters and temporal resolution of 1 to 5 days, covering a swath width of about 400 meters (Xiao et al., 2021). In this study, ECOSTRESS LST and Emissivity data, obtained from Level-2 products, were utilized. These data undergo atmospheric correction and georeferencing processes to generate precise land surface temperature and emissivity (LST&E) values that are acquired from these 5 TIR bands using a physics-based Temperature and Emissivity Separation (TES)

algorithm (Hulley & Hook, 2022). Moreover, special attention is required for geometric correction of this data due to its unique acquisition from the ISS, which differs from regular satellite missions. An additional noteworthy advantage of ECOSTRESS is its recent transition back to the 5-band mode on April 28, 2023. This transition occurred after a period of operating in the 3-band mode, which was a result of an anomaly in the Mass Storage Unit (MSU) of the instrument (Logan & Smyth, 2019)

Initially, ECOSTRESS data was obtained from NASA's EarthDataSearch platform, but several challenges were encountered such as scan line errors and absence of georeferencing. Later, acquisition from Application for Extracting and Exploring Analysis Ready Samples (AρρEEARS) Platform resolved these issues (https://appeears.earthdatacloud.nasa.gov/). The platform provides a straightforward and effective method for accessing and manipulating geospatial data sourced from diverse federal archives (NASA, n.d.) It automatically extracts the LST end product in Kelvin for the user-defined area of interest, eliminating the need for various pre-processing steps. Moreover, it also offers interactive visualizations such as temperature distribution histograms and quality assessment graphs along with summary statistics in .csv format for each sample within the application, facilitating in-depth exploration of the data. The details about the selection and pre-processing of the ECOSTRESS LST images have been discussed in Section 4.1.1.

3.2.2 Building data

The building data was acquired from EUBUCCO v0.1 (https://eubucco.com/data/), which is a comprehensive database containing ~202 million building footprints with 2D&3D attributes. These attributes include building height, type, and construction year, which are available for 73%, 46%, and 24% of the buildings, respectively, across the entire dataset. It is important to note that these percentages may vary across different cities and regions. This dataset serves as the foundation for in-depth studies of urban sustainability across different levels—ranging from continental to local studies—utilizing a centralized database. It holds significance for numerous applications, such as urban morphological analysis and assessing risks associated with natural hazards. It collects up-to-date data for detailed analysis of the European Union (EU) building stock, a critical resource for informing policy decisions at the EU, national, and municipal levels, guiding urban planning efforts, and supporting academic research. 50 open government datasets and OpenStreetMap data have been harmonized and validated to generate the EUBUCCO building dataset. It covers 27 EU countries and Switzerland, representing 378 regions and 40,829 cities (Milojevic-Dupont et al., 2023).

The dataset for Paris comprises of 645,265 building footprints, with height data available for 83.25% of the buildings. In Rotterdam, 430,038 building footprints are covered, with 88.55% having height data. Milan's dataset consists of 176,207 building footprints, with 86.69% having height data. In Vienna, 202,620 building footprints are present, with 95.18% having height data. The details of the buildings are summarized in Table 3.2. The buildings with missing height data are distributed throughout the study areas and are not concentrated in any specific locations. Thus, it did not impact the analysis, as there was still sufficient diversity among the remaining buildings and no particular building type was affected.

Table 3.2 Number of buildings and coverage of height data of four cities

CITY	NUMBER OF BUILDINGS	COVERAGE (%) OF HEIGHT DATA
Paris	645,265	83.25
Rotterdam	430,038	88.55
Milan	176,207	86.69
Vienna	202,620	95.18

An example of the building dataset has been shown in Figure 3.2. Furthermore, the quality of the dataset was ensured through several levels of pre-processing steps for cleaning, which are discussed further in detail in Section 4.2.1.

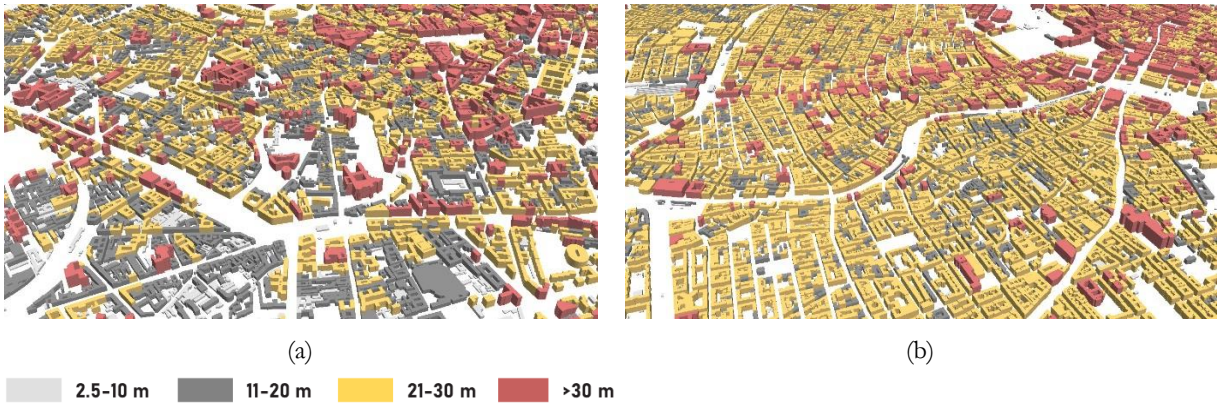

Figure 3.2 Examples of EUBUCCO building dataset of a) Milan and b) Vienna rendered by building height

4 Methodology

This chapter is structured into six main sections, outlining the methodology employed for analyzing UM and LST variations in this study. Section 4.1 ('LST variations') details the selection and the preprocessing steps of the LST images as well as the steps for conducting the hotspot analysis to identify temperature anomalies across the study areas. Section 4.2 ('Urban morphological analysis') explains how the building data was cleaned and pre-processed. Following this, it discusses about the UM analysis conducted in this study using the *momepy* toolkit in Python. Section 4.3 ('Consolidation of LST and UMMs') elaborates on the consolidation of LST values and UM metrics at a consistent spatial scale for further analysis. Section 4.4 ('Relation between LST and UM') introduces the training and testing of the Random Forest Regression (RFR) model to examine the relationship between UM and LST. Furthermore, it provides a framework for investigating the most important driving factors behind LST variations in the study areas. Section 4.5 ('Expert interviews') explains how the interviews with the city experts were conducted for validating the results of this study. Lastly, Section 4.6 ('Tools') discusses the tools utilized for data collection, processing, and analysis of UM and LST data.

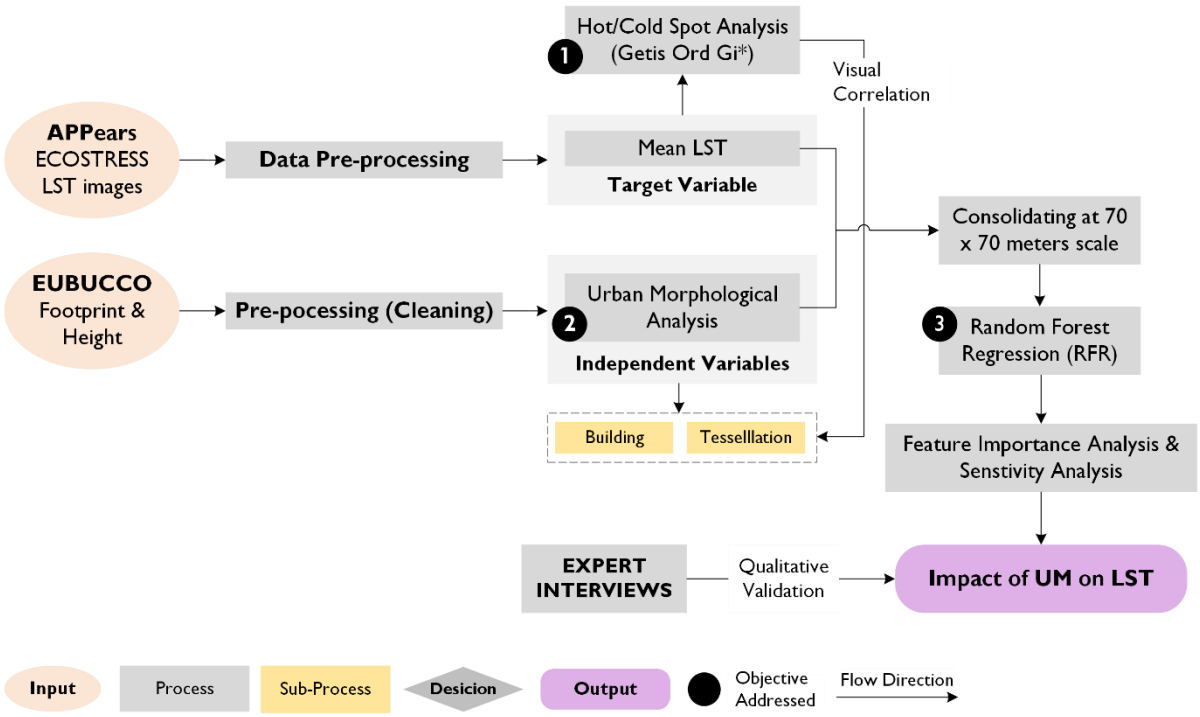

Figure 4.1 Research methodology (Source: Author, 2023)

The study's overall methodology is based on the given workflow (Figure 4.1). As already mentioned, two primary datasets have been used, ECOSTRESS LST images and EUBUCCO building data. The former

underwent pre-processing steps to derive the mean LST image for each city. Meanwhile, the latter underwent cleaning procedures to address various quality issues, followed by an UM analysis performed using momepy. Additionally, a hotspot analysis was conducted on the mean LST images to identify areas of significant temperature variation within each city. After consolidating both the datasets on a grid level at 70 meters by 70 meters scale, a RFR model was applied to explore the relationship between the UMMs and LST. The RFR model was further analysed to determine the importance of different UMMs in influencing LST and assess the sensitivity of those UMMs. To validate the results obtained from the RFR modelling, expert interviews were conducted to provide additional insights and confirm the robustness of the findings.

4.1 LST variations

The detailed methodology for studying the LST variations has been illustrated in Figure 4.2. These steps involved the selection and pre-processing of LST images, followed by the process of conducting the hotspot analysis.

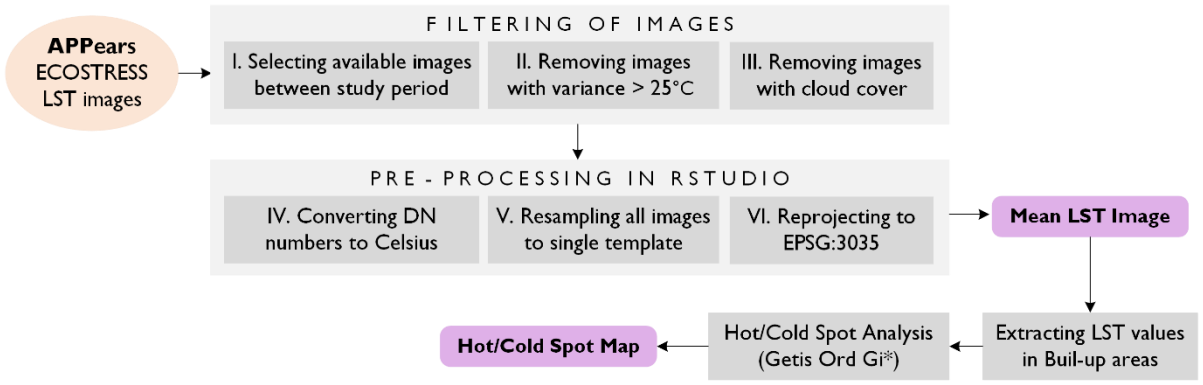

Figure 4.2 Detailed methodology for analysing LST variations (Source: Author, 2023)

4.1.1 Selection and pre-processing of ECOSTRESS images

Due to the variable temporal resolution of the ISS, finding intersecting acquisition dates across the study areas was infrequent. Consequently, a time range was selected, and all relevant images within this range were averaged to produce a single mean approximate image of LST for each city. To ensure accurate approximation between images, the time range was carefully considered with closer proximity. Keeping this in mind, multiple ECOSTRESS images during the summer period (June-August) of 2023 were retrieved. Considering that the summer solstice typically occurs around June 21st in the Northern Hemisphere, the chosen time range aligns with the period of peak solar radiation, thus resulting in higher LSTs. Figure 4.3 shows all the available images between the study period. The images from 10.00 hrs to 17.00 hrs (daytime) were filtered out from the available dataset. This was to have a similar temperature range and avoid misleading interpretations of temperature patterns.

Subsequently, many images from the filtered dataset either had a high cloud cover, scanning error or were not covering the whole region. To address this issue, images exhibiting high cloud cover and a temperature variance exceeding 25 °C that highlighted the outliers with significant deviations from the mean temperature values were eliminated. This was done with the help of summary statistics .csv files. Interestingly, these images corresponded to those with notably high temperature ranges, as evidenced by the histograms in Figure 4.3. Following this approach, six images were selected for Paris, thirteen for Rotterdam, six for Milan and three for Vienna.

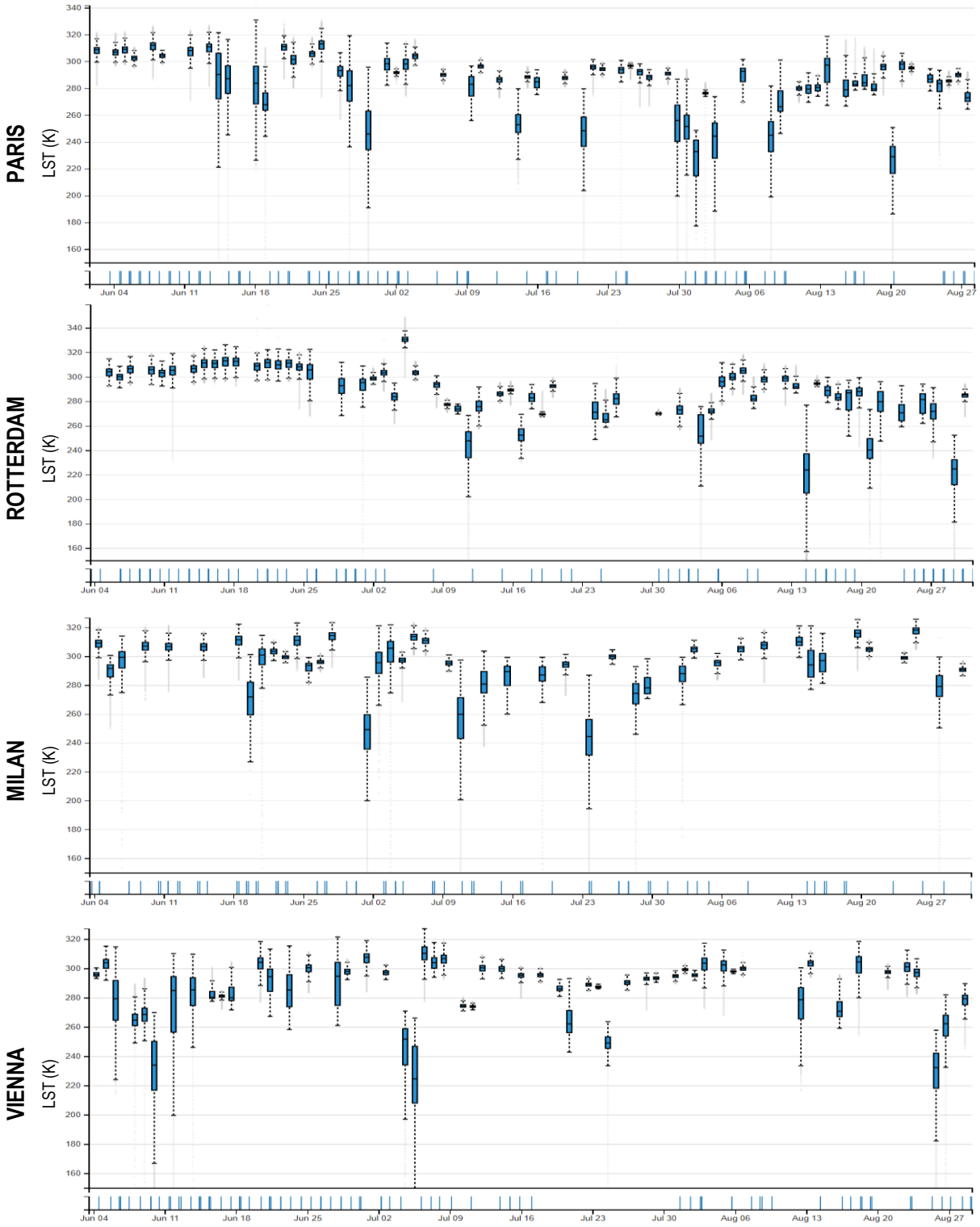

Figure 4.3 Temperature variations of all the available images between June and August, 2023 for Paris, Rotterdam, Milan, and Vienna

The selected acquisition dates along with the statistics of the ECOSTRESS images utilized in this research are summarized in Table 4.1. These sets of images for each city underwent essential preprocessing steps, which involved converting Digital Number (DN) values to Celsius, resampling, reprojecting, and ultimately aggregating them to obtain a single mean LST image for each city.

Table 4.1 Summary statistics for the selected ECOSTRESS images of Paris, Rotterdam, Milan, and Vienna

CITY	ACQUISITION DATES & TIME (UTC)	MINIMUM (K)	MAXIMUM (K)	MEAN (K)	STANDARD DEVIATION	VARIANCE
Paris	2023-06-01 14:21:09	282.10	322.16	308.16	3.63	13.18
	2023-06-03 14:20:40	296.90	321.50	306.75	3.36	11.27
	2023-06-04 13:31:49	297.68	322.12	308.55	3.72	13.86
	2023-06-04 16:45:25	295.34	310.88	302.57	2.30	5.30
	2023-06-05 12:43:21	286.52	326.52	311.26	4.14	17.13
	2023-06-13 12:38:21	286.80	330.02	310.68	3.64	13.23
Rotterdam	2023-06-03 14:21:32	291.86	315.74	303.82	3.70	13.72
	2023-06-03 15:57:53	291.24	309.40	300.01	2.82	7.95
	2023-06-04 13:32:41	292.94	318.10	305.98	4.03	16.22
	2023-06-08 13:30:24	293.72	320.16	306.53	3.80	14.47
	2023-06-09 12:41:34	295.02	325.26	310.81	4.51	20.33
	2023-06-09 14:18:30	294.38	322.22	310.43	4.41	19.41
	2023-06-10 13:29:28	295.94	326.88	312.50	4.80	23.01
	2023-06-11 11:03:11	292.38	325.56	312.14	4.45	19.78
	2023-06-13 12:38:21	296.40	359.12	310.97	4.36	19.04
	2023-06-14 11:49:14	296.38	332.42	309.90	4.35	18.94
	2023-06-14 11:50:06	296.46	323.64	310.75	4.31	18.58
	2023-08-09 13:59:05	285.36	312.80	300.28	3.33	11.08
	2023-08-16 10:00:50	287.24	310.92	297.88	3.18	10.14
Milan	2023-06-03 12:44:50	284.18	321.32	308.77	3.75	14.08
	2023-06-19 11:00:56	292.20	324.26	313.92	3.53	12.48
	2023-07-23 16:24:41	298.98	312.02	304.96	2.19	4.81
	2023-07-26 15:36:47	297.68	314.04	305.15	2.56	6.54
	2023-07-27 14:48:35	281.72	319.08	307.49	3.71	13.78
	2023-08-14 13:14:41	290.10	326.86	315.63	4.05	16.44
Vienna	2023-06-03 12:46:34	292.14	315.34	302.94	4.51	20.34
	2023-06-13 12:40:57	276.78	318.48	303.33	5.37	24.79
	2023-06-18 10:13:09	284.06	320.16	307.00	4.27	18.25

4.1.2 Getis-Ord Gi* hotspot analysis

A hotspot analysis was achieved, using the Getis-Ord Gi* statistics, on the mean summer LST image of each city. This was to identify areas where daytime LST values exhibited spatial clustering, resulting in either positive (hotspots) or negative (coldspots) anomalies in the LST patterns. The LST values corresponding to the building footprints were initially extracted from the image. Thus, the hotspot analysis was conducted only on the LST data within the built-up areas to observe spatial variations. This approach helped in identifying areas with significant temperature anomalies within urban environments and understanding their correlation with specific land uses. Getis-Ord Gi* is a local statistical method that groups the neighbouring pixels of similar values into statistically significant clusters at a local scale (Ord & Getis, 1995). The criterion for identifying these hot/coldspots is that the area in an image should be relatively different than the rest of the image (NV5 Geospatial, n.d.). The algorithm examines each pixel and its nearby pixels within a specified range, classifying them as 'hot', 'cold' or 'neutral' based on statistically significant clusters of high or low values. It is a reliable and effective hot-spot detection

technique that has been employed in prior research (Feyisa et al., 2016; Grigoraş & Urițescu, 2018). In the context of LST, it is computed using the following formula:

$$G_i^* = \frac{\sum_j W_{ij} T_j}{\sum_j T_j} \quad (1)$$

Where T_j is the LST value for feature j, W_{ij} is the spatial weight between pixel i and neighbouring pixel j.

The Gi* statistic was calculated for each feature in the image, which was represented in terms of probability (p-value) and standard deviation (z-scores). The z-score is the degree of clustering among features, and p-value is the likelihood that the observed hotspot patterns are only a result of Complete Spatial Randomness (CSR). A higher positive z-score means there's a stronger clustering of high values (hotspot). Whereas a lower negative z-score means there's a stronger clustering of low values (coldspot). A z-score close to zero suggests that there is no notable clustering observed in the study area, thus confirming the null hypothesis of CSR. After calculating the z-scores, False Discovery Rate (FDR) correction was applied to the p-values associated with these scores. FDR correction helps control for the inflated risk of false positives that arises from conducting multiple statistical tests (Caldas de Castro & Singer, 2006). By adjusting the p-values, it ensures a more accurate determination of significance. Three groups of thermal patterns were identified in this study:

1. **Hot Spots:** z-score > 1.65, statistically significant clustering of high LST values
2. **Cold Spots:** z-score < -1.65, statistically significant clustering of low LST values
3. **Neutral Areas:** -1.65 < z-score < 1.65, no significant spatial autocorrelation

The results of the hotspot analysis were further utilized for visual interpretation in conjunction with the findings of the UM analysis.

4.2 Urban Morphological (UM) analysis

The detailed methodology for the UM analysis involved several steps, as illustrated in Figure 4.4. These steps encompassed the processing of building data and the computation of UMMs using the momepy toolkit.

Figure 4.4 Detailed methodology for analysing UM (Source: Author, 2023)

4.2.1 Cleaning of EUBUCCO building data

The EUBUCCO building dataset, exhibited various quality issues such as long and extremely narrow or overlapping buildings, since it has been integrated from 50 different sources. To have the same quality across all the cities and make it fit for the analysis, it underwent a few validating and pre-processing (cleaning) steps. Initially, the quality of the building data was validated using the *Topology Checker* plugin in QGIS software, employing five topological rules. These rules identified common geometric errors such as

overlaps, duplicates, gaps, invalid and multi-part geometries within the building dataset. Subsequently, the *v.clean* tool (a part of GRASS GIS) was used to automatically rectify these errors. This tool facilitated the data cleaning process by addressing common issues without requiring manual intervention, thereby streamlining the overall process. The data was further pre-processed in momepy, which also offered a set of tools that were used to fix (to an extent) the issue of imprecise data. The basic steps involved (as shown in Figure 4.5):

1. Removing too small/large buildings that might be sensitive to certain morphometric computations.
2. Combining adjacent buildings that are long and narrow into a single building.
3. Merging buildings that are completely enclosed within other buildings into the parental buildings.

Additionally, buildings with missing height data were removed from the dataset. Although this might have slightly affected the morphometric analysis, the influence was deemed minimal due to the low percentage of buildings with incomplete information.

Figure 4.5 Example of pre-processing building datasets of (a) Rotterdam (where small and narrow buildings shown in red were removed) and (b) Paris (where long and narrow adjacent buildings were combined and enclosed buildings were merged into the parent buildings)

4.2.2 Computation of Urban Morphometrics (UMMs)

After the quality assessment of the building data, the UM of the selected cities was analysed using Urban Morphometrics (UMMs) in Python. UMM is a novel method for analysing UM that delivers a comprehensive and systematic measurement of urban characteristics in the form of numerical place codes (Dibble et al., 2019). An open-source python toolkit called momepy developed by Fleischmann (2019) has six modules of those morphometric characters - *dimension, shape, distribution, intensity, diversity,* and *connectivity*.

The *dimension* module is designed for measuring the physical size of morphological elements, their constituent parts, and the aggregated structures they form within an urban environment. The *shape* module facilitates the quantification of the diverse geometries representing various morphological features found within a built environment. The *distribution* module enables the capture of the arrangement and dispersion patterns of elements belonging to a specific category, as well as the relationships between different types of elements across the built environment. The *intensity* module focuses on computing density and other intensity-related characteristics, providing insights into the concentration of urban features. The *diversity* module calculates various aspects of diversity within urban forms, offering insights into the heterogeneity and complexity of the built environment. Lastly, the *connectivity* module is dedicated to capturing the connectivity of urban street networks, providing valuable information on the accessibility and

interconnectedness of urban spaces. Together, these modules offer a comprehensive toolkit for analysing and understanding the multifaceted nature of urban form and structure (Fleischmann, 2018).

The focus of this study was primarily on the first four modules of the momepy toolkit. This encompassed an examination of various metrics associated with each module, as proposed by Fleischmann et al. (2021) and an exploration of their potential influence on LST. It is to be noted that the metrics under the connectivity module were not considered in this study as they typically require a street layout as a base for analysis. The main units for the morphometric analysis in this study were buildings and morphological tessellations (MT) i.e. spatial segmentation based on building footprints (illustrated in Figure 4.6). MTs are similar to Voronoi tessellations but are generated around the building features rather than points. Fleischmann et al. (2020) suggested that spatial units such as MTs can serve as proxy data in capturing cadastral plot-scale spatial information of urban forms. The concept of a plot often presents challenges due to its ambiguity, resource-intensive nature, and inconsistent representation across different geographical contexts. In contrast, MTs remain consistent and contiguous throughout as they rely solely on the building footprint layer. This uniformity ensures reliable spatial data across diverse urban environments, facilitating comparative analyses with greater efficiency and reduces data dependency. Metrics such as floor area ratio and coverage area can be readily computed using MTs, offering results comparable to those derived from plot data. The steps to generate these MTs were conceptualised by Fleischmann et al. (2020) and were implemented into a Python script which was integrated as a part of the momepy toolkit. Therefore, based on the building data, the MTs were generated for each city, where each MT was linked to its parent building using a common *unique_id*.

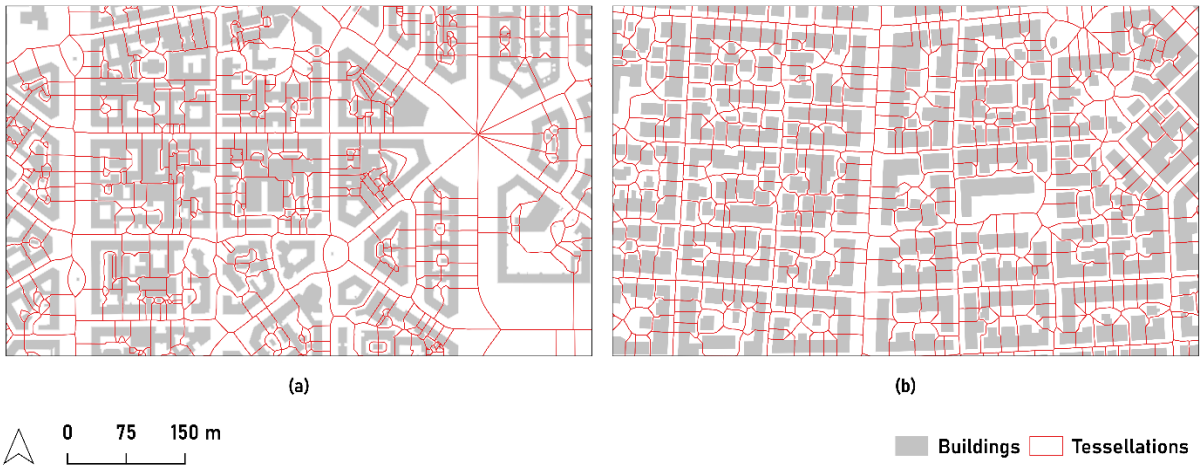

Figure 4.6 Units of morphometric analysis – building and morphological tessellation (MTs) cells across different areas of (a) Milan and (b) Vienna

Momepy utilizes GeoDataFrame objects from the geopandas library as its foundation. The initial step involved providing the necessary data in the form of a GeoDataFrame. Each city had two of them, one containing the spatial information of building footprints and the other containing the MTs. Subsequently, the analysis was performed, which allowed for the computation of relevant metrics for the provided GeoDataFrames. The results of this analysis were returned as pandas series, where each of the metrics were integrated as additional columns within the existing GeoDataFrames

The metrics computed in the study were divided into two types – *simple* and *relational* metrics. Simple metrics relied on a single GeoDataFrame (either building footprints or MTs in this case) as the primary data source. These metrics offered straightforward measurements of various morphological aspects and provided information regarding individual features.

Table 4.2 List of UMMs computed using momepy for analysing UM of Paris, Rotterdam, Milan, and Vienna

CHARACTERS	MORPHOMETRICS	URBAN UNIT	SPATIAL CONTEXT
Dimension	*Simple Metrics*		
	Area	Building & MT	Building & MT
	FloorArea	Building	Building
	LongestAxisLength (LAL)	Building	Building
	Perimeter	Building	Building
	Volume	Building	Building
	Relational Metrics		
	CoveredArea	MT	Spatial Weight
	MeanHeight	Building	Spatial Weight
Shape	*Simple Metrics*		
	CircularCompactness	Building	Building
	Convexity	Building	Building
	Elongation	Building	Building
	EquivalentRectangularIndex (ERI)	Building	Building
	FormFactor	Building	Building
	FractalDimension	Building	Building
	Rectangularity	Building	Building
	ShapeIndex	Building	Building
	SquareCompactness	Building	Building
	Squareness	Building	Building
	VolumeFacadeRatio (VFR)	Building	Building
Distribution	*Simple Metrics*		
	Orientation	Building & MT	Building & MT
	SharedWalls	Building	Building
	Relational Metrics		
	Alignment	Building	Spatial Weight
	BuildingAdjacency	Building	Spatial Weight
	CellAlignment	Building	MT
	NeighbourDistance	Building	Spatial Weight
	MeanInterbuildingDistance (MID)	Building	Spatial Weight
Intensity	*Relational Metrics*		
	FloorAreaDensity	MT	Spatial Weight
Diversity	*Relational Metrics*		
	Gini	MT	Spatial Weight
	Range	MT	Spatial Weight
	Shannon	MT	Spatial Weight
	Simpson	MT	Spatial Weight

While relational metrics assessed the relationships between two elements, building footprints and MTs, represented as separate GeoDataFrames. Some of the relational metrics also assessed relationships based on spatial weights matrices. To analyse the patterns of morphometric characters within a spatial context,

spatial weights take into the account the neighbouring elements and capture the relationship between them. Specifically, in this case, focusing on building footprints, spatial weights were represented as a binary matrix where a value of 1 signified neighbouring elements and 0 indicated the absence of such proximity. These metrics enabled the exploration of spatial interactions and dependencies between both the units. A detailed list of metrics used in this study can be found in Table 4.2, which includes a total of thirty UMMs. Descriptions of these UMMs are provided in Annexure IV. Additionally, more information about momepy can be found in https://docs.momepy.org/en/stable/index.html.

4.3 Consolidation of LST and UMMs

Consequently, all the metrics and LST data were consolidated at an appropriate and comparable scale of 70 meters, mirroring the spatial resolution of ECOSTRESS data (Figure 4.7). This integration process involved generating a vector grid covering the study area, with each grid cell representing a uniform spatial unit of 70 meters by 70 meters. By employing spatial analysis techniques such as *Spatial Join* and *Zonal Statistics*, the metrics pertaining to building morphology and its corresponding LST values were attached to the grid cells.

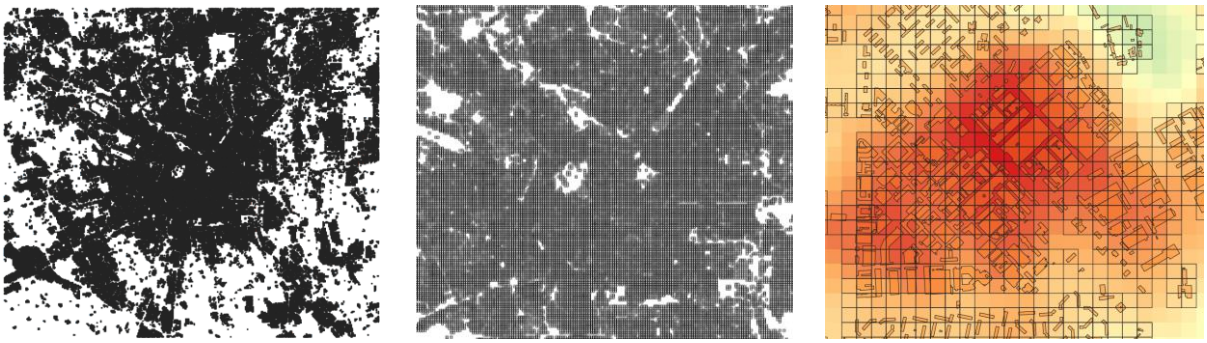

Figure 4.7 Consolidation of LST and UMM at a grid of 70 m by 70 m resolution for Milan

This approach, being used by various authors (Estoque et al., 2017; Han, 2023) in the past, ensured spatial homogeneity by representing the study area in consistent spatial units and helped reduce computational complexity and noise in the data. Additionally, the structured grid format simplified model interpretation and allowed for the examination of UM's influence on LST at a broader level across the study areas. However, it's important to acknowledge potential disadvantages, including the loss of fine-scale spatial detail present in individual buildings and the generalization of unique building characteristics within grid cells.

4.4 Relation between LST and UM

While several traditional statistical methods have been used (as shown in Annexure I), many of them (e.g., Pearson's correlation, OLS regression, PCA) often provide limited interpretability, especially when dealing with complex relationships or high-dimensional data. As discussed in Section 2.4, these methods may encounter issues related to collinearity (Hu et al., 2022) and find it challenging to calculate the importance of all independent variables (Yao et al., 2022).

Hence, RFR was employed as the fundamental model for examining the relationship between UM and LST in this study, where the twenty-four UMMs (mentioned in Table 4.2 excluding the metrics with MTs as the urban unit) and LST were considered as the independent and dependent variables, respectively. Six UMMs (CoveredArea, FloorAreaDensity, Gini, Range, Shannon and Simpson) were not included in the

model due to high computation demands. The detailed methodology for the RFR modelling has been illustrated in Figure 4.8.

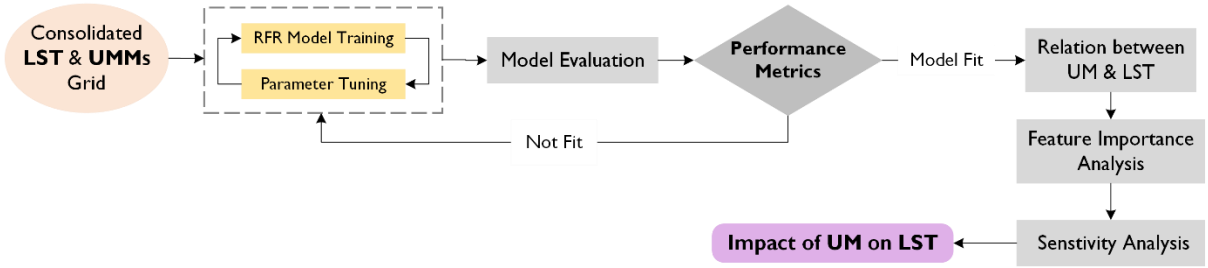

Figure 4.8 Detailed methodology for RFR modelling (Source: Author, 2023)

4.4.1 Model training

To train the RFR model, the entire consolidated dataset for all the cities underwent a randomized split into an 80-20 ratio, allocating 80% for training and 20% for testing. Following this, hyperparameter tuning was conducted utilizing the k-fold cross-validation technique to obtain the optimal n_{tree} (optimal number of trees) and m_{try} (number of input variables randomly sampled as candidates at each split) for constructing a more accurate model (Jung & Hu, 2015). This technique divides the dataset into k subsets (or folds), where the model is trained on k-1 folds and validated on the remaining fold. This process iterates k times, where each fold is utilized as the validation set once. By averaging the performance metrics across the k iterations, k-fold cross-validation provides a more reliable estimate of the model's performance and helps prevent overfitting by leveraging all available data for both training and validation (Raschka, 2018). The k-fold cross-validation technique, with k set to 5 in this study, was employed to iteratively train and validate the model on different subsets of the data. The number of trees was systematically adjusted from 100 to 300, with increments of 100, to explore its impact on model performance. The optimal n_{tree} varied across cities, with both Rotterdam and Paris achieving peak accuracy with 300 trees. Conversely, Milan and Vienna demonstrated their highest accuracies with 100 trees. Notably, the m_{try} value was set to 8 for all cities, nearly one-third of the total number of variables (twenty-four in this case), which is the ideal m_{try} value in a RFR model (Liaw & Wiener, 2002).

4.4.2 Model evaluation

The performance of the model was evaluated using three main metrics, namely, i) Co-efficient of determination (R^2), ii) Mean Absolute Error (MAE), and iii) Root Mean Square Error (RMSE). Co-efficient of determination or r-squared is a statistical measure that indicates how much of the variability in the dependent variable can be explained by the independent variables. It ranges from 0 to 1, where 1 indicates a perfect fit. A higher R^2 value indicates a better fit of the model to the data. Mean Absolute Error (MAE) represents the average absolute difference between the predicted values and the actual values. Lower MAE values indicate smaller average errors between predicted and actual values, implying better model performance in terms of accuracy. Root Mean Square Error (RMSE) calculates the square root of the average of squared differences between predicted values and actual values. RMSE, similar to MAE, computes the average magnitude of errors but penalizes larger errors more heavily because of the squaring process, making it more sensitive to outliers. A low RMSE value indicates that the model's predictions are, on average, closer to the actual observed values.

$$R^2 = 1 - \frac{\sum_{i=1}^{n} (y_i - \hat{y}_i)^2}{\sum_{i=1}^{n} (y_i - \bar{y})^2} \quad (2)$$

$$MAE = \frac{1}{n} \sum_{i=1}^{n} | y_i - \hat{y}_i | \quad (3)$$

$$RSME = \sqrt{\frac{1}{n} \sum_{i=1}^{n} (y_i - \hat{y}_i)^2} \quad (4)$$

Where, y_i represents the observed LST values, $\hat{y}_i$ represents the predicted LST values from the model, $\bar{y}$ represents the mean of the observed LST values and n is the number of data points. The combination of these three metrics offered a comprehensive evaluation of the model's performance and accuracy.

4.4.3 Feature importance

Based on this model, the influence of each UM metric on the LST was evaluated by quantifying the *%IncMSE* (percentage increase in mean squared error) and *IncNodePurity* (increase in node purity) for each city. %IncMSE is calculated by comparing the change in MSE of the out-of-bag (OOB) samples before and after permuting a predictor variable. A high value indicates a strong correlation between the variable and the dependent variable, suggesting that the variable is essential for the model and contributes significantly to its predictive accuracy. It assesses variable importance based on its impact on the overall predictive accuracy of the RF model. Whereas IncNodePurity is calculated based on the improvement in node purity achieved by splitting nodes using a particular variable. A higher value indicates significant contribution of the variable to creating more homogeneous partitions within decision tree nodes, thus enhancing the model's ability to effectively separate data points into distinct categories or predicted values. It evaluates the variable importance within individual decision trees and their contribution to node purity (Yan & Bai, 2020) After this process, a relative importance (RI) percentage was derived by normalizing the %IncMSE values of the UMMs for each city to obtain the contribution of each UMM to LST.

4.4.4 Sensitivity analysis

Following the assessment of variable importance, a sensitivity analysis was conducted to delve deeper into the relationships between UMMs and LST within each city. Partial Dependence Plots (PDPs) were generated for the most important independent UMMs to see whether they have a positive or negative effect on the LST. They can help understand how changes in a particular UMM impact the LST, while keeping other features constant or averaging over them (Friedman, 2001). These plots not only revealed the direction of influence but also provided insights into the nature of the relationship, whether it is linear, non-linear, or subject to interactions with other features.

Following this, a comparative analysis was conducted across different cities to discern how the influence of UM on LST varies spatially.

4.5 Expert interviews

The results of this research were backed up by qualitative interviews with city experts in the field. Three experienced city experts, each from Rotterdam, Milan (with additional knowledge of Paris), and Vienna, were engaged in semi-structured interviews. These interviews adhered to the framework outlined in the manual by Groenendijk & Dopheide (2003), during which they were presented with the hotspot and UMM maps, alongside PDP plots. Open-ended questions were posed to them, focusing on the behaviour of the hotspot patterns with different land uses as well as the potential reasons behind the relationship

between important UMMs and LST. They primarily supported the results by helping to explain the observed patterns and the possible implications of this study in mitigating heat in urban areas. The interviews provided a deeper understanding and context for the findings, enhancing the overall analysis.

4.6 Tools

Pre-processing of the LST images, involving steps such as resampling, reprojection and aggregating, were conducted in RStudio, followed by the hotspot analysis which was performed using the *elsa* package. Initial cleaning of the building data was done in QGIS software. Subsequent levels of cleaning and the UMM computations were carried out in Python programming language, particularly using the *momepy* module developed by Fleischmann (2019). Development, testing and evaluation of the random forest regression models were undertaken in RStudio, using the *randomForest, caret* and, *pdp* packages. All these scripts and software tools were utilized within the CRIB, university's geospatial computing platform. Its high computational capacity helped in reducing significant processing time.

5 Results

This chapter presents the findings of the study, organized into three main sections. Each section addresses specific aspects of the research aligned with its corresponding objectives. Sections 5.1 ('LST variations and hotspot analysis') and 5.2 ('UM analysis') presents the results related to understanding of the LST variations and hotspot analysis (Objective 1) and urban morphological characteristics (Objective 2) of the four cities, respectively. Section 5.3 ('Relation between LST and UM') presents the results obtained from the RFR regression modelling to examine the influence of UM on LST (Objective 3).

5.1 LST variations and hotspot analysis

This section addresses Objective 1 of this research. It presents the processed mean LST images obtained from the filtered ECOSTRESS dataset, along with the results derived from the hotspot analysis conducted using the Getis Ord Gi* statistics based on these processed images.

Figure 5.1 illustrates the boxplot representing the mean LST variation across the selected raw images (refer to Table 4.1). Notably, all images for each of the cities exhibited mean temperatures exceeding 300.00 K, with the exception of one, in Rotterdam, which recorded a mean temperature of 287.88 K. Across all cities, the temperature variance remained relatively low, with a maximum variance of 14.62 K observed in Rotterdam due to the higher number of available images. The highest mean temperature observed was in one of the images of Milan (315.63 K). Furthermore, even the lowest mean temperature recorded in Milan surpassed the lowest temperatures observed in the other three cities. Vienna, despite having only three images, demonstrated closely clustered mean temperatures, with a variance of 4.06 K between them. Hence, the limited dataset size didn't significantly affect the LST consistency in Vienna.

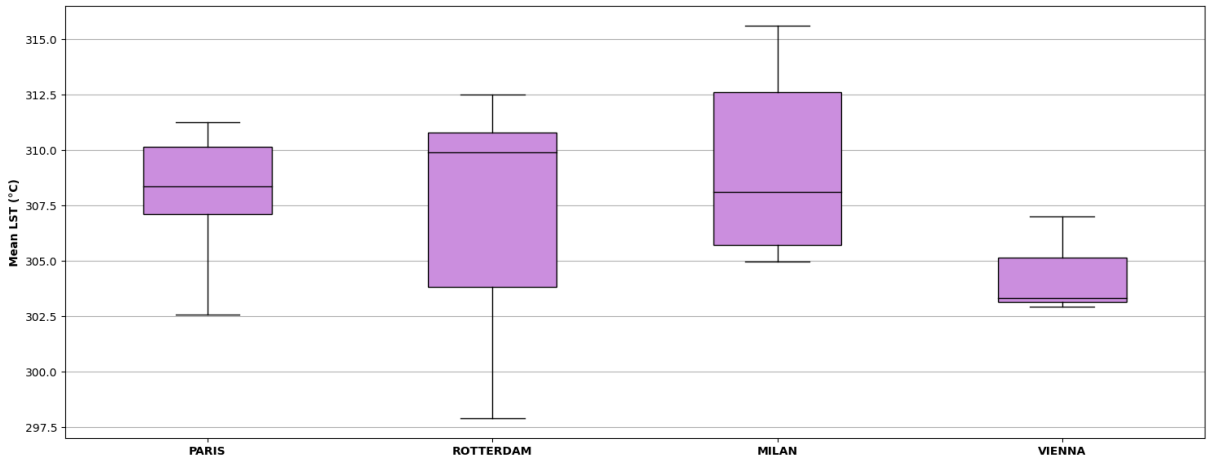

Figure 5.1 Boxplot of the distribution of mean LST values of the selected ECOSTRESS images of Paris, Rotterdam, Milan, and Vienna

Figure 5.2 shows the processed mean LST images of the study areas during the summer period (June-August) of 2023 between 10.00 hrs to 17.00 hrs alongside their corresponding hotspot maps. Paris experienced a mean LST ranging from 28 to 41 °C. Rotterdam showed the mean LST ranging from 25 to 41 °C. Milan showed the mean LST ranging from 31 to 41 °C and Vienna had a mean LST range of 23 to 38 °C. Milan experienced the highest mean LST during the study period indicating relatively higher temperatures as compared to the other cities. Furthermore, these LST images were used as the target variable for the RFR modelling for each city which has been discussed in more detail in Section 4.4.

The summary of the hotspot analysis has been given in Table 5.1 including the minimum, maximum, and mean temperatures for each Gi* spot category in these cities. In Paris and Rotterdam, results show that the spatial coverage of hotspots exceeds that of coldspots within the built-up areas. Specifically, in Paris, hotspots cover approximately 9.42% of the built-up area with a minimum LST of 38 °C and a maximum of 41 °C, while in Rotterdam, they cover approximately 10.24% with LST minimum and maximum values same as that of Paris. In Paris, the most pronounced instances of extreme LST hotspots are predominantly observed in two main areas. From Figure 5.3, it can be observed that these areas are mostly prevalent in the northeastern section of the city, including a major business park (1) and warehouse districts (2). Additionally, they are present in the southeastern region, particularly in sections along the left bank of the Seine River, which feature a commercial area adjacent to a railway station (3) and an industrial area (4). Hotspots in Rotterdam are primarily concentrated in the central part of the city (as shown in Figure 5.4), running perpendicular to the Nieuwe Maas River which mainly is the business park and an industrial neighbourhood (2). Additionally, smaller clusters of hotspots are scattered across various parts of the urban area, including the port area (3) and another industrial estate (4) in the south.

Table 5.1 Area covered by Gi* spots, along with their corresponding descriptive statistics of LST

CITY	SPOTS	RELATIVE AREA (KM²)	LST (°C)		
			MINIMUM	MAXIMUM	MEAN
Paris	Cold	31.47 (8.97%)	25	35	33
	Neutral	286.26 (81.61%)	32	40	36
	Hot	33.01 (9.42%)	38	41	40
Rotterdam	Cold	19.79 (10.06%)	24	36	31
	Neutral	156.67 (79.70%)	30	38	34
	Hot	20.09 (10.24%)	38	41	40
Milan	Cold	23.46 (9.98%)	29	37	34
	Neutral	193.66 (82.39%)	32	39	38
	Hot	17.92 (7.63%)	39	41	40
Vienna	Cold	20.52 (9.98%)	22	32	28
	Neutral	166.87 (81.21%)	27	39	34
	Hot	18.07 (8.81%)	36	38	37

In contrast, Milan and Vienna exhibited different spatial distribution patterns, with a relatively larger area covered by the coldspots as compared to hotspots within their built-up areas. Hotspots accounted for 7.63% and 8.81%, respectively of the areas. In Milan, hotspots were dispersed radially across the southeastern part of the city as shown in Figure 5.5. These hotspots are particularly noticeable on the outskirts, away from the urban centre, and are mainly found in manufacturing units (2 and 4) and wholesale markets (3). Whereas hotspots in Vienna (Figure 5.6) are predominantly concentrated within the urban centre (3), which includes a large portion of a residential area. These hotspots also extend to some parts of the southern regions (4 and 5).

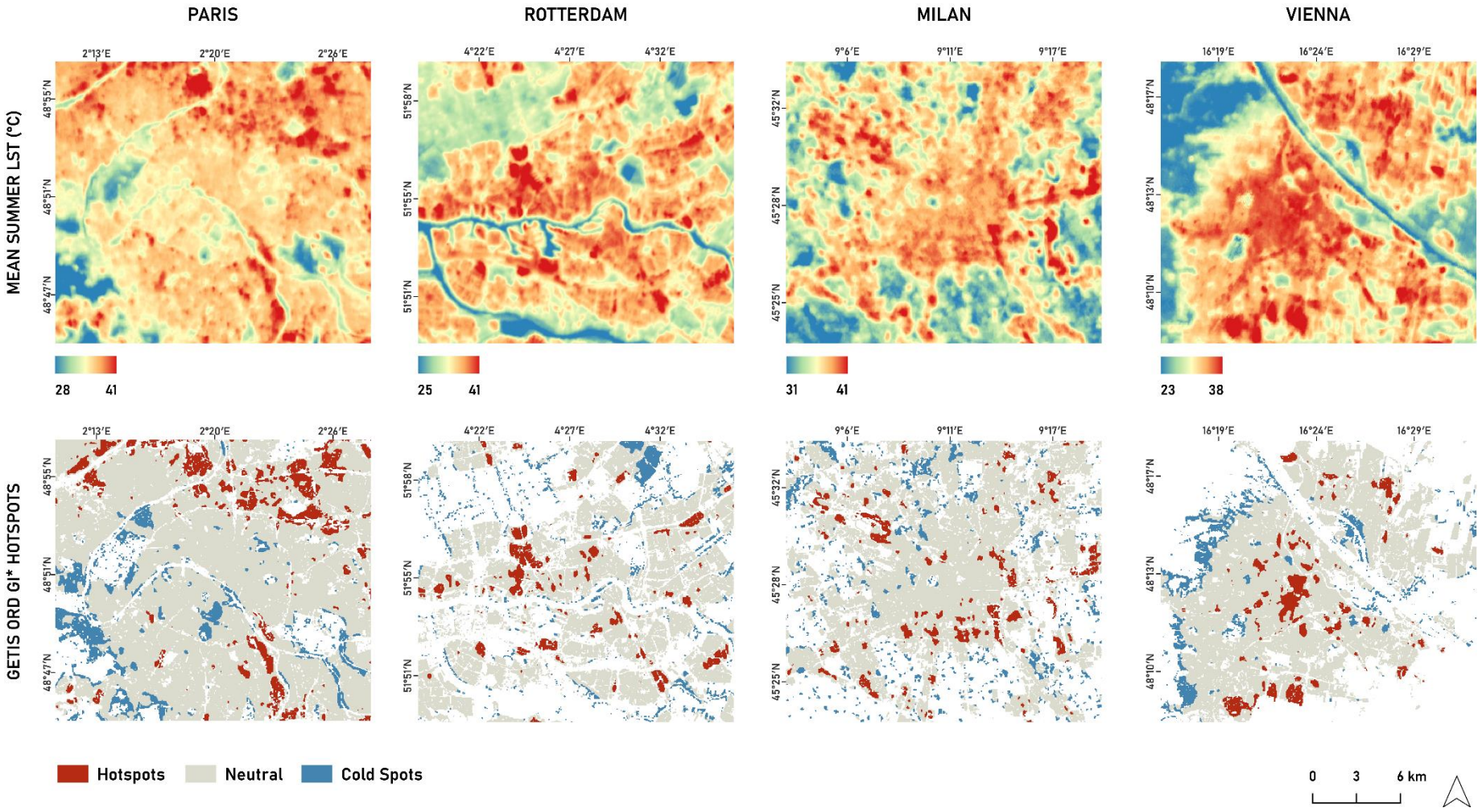

Figure 5.2 Processed mean LST images of Paris, Rotterdam, Milan, and Vienna obtained from the filtered ECOSTRESS and their corresponding hotspot maps within the built-up area

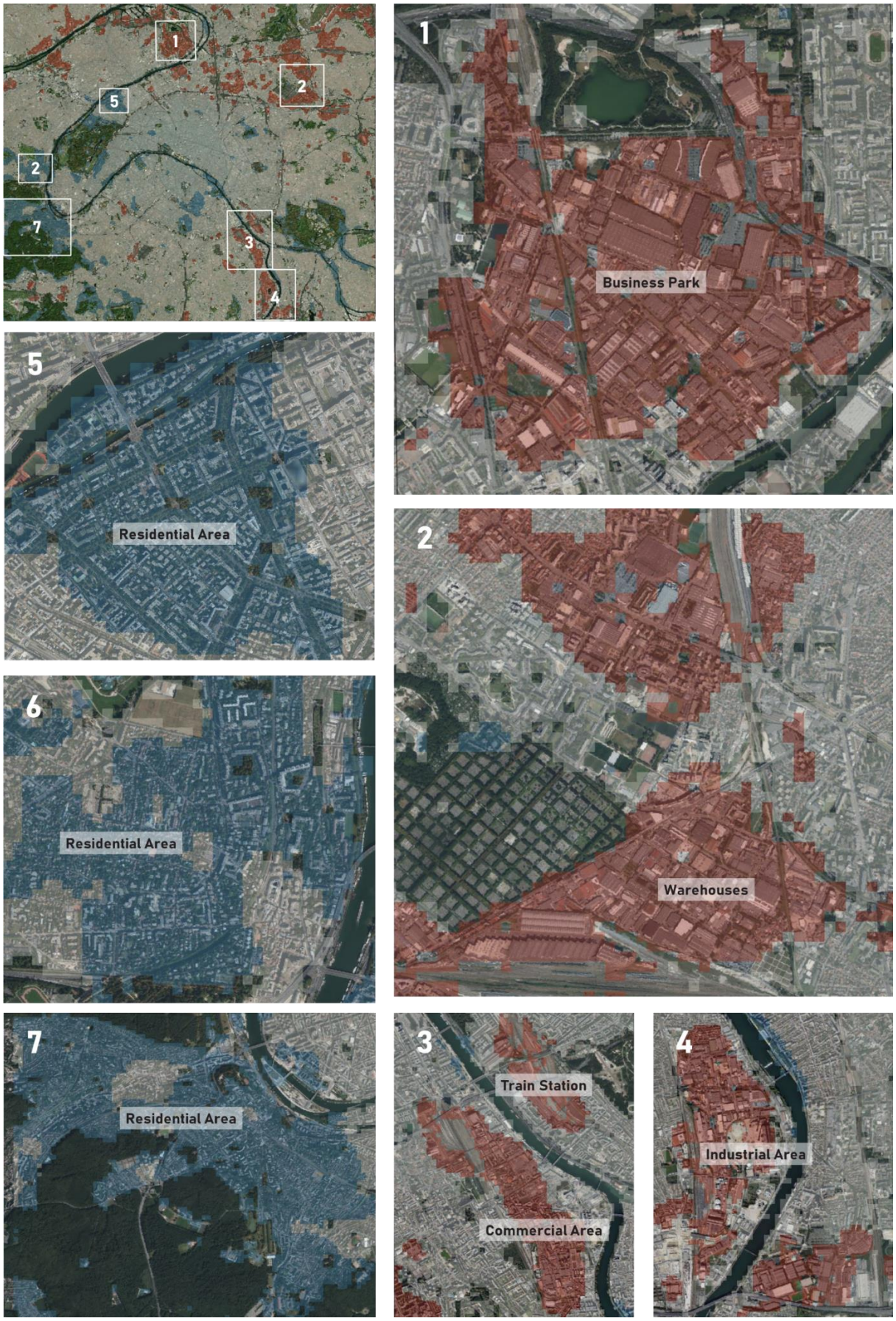

Figure 5.3 Built forms in hot and coldspots of Paris at a detailed level

Figure 5.4 Built forms in hot and coldspots of Rotterdam at a detailed level

The observed coldspots across all cities are predominantly situated in the residential areas. These areas are generally featuring several characteristics that contribute to lower LST. It can be observed that the residential areas have much lower building densities compared to commercial or industrial zones. This means there are fewer buildings per unit area, which might reduce the amount of heat absorbed and retained by structures and paved surfaces. Moreover, lower building density allows for more space between the buildings, potentially enhancing air circulation, which could contribute to the lower LST observed in these areas. The extremes in the LST could also be attributed to the design and materials used in residential buildings. For example, residential buildings might have reflective roofs or lighter-colored surfaces that absorb less heat compared to the darker, heat-absorbing materials often used in industrial or

commercial buildings. In case of Rotterdam, one of the notable coldspots includes areas with several florist shops and greenhouses (Figure 5.4, 1). Greenhouses are designed to control their internal environment, often using shading, ventilation, and evaporative cooling techniques. The presence of extensive vegetation within these greenhouses might also contribute to cooling through evapotranspiration.

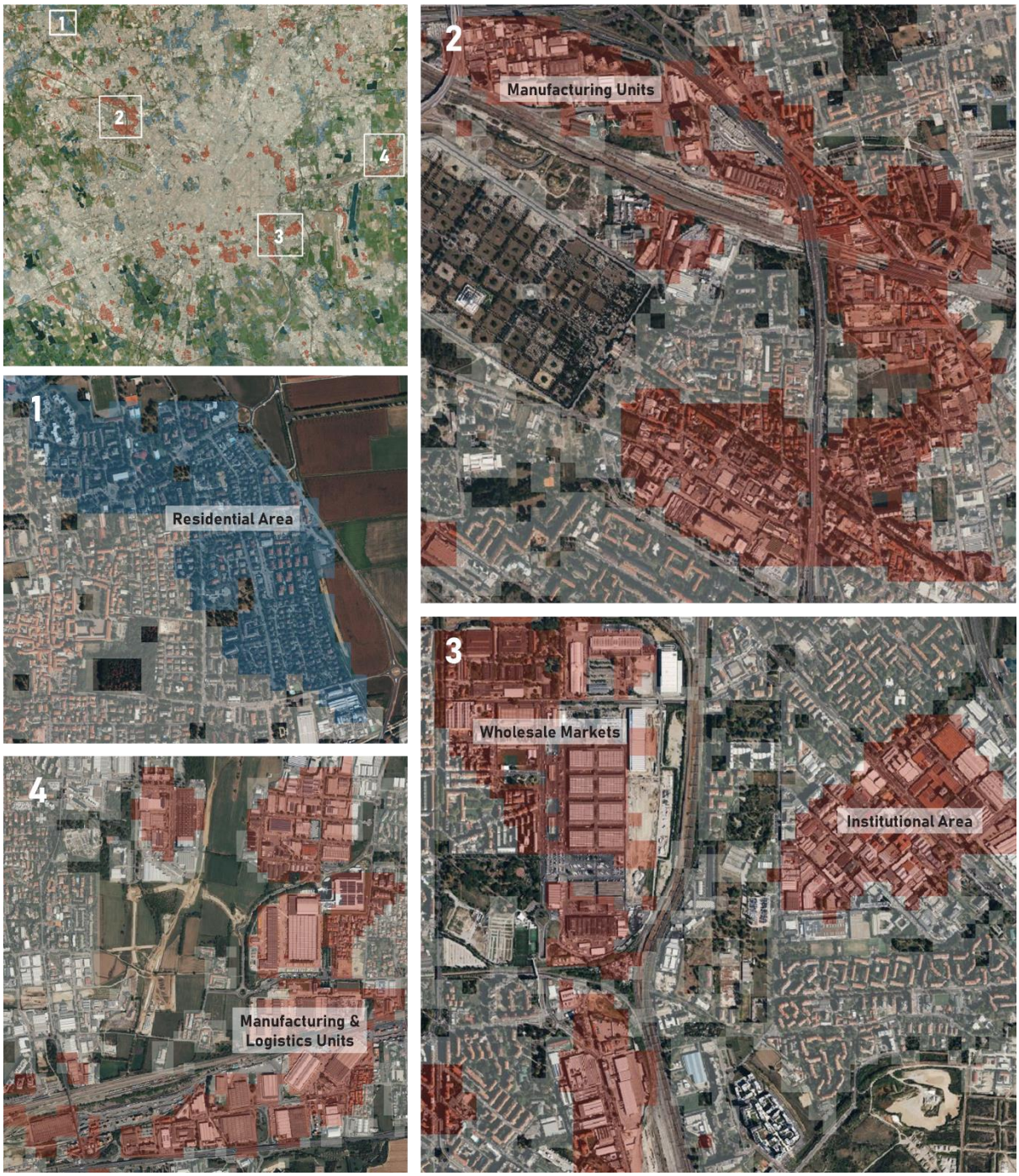

Figure 5.5 Built forms in hot and coldspots of Milan at a detailed level

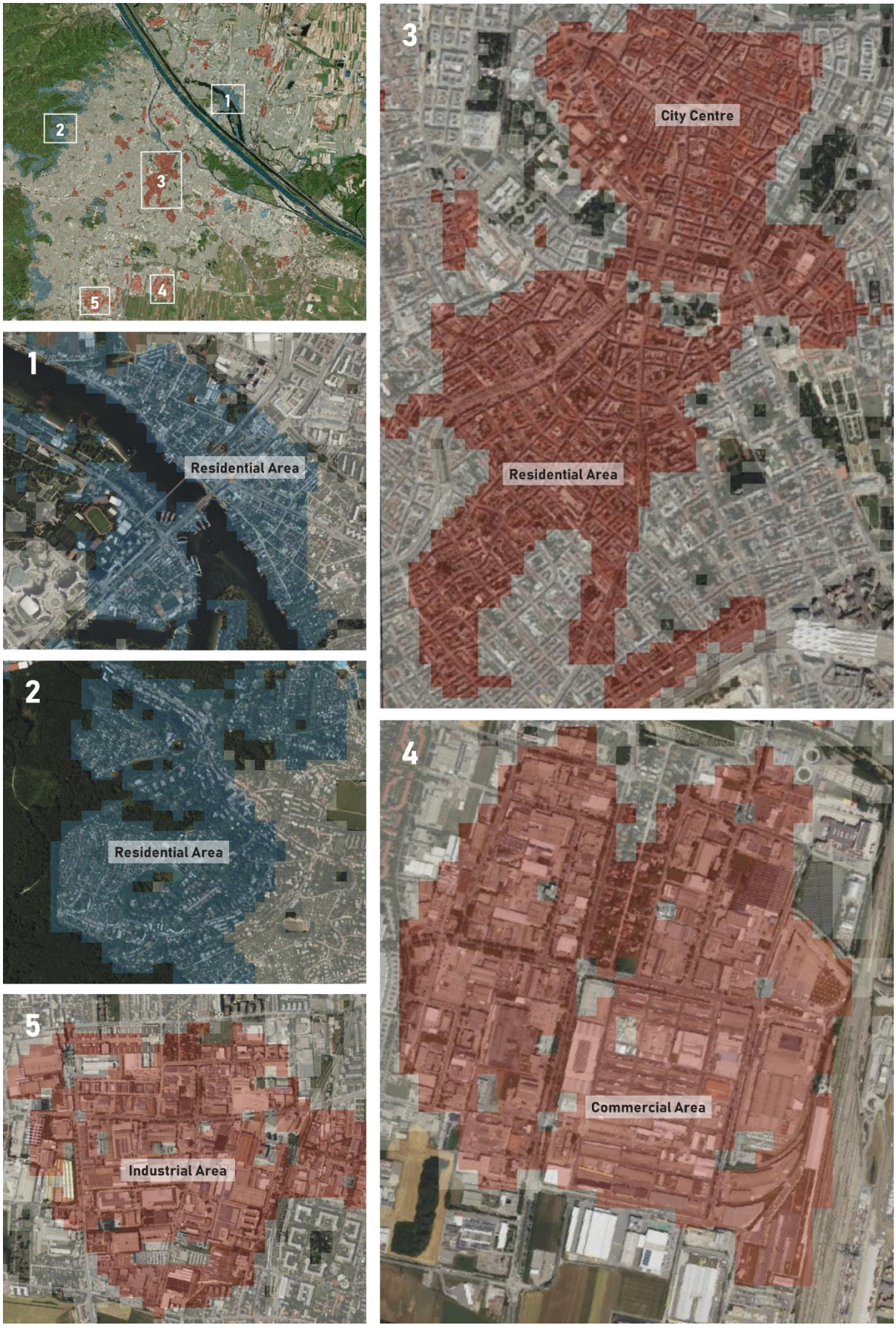

Figure 5.6 Built forms in hot and coldspots of Vienna at a detailed level

5.2 UM analysis

This section addresses the Objective 2 of this research. Thirty different UMMs for Paris, Rotterdam, Milan, and Vienna at a building level have been presented in Figure 5.7-Figure 5.11, that were computed using momepy. These maps reveal both consistent and varying UM patterns across the cities.

For example, one notable pattern is the distribution of Mean Height, which is relatively higher in the urban centres and lower in the surrounding areas. This indicates the presence of high-rise buildings and denser development in the urban core, which are typical characteristics of central business districts and densely populated urban areas. Figure 5.8, column one, clearly illustrate this pattern, with lighter shades indicating higher values of Mean Height clustering in the central areas. Conversely, as one moves towards the periphery of these urban areas, the Mean Height values decrease, signifying a transition to lower-rise residential and commercial buildings typical of suburban and rural landscapes. A notable difference among these cities is that Milan and Vienna have the highest mean building heights, both having an average (μ) height of 14 meters, compared to Paris (μ = 12 meters) and Rotterdam (μ = 9 meters). This indicates that buildings in Milan and Vienna tend to be taller on average.

Similarly, the Mean Interbuilding Distance (MID) of the buildings are significantly lower in the central urban areas, reflecting a closely spaced buildings and compact development which is common in city centres. This is shown in Figure 5.11, column one, with darker shades indicating smaller interbuilding distances in these densely built-up areas. On the other hand, the surrounding suburban and rural areas, characterized by more spread-out development and lower density, show higher MID values. The maps highlight this gradation, with lighter shades representing larger distances between buildings as one moves away from the urban core. One significant distinction is observed in the average MID across the cities studied. In Paris, it is ~88 meters, which is notably the lowest among the four cities. In comparison, Rotterdam, Milan, and Vienna have average MIDs of ~95, ~145, and ~125 meters, respectively. The combination of shorter distance between buildings and the average building height in Paris indicates that it exhibits a relatively higher density of buildings within the designated study area as compared to the more spaced-out building configurations seen in other cities.

Furthermore, these UMMs were visually interpreted for each city alongside the hotspot areas identified in Section 5.1. While all UMMs were examined, it was particularly evident that certain metrics exhibited clear patterns and relationships with the distribution of hotspots across the four cities. In the following sections, some of the examples from each city have been discussed.

In Paris, Orientation (Figure 5.10, column one) reveals that most coldspots in the city are situated in areas characterized by lower orientation, represented in shades of purple and blue (~0-20°). These coldspots are predominantly located in the southwest mainly comprising residential areas. Conversely, hotspots are heavily concentrated in the northeast of the city and correspond to areas with higher orientation values (~28-45°). These zones largely correspond to the industrial estates discussed earlier in Section 5.1.

In Rotterdam, the Mean Height (Figure 5.8, column one) illustrates that the regions shaded in purple, spanning ~3 to 7 meters in height, predominantly appear as coldspots. These areas are notably prominent in the north section of the city, characterized by the presence of large buildings which are primarily florist shops and expansive greenhouses, along with scattered small structures. Whereas areas with buildings ranging from ~7 to 11 meters in height, depicted in light blue and green hues, mostly emerge as hotspots. These areas encompass a major business park and an industrial neighbourhood located centrally, along with another estate and a port area situated in the southern region, as depicted in Figure 5.4.

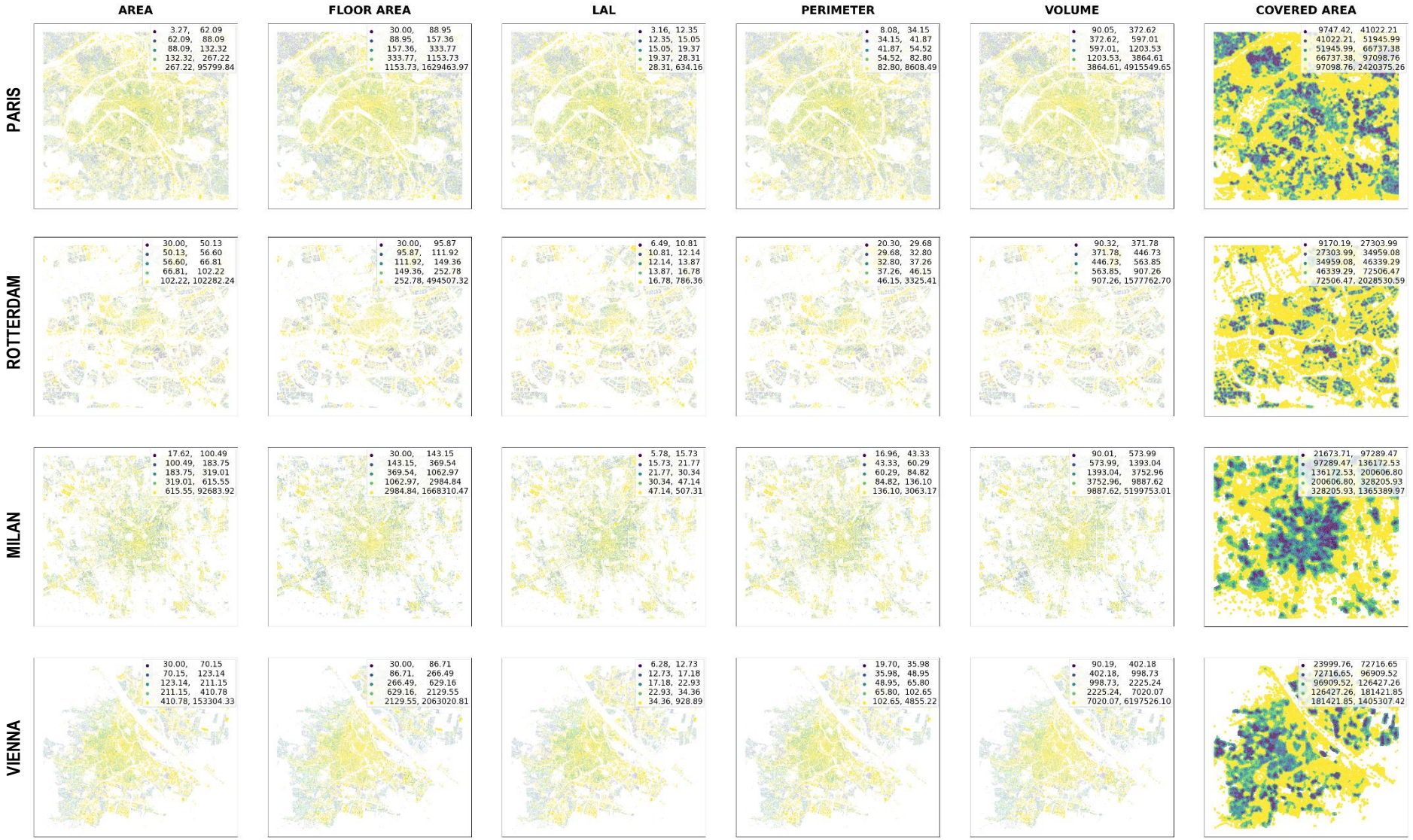

Figure 5.7 Different UMMs computed for Paris, Rotterdam, Milan, and Vienna (Part 1)

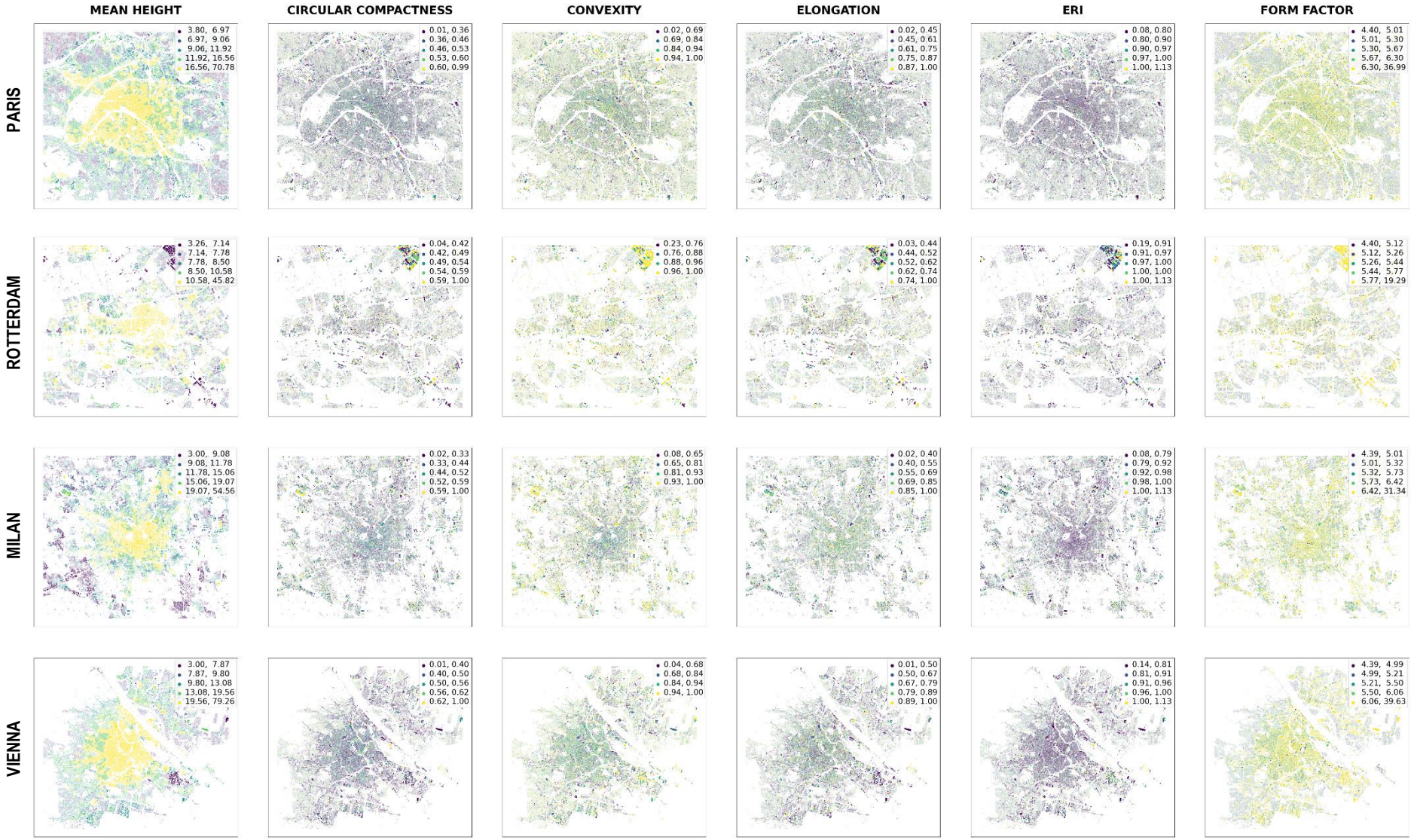

Figure 5.8 Different UMMs computed for Paris, Rotterdam, Milan, and Vienna (Part 2)

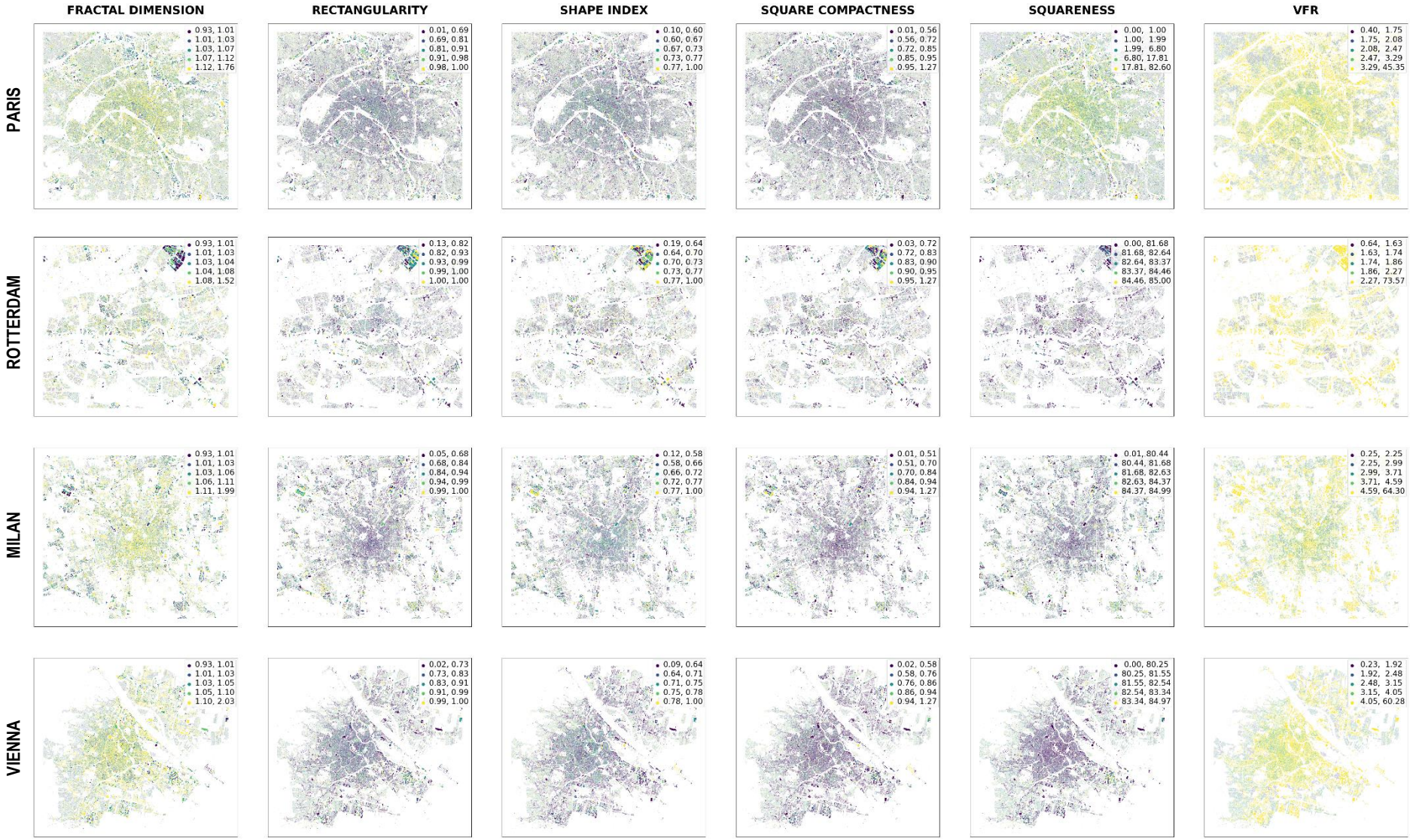

Figure 5.9 Different UMMs computed for Paris, Rotterdam, Milan, and Vienna (Part 3)

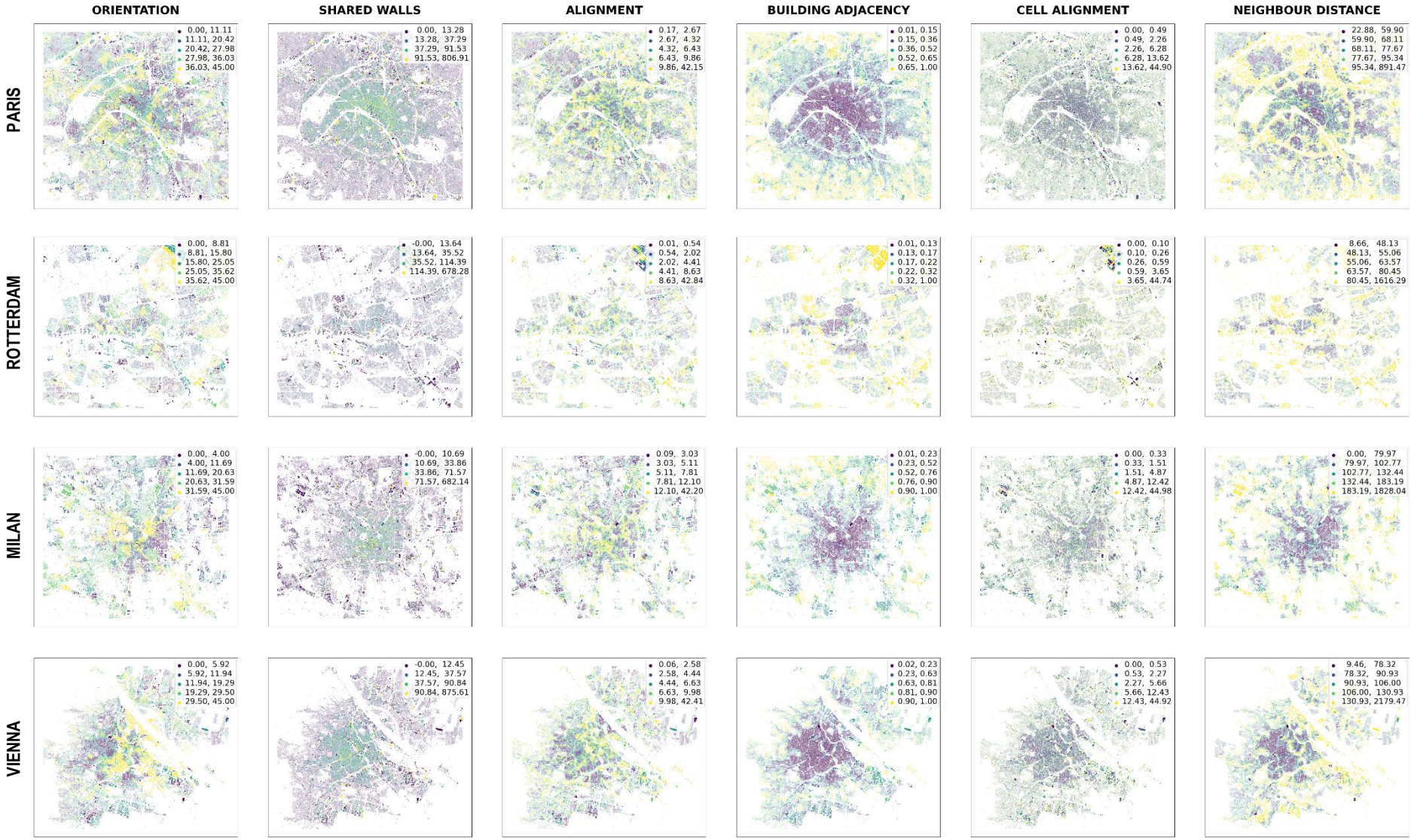

Figure 5.10 Different UMM computed for Paris, Rotterdam, Milan, and Vienna (Part 4)

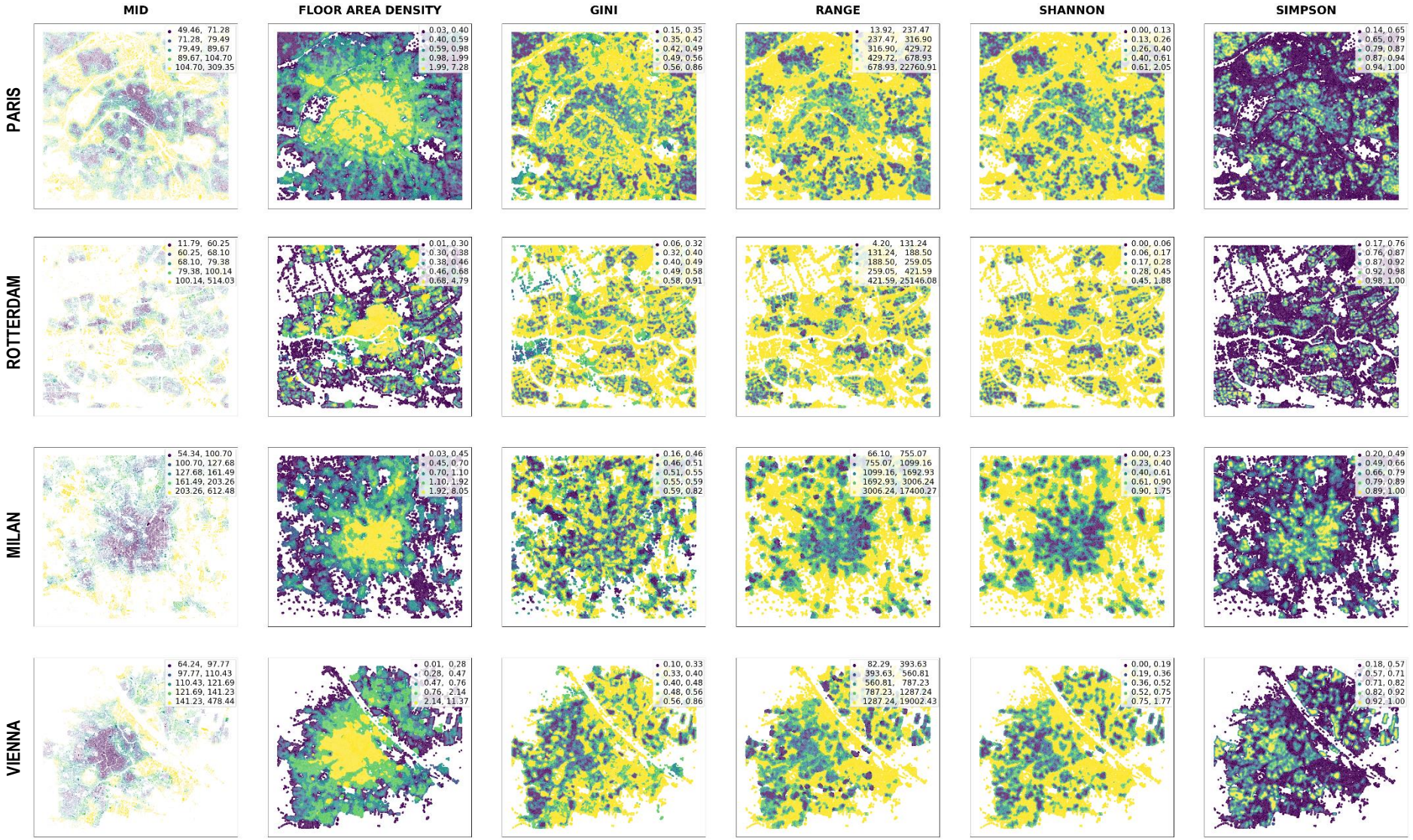

Figure 5.11 Different UMM computed for Paris, Rotterdam, Milan, and Vienna (Part 5)

In context of Orientation (Figure 5.10, column one), hotspots are mostly evident in areas shaded in dark blue (~8-16°), with some regions displaying purple hues (~0-8°). Additionally, both hot and coldspots can be found in areas characterized by light blue and green colour with values ranging from ~15 to 25°. In MID (Figure 5.11, column one), coldspots predominantly emerge in regions where MID is represented in yellow (above ~100 meters). On the other hand, hotspots can be identified across a range of colours spanning from purple (lowest MID) to blue to green hues, and occasionally in specific regions marked by yellow shading.

In Milan, Orientation (Figure 5.10, column one) shows hotspots primarily coinciding with regions shaded in purple (~0-4°). These areas are particularly concentrated in the extreme eastern and southwestern parts of the city. Certain hotspots are also observed in the light green (~20-31°) coloured region, especially prominent in the northwest and in yellow (~31-45°), in the southwest. In the case of Building Adjacency (Figure 5.10, column four), coldspots are predominantly located within the yellow and light green regions, which correspond to higher values. Conversely, as the values transition from high to low, represented by shades of light blue, dark blue, and purple, these areas essentially correspond to the hotspots. Vienna also exhibits similar patterns with Building Adjacency, where the coldspots are also primarily situated within the yellow and light green regions, often found on the outskirts of the city. In Alignment (Figure 5.10, column three), areas shaded in purple, indicating the lowest alignment, coincide with the hotspots, with two major concentrations in the south of the city. Additionally, hotspots are also observed in certain regions shaded in blue and green hues (~2-7°), particularly in the central areas of the city.

5.3 Relation between LST and UM

This section addresses Objective 3 of this research and is structured into three subsections. Subsection 5.3.1 presents the results obtained from the RFR model for all the cities, detailing its performance metrics and model evaluations. Subsection 5.3.2 shows the results of the feature importance analysis, identifying the key contributors of LST variations in each city. Lastly, Subsection 5.3.3 presents the outcomes of the sensitivity analysis, elaborating on the nature and direction of the influence of UMMs on LST.

5.3.1 RFR Model performance

As mentioned in Section 4.4, the RFR model considered twenty-four UMMs (mentioned in Table 4.2 excluding the metrics with MTs as the urban unit) as the independent variables and the processed mean LST image (shown in Figure 5.2) as the target variable for each city. As outlined in the methodology, the datasets after splitting into training and testing sets varied for each city, which have been summarized in Table 5.2.

Table 5.2 Distribution of training and testing samples for the RFR model for Paris, Rotterdam, Milan, and Vienna

CITY	TOTAL SAMPLES	TRAINING SET	TESTING SET
Paris	737,597	590,077	147,520
Rotterdam	446,275	357,020	89,255
Milan	249,032	199,225	49,807
Vienna	283,973	227,178	56,795

Table 5.3 shows the performance metrics of the RFR model applied to Paris, Rotterdam, Milan, and Vienna. For each city, the table outlines the hyperparameter values (m_{try} and n_{tree}), and their corresponding performance metrics of the trained (mean of squared variables and percentage of variables explained) and tested model (RSME, MAE, R^2).

The model demonstrated similar performances for different number of trees across each city as shown in Table 5.3. Moreover, the feature importance remained relatively stable across various tree numbers which have been discussed in detailed in Section 5.3.2. In case of Paris, the model yielded the best results with 300 trees where 80.04% of the variability in LST can be explained by the UMMs. It also achieved the highest R^2 of 0.812, lowest RMSE and MAE values of 0.659 and 0.418, respectively on the testing set. For Rotterdam, the best results were once again achieved using 300 trees with 89.48% variability explained in the LST. The RMSE, MAE and R^2 values were 0.610, 0.389, 0.902, respectively. For Milan and Vienna, the most accurate results were achieved with 100 trees, where the model was able to account for 85.06% and 87.87% of the variation in the LST, respectively. They also had high R^2 values of 0.865 and 0.899, respectively, indicating a good model fit of the data.

Table 5.3 Performance metrics of the RFR model for Paris, Rotterdam, Milan, and Vienna (best performance highlighted in green color)

CITY	Hyperparameters		Training Performance		Testing Performance		
	ntree	mtry	Mean of squared residuals	% Var explained	RMSE	MAE	R^2
Paris	100	8	0.4522794	79.35	0.6649854	0.4225103	0.8083977
	200	8	0.4409825	79.86	0.6609585	0.4198395	0.8113810
	300	8	0.4371835	80.04	0.6594360	0.4185121	0.8124834
Rotterdam	100	8	0.3904680	89.10	0.6137751	0.3922143	0.9006409
	200	8	0.7500006	88.17	0.8545865	0.5341727	0.8904171
	300	8	0.3766988	89.48	0.6102121	0.3893371	0.9020464
Milan	100	8	0.3422951	85.06	0.5753788	0.3732098	0.8656429
	200	8	0.4368008	81.72	0.6040958	0.3759762	0.8490204
	300	8	0.4316374	81.94	0.6013489	0.3749244	0.8507018
Vienna	100	8	0.7687621	87.87	0.8561070	0.5355361	0.8998065
	200	8	0.7512704	88.15	0.8541133	0.5338468	0.8904862
	300	8	0.7415837	88.30	0.8517708	0.5321406	0.8912356

Overall, the RFR models effectively captured the underlying patterns and relationships between the UMMs and LST with more than 80% variability explained across all the cities and also generalized well on the unseen dataset. Among all the cities, Rotterdam and Vienna exhibited the best performance.

5.3.2 Relative importance of UMMs on LST

The relative importance (RI) of the UMMs on LST for each city has been shown in Figure 5.12. Among the top ten UMMs, six UMMs consistently emerged across all cities. These UMMs include Alignment, Orientation, Mean Height, MID, Building Adjacency, Neighbour Distance. Alignment refers to the mean deviation of solar orientation of objects on the neighbouring cells from a reference building. Orientation can be defined as the angle of the longest axis of a building's bounding rectangle relative to the cardinal directions, ranging from 0 to 45°. This angle represents the deviation of the building's orientation from the perfect alignment with cardinal directions (North-South or East-West). Mean Height, as the name suggests, is the average height of buildings within 100 meters of its neighbours. MID is the mean interbuilding distance between buildings on neighbouring cells. Building Adjacency reflects the extent to which buildings join together into larger structures. Lastly, Neighbour Distance is the mean distance from its adjacent buildings.

The above mentioned UMMs have the maximum role in influencing the LSTs in these cities, which enhanced the overall predictive power of the RFR model. This observation aligns with the findings from the visual analysis of the UMMs and distribution of hotspots detailed in Section 4.2.

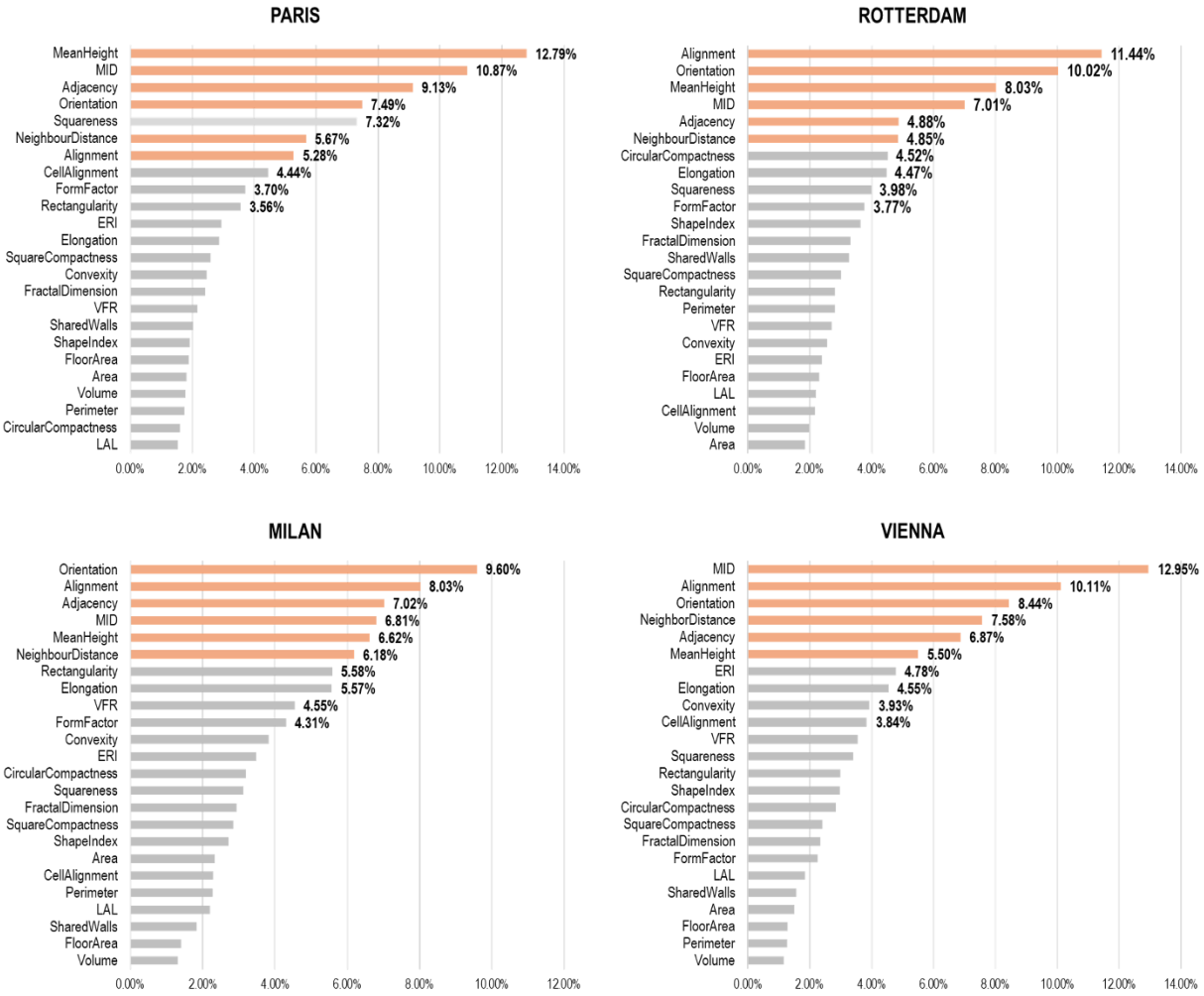

Figure 5.12 Relative importance of UMMs in influencing the LST in Paris, Rotterdam, Milan, and Vienna revealed by the RFR model (common UMMs in all cities under top ten in brown colour)

Additionally, Squareness emerged as a noteworthy UMM in Paris, securing the fifth position in importance rankings. Interestingly, it stood out as the only distinctive UMM among the top six important features in Paris, distinguishing it from the UMM rankings of other cities.

Although, the UMMs mentioned above were common across all the cities, there was a difference in their importance ranking. The five most important UMMs contributing to the maximum change in the LST for Paris were Mean Height (RI=12.79%), followed by MID (10.87%), Building Adjacency (9.13%), Orientation (7.49%) and Squareness (7.32%). For Rotterdam, Alignment, Orientation, Mean Height, MID, and Building Adjacency had the highest influence on LST with RI of 11.44%, 10.02%, 8.03%, 7.01%, and 4.88%, respectively. In case of Milan, Orientation (9.60%), followed by Alignment (8.03%), Building Adjacency (7.02%), MID (6.81%), and Mean Height (6.62%) had the greatest influence on LST. Lastly, for Vienna, MID (12.95%), Alignment (10.11%), Orientation (8.44%), Neighbour Distance (7.58%), and Building Adjacency (6.87%) were the most important UMMs for explaining the variability in LST. A more detailed analysis of how the LST of each city varies with these UMMs is discussed in Section 5.3.3. It

should be noted that these UMMs among other metrics also contributed the most in improving the purity of nodes in the decision trees.

Apart from this, Elongation was common in Rotterdam (4.47%), Milan (5.57%), and Vienna (4.55%) coming in the eight positions in the ranking for all three cities. Similarly, Form Factor was common among Paris (3.70%), Rotterdam (3.77%), and Milan (4.31%), coming on the ninth position for Paris and tenth position for the other two cities. Although their rankings are slightly lower, they also have some amount of influence on LST.

Conversely, UMMs like Area, Perimeter, Volume, Long Axis Length (LAL) and Floor Area had the least effect on LST variations across all cities as compared to the other UMMs with less than 3% of RI.

5.3.3 Sensitivity analysis

The intricate relationships between the important UMMs and LST were revealed by using the PDPs based on the RFR results for each city. PDP offered insights into the variation of LST along with the UMMs, where the curves in Figure 5.13 (showing six common UMMs) and Figure 5.14 (showing distinct UMMs) represents the mean marginal effect. The subsequent sections will initially delve into the shared findings across the cities derived from Figure 5.13, followed by a discussion of the distinct outcomes depicted in Figure 5.14.

For Paris, the most important UMM contributing to the variations in LST was the Mean Height. It can be observed from Figure 5.13 that the direction of change in Mean Height in relation to LST is negative. This implies as the building height increases the LST rapidly decreases, following an almost linear pattern. This persists until the height reaches approximately ~20 meters, beyond which LST stabilizes at lower temperatures, exhibiting minimal variation. As the second important UMM, the effect of MID on LST was non-linear. The results revealed that LST experiences a rapid decrease until MID reaches ~100 meters. Subsequently, there are further declines in LST from ~170 to 200 meters, with spikes observed at ~120 and 150 meters. Following this, LST exhibits a positive pattern until ~250 meters, after which it remains relatively constant for the remaining range of MID values. The relation of LST with the next important UMM, Building Adjacency, predominantly exhibited a negative direction, beginning from ~0.25 and remaining relatively stable. This consistent negative association suggests that as Building Adjacency increases, LST tends to decrease, indicating a potential cooling effect on the environment. The fourth significant variable, Orientation, demonstrated an increasing effect on LST with an almost linear pattern, albeit with a slight dip observed at ~40°. This finding suggests that as the orientation angle of the building increases, LST tends to rise consistently, indicating a positive correlation between orientation and surface temperature. This pattern is further corroborated by the visual interpretation done in Section 5.2 for Paris.

In Rotterdam, the most crucial UMM was Alignment, characterized by a stable and almost linear negative pattern from ~2° to 27°. Beyond this range, the relationship between Alignment and LST remained relatively unchanged despite increasing values. Orientation emerged as the second most important UMM, characterized by several fluctuations but with an overall negative pattern. This suggests that as the orientation of the buildings varies, LST tends to decrease, with a notable peak observed at ~35°. This observation was also verified by the visual interpretation done in Section 5.2 for Rotterdam. The pattern for Mean Height, the third most important UMM, grows positively from 0 till ~15 meters. Beyond this point, the LST begins to decrease till ~25 meters, eventually flattening out. This suggests that taller buildings may contribute to higher temperatures only up to a certain point. The next significant UMM influencing LST was MID. The analysis revealed a stable negative relation between MID and LST. LST exhibited a gradual and steady decrease with the increase in MID until ~300 meters. Beyond this

threshold, LST remained relatively constant. This pattern suggests that as the distance between the buildings increases, surface temperatures tend to decrease consistently.

For the city of Milan, the most significant UMM influencing LST was Orientation, which exhibited a partial U-shaped pattern. The centre of the dip in the U-shape was observed at ~20°. Following this, the right side of the U-shaped curve showed a slight increase before sharply dropping from ~30° till ~40°. The subsequent UMM in line, Alignment, exhibited a relatively complex relationship with LST. The graphs revealed a notable dip in temperature around 2-3°, resulting in a sharp decrease from the highest temperature to 0 °C. While this anomaly may seem unusual, it can be considered negligible or disregarded in the overall pattern. Following this, it started stabilizing after an alignment of ~5° and displayed a negative pattern until ~20°. Beyond this point, the relation remained relatively unchanged. This suggests that within the observed range, deviations between the buildings from the optimal alignment angle are associated with lower surface temperatures, indicating a cooling effect. The next significant UMM, Building Adjacency, exhibited a monotonic negative effect on LST in Milan. The relation indicates that as building adjacency values increase, temperatures tend to decrease. MID was the next important UMM influencing the LST in this city. The pattern observed in the relationship between MID and LST starts with a slight decrease in slope, followed by a sharp increase until ~200 meters. Beyond this threshold, LST gradually decreases with the increase in MID, albeit with a few peaks in between.

For Vienna, the most crucial UMM was MID, which displayed a relatively non-linear pattern. The results reveal a deep and narrow dip between 100 and 300 meters, indicating a significant fluctuation in LST within this range of interbuilding distances. The pattern for Alignment, the second most important UMM, exhibited a smooth monotonic negative relation with LST. This pattern was also observed in the visual interpretation in Section 5.2. Next important UMM was Orientation, characterized by a complex relationship resembling an inverted U-shape. Initially, the pattern exhibited a positive association between orientation and LST. However, beyond a certain threshold, from ~20 to ~45°, this relationship abruptly changes to negative, resulting in a substantial drop in the temperature. The fourth important UMM, Neighbour Distance, exhibited a negative relation with LST. The LST decreases sharply as the distance increases up to approximately 750 meters, beyond which the pattern stabilizes.

In summary, while commonalities existed in the patterns and relationships between UMMs and LST across Paris, Rotterdam, Milan, and Vienna, variations were also apparent. From Figure 5.13, it is evident that LST exhibited a positive correlation with Mean Height across all cities except Paris. It has a fluctuating ascent pattern: when the height of the buildings is below a certain threshold—15 meters for Rotterdam and 20 meters for both Milan and Vienna—the LST tends to be higher. As the height of the buildings starts increasing from that threshold, those areas become cooler, showing a negative relationship with LST. This pattern is particularly evident in the cases of Rotterdam and Milan, while Vienna exhibits comparatively a weaker negative relation. Moreover, beyond the threshold, the height has no influence on the LST in Rotterdam and Vienna, while it increases slightly and then remains constant for Milan. There is an initial positive pattern in the relationship between MID and LST across Paris, Milan, and Vienna and afterwards, a notable dip at around 200 meters. Once the MID reaches a certain threshold (which varies for each city), the LST stabilizes indicating a diminishing effect of MID on temperature at larger scales. The results also reveals a generally negative relationship between Orientation and LST, with some positive patterns observed in the middle (~20 to 35°) for both Milan and Rotterdam. However, the pattern was entirely opposite in Paris. Both Building Adjacency and Neighbour Distance demonstrates non-linear cooling effects on the urban environment across all cities.

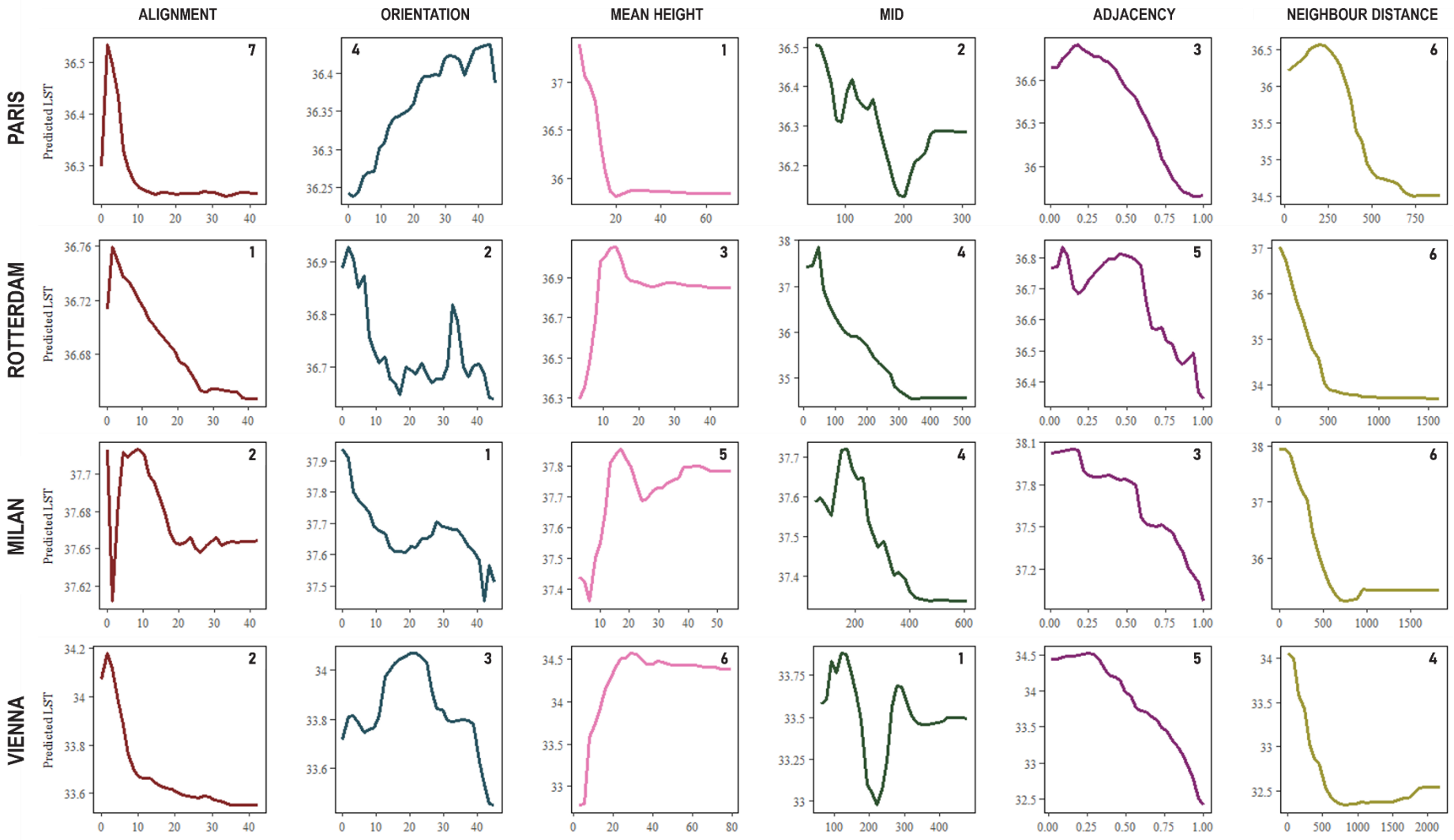

Figure 5.13 Partial dependence plots of the important UMMs under top ten that were common across Paris, Rotterdam, Milan, and Vienna with their corresponding rank of RI

Figure 5.14 shows the pattern and direction of the distinct UMMs for each city which were coming under top ten important UMMs. It is noteworthy that Squareness, which ranked fifth in importance for Paris, exhibited a monotonic negative pattern with LST, indicating a cooling effect on the urban environment. Additionally, Rectangularity contributed to LST variations in both Paris and Milan, displaying a positive pattern. Cell Alignment was a common UMM observed in Paris and Vienna, characterized by a negative and an almost linear relation. Convexity and Equivalent Rectangular Index (ERI) had a positive influence on LST in Vienna.

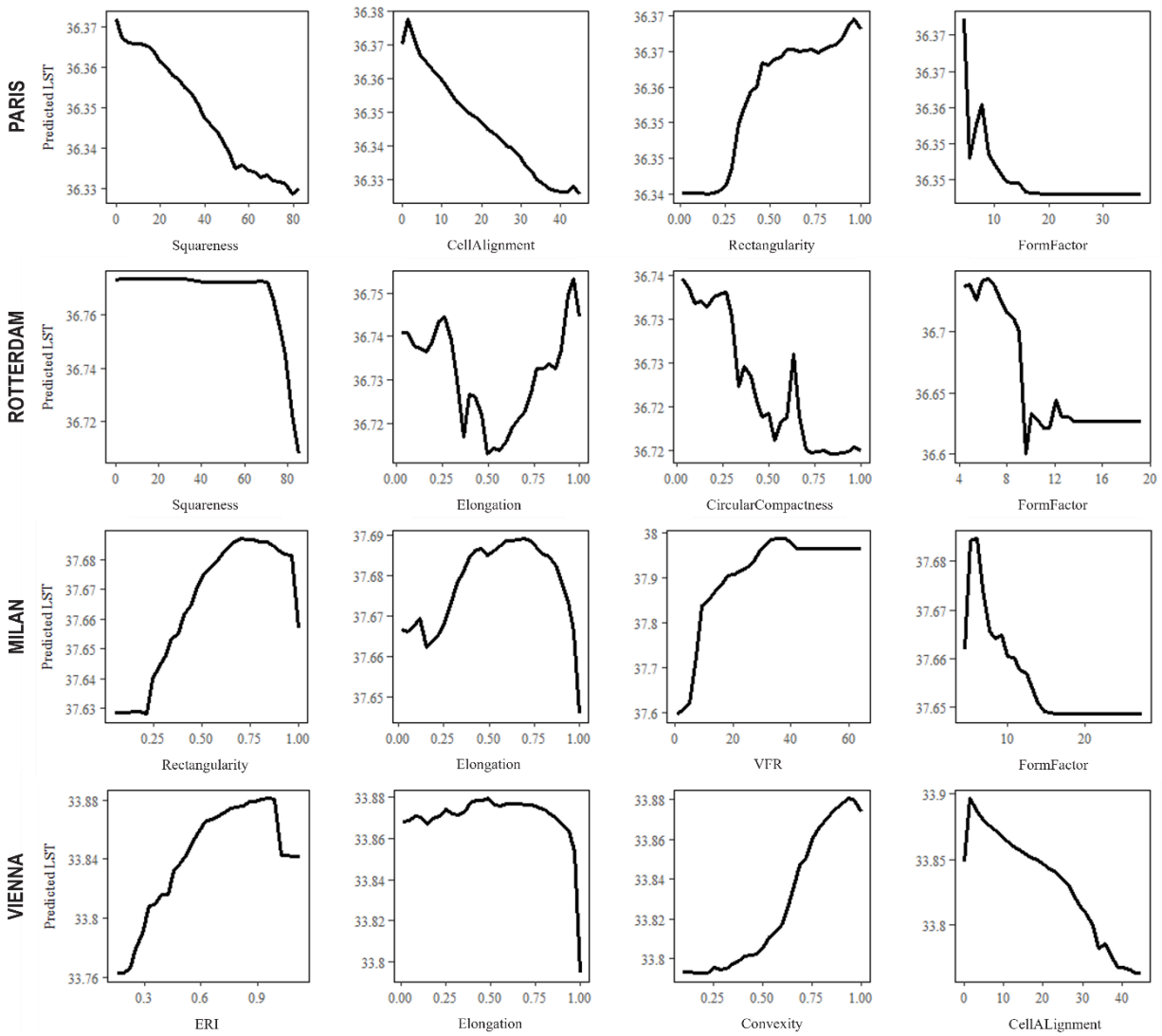

Figure 5.14 Partial dependence plots of the important but distinct UMMs under top ten RI

5.4 Expert validation

This research included in-depth semi-structured interviews with three city experts on urban planning, each from Rotterdam, Milan and Vienna. They provided valuable insights into these findings regarding the potential reasons underlying these patterns and the heat dynamics across these cities. According to them, the diverse range of building metrics employed in this study is both heuristic and highly relevant within this field of research.

The experts from Rotterdam and Vienna noted that some UMMs, such as Orientation, may not directly impact LST and could be influenced by factors such as reflective building materials or the slope of the roofs. They also cautioned that the patterns seen in the PDPs may not fully represent their actual impact unless the original data points are plotted. This is because PDPs illustrate the effect of a particular variable on the outcome while averaging out the effects of other variables.

The expert from Milan explained the contrasting relationship between Mean Height and LSTs in Rotterdam and Milan, where mid-rise buildings have a cooling effect on the environment, by drawing upon the historical backdrop of these cities. She highlighted that, European cities, including those analysed in this study, often have deeply ingrained and historically significant planning regimes. For instance, figures like Georges-Eugène Haussmann, known for transforming Paris with wide boulevards, significantly shaped the city's urban fabric. Many buildings constructed during his time still remain today. However, the design and construction materials from that era may not be able to withstand today's extreme temperatures. Both Rotterdam and Milan were heavily bombed during the Second World War, leading to extensive rebuilding efforts. As a result, the modern urban landscape of Rotterdam, in particular is characterized by taller buildings compared to other Dutch cities, which generally have lower building heights. This extensive reconstruction has influenced the urban heat dynamics, contributing to the observed patterns in LST. She emphasized on the importance of balancing historical preservation with the integration of sustainable urban principles, particularly when retrofitting older buildings for energy efficiency.

Additionally, she confirmed the hotspot analysis and supported the observation that industrial areas on the periphery of Milan, especially near the ring road are mostly hotspots. This can be attributed to high heat emissions from manufacturing processes and energy consumption, lack of vegetation, and heat-retaining materials like metal and concrete. The proximity to the ring road exacerbates this by contributing additional heat through heavy traffic and vehicle emissions, with asphalt absorbing and slowly releasing heat.

In addressing the implications for urban heat mitigation, she highlighted the need to recognize that each city faces unique challenges and requires tailored strategies that must be carefully balanced by local governments. The integration of innovative projects, such as rooftop initiatives of Milan and Rotterdam, highlights the potential to reshape urban environments while enhancing resilience to urban heat.

6 Discussion

This thesis aimed to analyse the effects of UM on LST using UMMs and ML techniques, focusing on four European cities—Paris, Rotterdam, Milan, and Vienna. This chapter discusses the results presented in Chapter 5), providing an in-depth examination of the findings in relation to existing literature and insights from expert interviews. The discussion is organized into three sections. Section 6.1 ('Reflection on influence of UM on LST') explores how UMMs influence LST and discusses the potential reasons for these effects. Section 6.2 ('Implications for urban heat mitigation') explores the implications of this study for mitigating urban heat in European cities. Finally, Section 6.3 ('Limitations') outlines the existing limitations of this study.

6.1 Reflection on influence of UM on LST

It has already been well established by several studies that building morphology is one of the most important factors in determining LST (He et al., 2023; Huang & Wang, 2019; Puche et al., 2023; Wang et al., 2022). Building on this foundation, the present study revealed that building UMMs play an important role in influencing LSTs across the four cities. After employing the RFR model, it was observed that the relative impact of UMMs on the LST varied significantly. Accordingly, the key UMMs influencing the variation in LST among cities were identified.

In Paris, a significant inverse statistical relationship between Mean Height and LST has been found, which is consistent with previous studies by Puche et al. (2023), Cilek & Cilek (2021) and Zhu et al. (2023). These studies demonstrated that an increase in building height can reduce LST. Theoretically, high rise buildings can cast larger shadows than low-rise buildings, which reduces the amount of solar radiation that reaches the ground and, consequently, lowers the surface temperatures (Li et al., 2011). Huang & Wang (2019) pointed out that taller buildings can also improve surface roughness that can lead to the creation of mechanical turbulence, which in turn enhances convective heat dissipation. In contrast, the relationship between Mean Height and LSTs in the other cities is found to be opposite to that of Paris, but with mid-rise buildings still having a cooling effect on the urban environment. Similar patterns have been reported by Hu et al. (2020) and Li et al. (2021) where the positive influence of building height on LST reached its peak at a height of 10-15 meters before gradually declining.

One of the underlying reasons explained by the Milan expert is the post-war histories of these cities. Both cities underwent extensive rebuilding after World War II, resulting in Rotterdam having taller buildings compared to other Dutch cities. Regional characteristics, such as proximity to water bodies or higher elevations, also play a significant role in shaping local climates. Research by Robitu et al. (2004) indicates that the cooling effect of water bodies can extend up to 30 meters from their banks. For Rotterdam, a city receiving water from two sources, the Maas River and the Rhine River, water has a significant influence on the temperature. According to Heusinkveld et al. (2014), the temperature variation of these rivers is less

than 2 °C even on hot days, which helps maintain a stable and cooler microclimate during the daytime in their vicinity. This impact is amplified because of the predominant southwest winds (Janssen, 2011). Moreover, in the north and southeast of Rotterdam, there are many florist shops and greenhouses, which emerged as coldspots in this study, that can positively influence airflow. The presence of large water bodies is a common feature in many Dutch cities, and it effectively reduces the daily maximum temperatures. Similarly, in Vienna, the Danube River plays a crucial role in moderating the local climate. The cooling influence of the Danube is evident in one of the major coldspots highlighted in this study, much like the effect seen in Rotterdam. The presence of hilly terrain near urban areas significantly alters airflow dynamics and can enhance the ventilation efficiency by two to three times within urban canyons—narrow street configurations flanked by tall buildings—compared to flat urban terrain (Sun et al., 2012). Therefore, the proximity of the Vienna Woods, a hilly region southwest of the city, to the other coldspots (mostly observed on the periphery of the city in the same direction), could also influence local wind patterns and temperature regulation.

The initial positive relation observed between MID and LST across Paris, Milan and Vienna may be attributed to heat accumulation. Previous research has shown that dense clusters of high buildings can elevate LST due to restricted air circulation, a phenomenon known as the 'canyon effect' (Kim et al., 2022). This effect is closely associated with UM factors such as building height and spacing among them (Guo et al., 2016). It is formed by high buildings along narrow streets, which tend to slow down air flow, weaken energy transfer, and cause more heat to accumulate on the surfaces, leading to a rise in LST (Wu et al., 2022). However, the relationship between MID and LST has a sudden dip after a certain distance. Studies like Wu et al. (2022) and Yuan & Chen (2011) have suggested that increasing the space between buildings may improve the efficiency of ventilation and rate of energy exchange and effectively reduce LST. But this cooling effect again starts to diminish after a certain point as the distance is further increased (You et al., 2017), which is also noted in the findings of this study.

Another interesting finding is that the correlation patterns between Orientation and LST varied among the cities, with Rotterdam and Milan displaying a negative pattern, contrasting with the positive pattern observed in Paris. The orientation of a building plays a crucial role in determining how much solar radiation it can receive (Habibi, 2023). Despite an extensive review of the existing literature, no studies were found that explicitly talks about the relationship between the orientation of buildings and LST. Theoretically, a building that is oriented perfectly towards the cardinal directions (0° or closer) will have less heat-absorbing surface area compared to a building that is oriented at an angle (45° or closer) from the cardinal directions. This principle helps explain the observed pattern in Paris, where buildings oriented closer to cardinal directions tend to exhibit lower LSTs.

As suggested by the expert from Rotterdam and Vienna, differences in Orientation patterns among cities can be attributed to factors such as the use of reflective building materials and types of roofs. Research suggests that roofs can contribute 70% of the building's heat gain (National Disaster Management Authority, 2021), with flat roofs particularly prone to absorbing heat easily due to their continuous exposure to sunlight throughout the day (Robyn, 2020). Steep-sloped roofs can reflect sunlight better than flat or low-sloped roofs. Moreover, a suitable orientation can facilitate sufficient wind speed and airflow to achieve successful and comfortable ventilation (Du, 2019). Givoni (1994) proposed that oblique winds, which approach the wall at angles between 30 and 120°, can accomplish cross ventilation if both the windward and leeward walls have openings.

The above factors are also closely linked to the unique architectural and historical integrity of these cities, which was highlighted by the expert from Milan, who gave the example of the Haussman's renovation of

Paris. Approximately 80% of its buildings were constructed before 1945. Many of these buildings (totaling around 110,000 properties) are characterized by zinc roofs (dark materials) and limestone façades, chosen for their affordability and durability during their time. In today's date, they contribute to increasing temperatures reaching upto 80 °C by absorbing heat from the sun (Willsher, 2023). These buildings feature inefficient heating and cooling systems, which collectively account for up to 15% of Paris' greenhouse gas emissions (AFP News, 2019). Similarly, around 20% of Vienna's building stock dates back to the Gründerzeit era, predominantly from the 1850s. These old buildings are still located in the city's historic centre and are now mostly privately owned residential properties (Mukati, 2021). The findings of this study revealed that a large portion of the residential area in the centre, coinciding with these historic areas, has emerged as a significant hotspot. According to the literature, these buildings require higher cooling demands due to their age and lower insulation levels, compared to more modern constructions from the 1960s to 1980s (Mukati, 2021). However, the occurrence of hotspot might also be due to the absence of green spaces in these central areas. In Rotterdam, the city centre and the pre-war districts in the west and south also experience significantly high temperatures (Hoeven & Wandl, 2015). In addition, this study confirmed that industries and port areas are the main hotspots, which were moved to new industrial zones on the outskirts of the city after the war (Thissen, 2013). Rotterdam's postwar reconstruction also led to 200 million square feet of flat rooftops which is capable of absorbing more heat (Rotterdamse Dakendagen, 2020). The industrial areas in Milan, were once connected by the famous Navigli canal network for transportation purposes. This is the reason why, most of the hotspots are located on the periphery of the city. After the war, the city's economic revival led to new buildings and industries (Tyson, 2021). Increased road transportation led to significant canal pollution, because of which the canal was covered up and replaced by a ring road.

Examining the contrasting Orientation-LST patterns of Rotterdam and Milan suggests they might already have some existing strategies encompassing urban planning regulations, architectural design principles, and material choices aimed at enhancing thermal comfort and alleviating high temperatures within the city. Despite Rotterdam having a large number of buildings with flat roofs, they have made efforts to utilize this area with innovative solutions. Many buildings have constructed cool roofs and façades, which can significantly decrease the surface temeratures. The city also has a Rethinking Rooftops movement, where Rooftop Days festival is organized by the government every year. This event highlights the potential of rooftops in addressing various urban challenges, including the reduction of urban heat (Rotterdamse Dakendagen, 2020). Similarly, Milan has an ongoing program to explore green roofs and innovative Nature-based Solutions (NbS) in its southern district, aiming to eventually implement these strategies throughout the entire city.

Building Adjacency shows an overall negative pattern across all cities with respect to LST. While there are not many studies specifically addressing this aspect, a possible explanation lies in the characteristics of adjacent buildings. Buildings that are joined together would have fewer exposed walls per unit area compared to standalone buildings. Consequently, these surfaces would absorb significantly less solar heat. Additionally, adjoined buildings would have limited exposure or interaction with external hot air from their surroundings. Hence, they may not experience as much convective heat transfer from the surrounding environment, which could contribute to lower LST compared to standalone buildings. Furthermore, adjacent buildings can shade each other, reducing direct sunlight exposure on the walls and roofs, further decreasing heat absorption.

Another crucial point to consider is the varying contributions of UMMs to LST variation at the building level. The present study indicates that the twenty-four UMMs can statistically explain more than 80% of the variation in LST across all cities using the RFR model. This level of explanatory power is noteworthy,

as it aligns closely with the results of some previous studies, such as those by Han (2023) and Yin et al. (2022). These studies have reported similarly high levels of explained variance, indicating a robust relationship between UM and LST. It is even higher than several studies (Li et al., 2021; Yao et al., 2022). These differences may be attributed to the type and number of UM factors considered for the modelling or the analytical methods these studies have employed. Although, the result of the statistical model shows that the considered UMMs explain much of the LST variation, this does not imply a direct causal relationship, as also suggested by the city experts. For instance, proximity to water bodies or the use of different building materials (among many others), which significantly influence the heat, may confound this relationship. Some UMMs might be correlated with the presence of a water body or the use of building materials that impact LST. Thus, the influence of UMMs on LST might partly be due to their association with wind speed and surface materials.

6.2 Implications for urban heat mitigation

European cities are increasingly at risk from the rising temperatures caused by global warming, which is significantly altering their local climates and heat patterns. Urban areas, expected to accommodate nearly 70% of the global population by 2050, will face twice the amount of heat stress compared to rural areas (Hayward et al., 2023). Given the associated risks such as heat stress, health problems, economic instability, and damage to infrastructure, there is an urgent need for European cities to adapt to climate change to safeguard themselves and their residents from its unavoidable impacts (Matt Rees, 2020). With buildings being one of the major contributors to climate change within these urban environments, it is essential to focus on making them a central part of the solution (IPCC, 2023). The results from this study have profound implications for mitigating urban heat in European cities. Despite numerous studies analysing UM factors at various scales (Hu et al., 2022; Huang & Wang, 2019; Cilek & Cilek, 2021; Yang et al., 2021; Zhu et al., 2023), obtaining a quantitative understanding at the building level remains challenging because of availability of suitable building data. This study emphasizes the importance of understanding these factors at the building level to aid urban planners, architects, and other concerned actors in improving urban thermal environment in European cities.

The most influential UMMs from this study were found to be Mean Height, Orientation, Alignment, Building Adjacency and MID. By strategically managing these factors, urban planners and policymakers can effectively mitigate urban heat, thereby creating more comfortable and sustainable city environments. The study outlines several implications for improving thermal comfort in existing as well as new urban developments across European cities, based on observed LST patterns and the varying impact of UMMs on LST.

Many of the older buildings in these cities, as discussed in the previous section, suffer from poor insulation, unsuitable locations, and a heavy dependence on air-conditioning, rendering them unfit for the extreme climate conditions of the 21st century (Goodell, 2023). Additionally, their outdated designs, absence of modern energy efficiency standards, insufficient thermal insulation, and poor ventilation result in higher energy usage, often derived from non-renewable sources, increases greenhouse gas emissions. To address these issues, it is essential to renovate and update historic and cultural heritage buildings, to improve their energy efficiency and enhance the thermal comfort of people. In addition, this study also acknowledges that implementing cooling measures can be challenging in densely populated areas, due to limited space availability. Alternative approaches can be adopted to make efficient utilization of available space.

Looking at the existing situation in Paris, adding insulation under the zinc roofs can be expensive. A more feasible solution could be painting the roofs white. The albedo or reflectivity of the buildings can significantly increase by using light coloured materials, thereby reducing the heat gain (Pal et al., 2020). The city should also promote rooftop strategies similar to those implemented in Rotterdam and Milan. Vertical greening strategies, such as green roofs, green walls, and street parks, can effectively enhance the urban ecological environment and lower surface temperatures in high-density areas (Zhang et al., 2022). Green walls with evergreen plants have the potential to lower daytime temperatures by as much as 9 °C on hot days (Vox et al., 2018). Given the constraints on reducing impervious surfaces in these urban settings, these vertical and rooftop greening methods can play a crucial role in mitigating high surface temperatures.

Additionally, designing buildings with sloped roofs at optimal angles to minimize solar exposure, along with incorporating shading devices like awnings and pergolas, is another solution to mitigate solar gain. A steep-sloped roof offers natural advantages in terms of insulation and ventilation, whereas a flat roof may necessitate extra insulation measures to uphold energy efficiency standards (Irwan et al., 2010). The substitution of flat roofs with sloped alternatives can yield a notable 6% reduction in the total annual energy consumption of buildings (Peng et al., 2017). High-density cities like Paris should consider adopting these strategies to reduce heat storage. These measures will not only help in lowering the LST in urban areas but also improve overall thermal comfort for their residents.

The above implications are specific to existing buildings. Addressing design implications for new urban developments, the findings of this study indicate that mid-rise buildings between 15 to 25 meters tend to reduce LST, suggesting that buildings within this range can promote cooling effects. However, these conclusions hold true only if the observed patterns are reliable. Traditional strategies have often relied on linear relationships between the UM factors and the surface temperatures (Zhang et al., 2020), like reducing the SVF by 0.2 can lower the average daytime temperatures by approximately 0.3 °C (Yang et al., 2011). Recent research, including this study, suggests that different building morphologies are interconnected and collectively impact the thermal environment (S. Du et al., 2022). Thus, it is essential to carefully balance the ideal height of the building with adequate inter-building distance to avoid creating urban canyons, which can trap heat. According to Cheung & Liu, (2011), increasing the distance between buildings (to approximately three times the width of a building) significantly enhances the ventilation rates. Moreover, ensuring greater distances between buildings can also help increase shadow coverage, especially for high-rise buildings, further contributing to lower LST and enhanced thermal comfort.

The RFR modelling in this study demonstrates strong generalization capabilities. This study has been conducted in four European cities, all showing a high percentage of variables explained. This consistency suggests that the model can be effectively applied to other European cities, which often share similar urban patterns and characteristics. Therefore, the model appears to have broader applicability across different European urban contexts, potentially serving as a useful tool for urban planners and policymakers in addressing LST variation and mitigating urban heat island effects.

Moreover, the findings of this study suggest that a grid measuring 70 meters by 70 meters could be an optimal scale for assessing the impact of building morphology on LST variations, particularly when compared to other studies that achieved their highest accuracy with larger grid resolutions. While other research found optimal scales ranging from 210 meters by 210 meters to 240 meters by 240 meters (Estoque et al., 2017), and even up to 600 meters (Han, 2023), these larger scales may miss finer variations in building morphology and LST. This scale of 70 meters by 70 meters proved effective as it balanced both detail and computational efficiency and allowed for a comprehensive analysis of UMMs without overwhelming data processing resources.

Lastly, the study also highlights the efficacy of the momepy toolkit in conducting detailed analysis of building morphology and exploring the relationships between UM and thermal dynamics. Notably, momepy exhibits versatility in handling complex spatial data, offering a spectrum of functionalities for processing and analyzing building datasets. These functionalities include data cleaning, generation of MTs, and computation of a comprehensive range of UMMs. Thus, momepy emerges as a reliable instrument for computing detailed building metrics, serving as a valuable resource for urban planners, designers, and architects. Its robust capabilities can enable them to conduct in-depth analyses of UM, facilitating informed decision-making aimed at mitigating heat-related issues.

6.3 Limitations

The selection of the study area faced several challenges due to the unavailability of building height and ECOSTRESS data, in many potential cities. Although some cities experiencing even higher temperatures than the chosen cities would have been ideal for the study, they could not be included due to these data constraints. Additionally, there was an initial plan to incorporate thermal data from SDGSAT-1, a recently launched Chinese satellite offering higher resolution, but time constraints prevented the submission of a proposal to acquire this data. The process of generating MTs and computing UMMs using the momepy at the city level proved to be extremely time-consuming. This computational demand often caused the server to crash, further complicating the research process. The MT files themselves were very large for each city, which further prevented the inclusion of UMMs based on them in the RFR model due to the high computational demands.

While the study extensively examined the influence of UMMs on LST, it's crucial to recognize that these findings are solely reliable on the data used and the results of this study. UMMs served as proxies for complex interactions within urban environments, and their role may not fully capture the dependencies and interactions affecting surface temperatures. The patterns observed indicate only a marginal effect of UMMs on LST. Due to the absence of actual data points the PDP curves may not accurately reflect the true nature of the relationship between the UMMs and LST. The direct causality between UMMs and surface temperatures could be influenced by additional factors beyond the scope of this analysis, such as the use of reflective building materials, roof types, wind speed, and regional factors such as water bodies and high elevations, as highlighted by the city experts. Additionally, the patterns of several UMMs, such as alignment and building adjacency, leave room for discussion regarding their possible causes. Due to the limited research available on these specific UMMs, it could not be determined if these patterns align with other studies, making interpretations regarding these metrics speculative and in need of further investigation.

7 Conclusion and recommendations

To conclude this thesis, this chapter is divided into three sections: Section 7.1 ('Conclusion) presents the final conclusion of this study, Section 7.2 ('Future research') gives recommendations for future research, and Section 7.3 ('Ethical considerations, risks and contingencies') details out the ethical considerations related to this study.

7.1 Conclusion

This study investigated the impacts of UM on daytime LST during the summer period across four European cities—Paris, Rotterdam, Milan, and Vienna—using a comprehensive set of thirty UMMs and ML techniques. By leveraging the capabilities of the MOMEPY toolkit and employing a RFR model, the study delivers a detailed understanding of how building morphology influences the thermal environment. The research identified key UMMs, such as Mean Height, Orientation, Alignment, Building Adjacency, and MID, which play a pivotal role in shaping urban LSTs. Taller buildings in Paris were found to have a cooling effect due to increased shadowing and mechanical turbulence, aligning with previous studies. In contrast, mid-rise buildings in Rotterdam, Milan and Vienna also contributed to cooling. The study highlighted the cooling effect of water bodies, particularly in Rotterdam and Vienna, where rivers played a crucial role in moderating the local climate. Additionally, it identified that building orientation and adjacency significantly affect LST; buildings oriented away from the cardinal directions in Paris exhibited higher LSTs, and adjacent buildings generally experienced less heat possibly due to reduced surface areas to absorb solar heat. Moreover, the city experts emphasized the importance of historical context, particularly the post-war reconstructions and associated building factors, such as building materials, in shaping modern urban heat dynamics. In relation to this, the study also correlated this insight with the occurrence of hotspots in regions characterized by older, less insulated buildings, particularly notable in Vienna, and in industrial zones across all cities. Furthermore, it also identified coldspots in areas featuring greenhouses, as observed in Rotterdam and in low-density residential areas across all cities. It is important to note that the patterns uncovered in this research highly rely on the data utilized and do not indicate a direct relationship between LST and UMMs. It acknowledges that LST could be influenced by additional factors beyond the scope of this study. Nevertheless, the RFR model demonstrated promising results, highlighting the potential for its broader applicability across other European cities. It also suggests that a grid scale of 70 meters by 70 meters can be optimum for assessing UMMs' impact on LST. Momepy can be used as a reliable tool for conducting morphological analysis at a building level and facilitating informed decision-making aimed at mitigating heat-related issues. Based on these results, the study outlines several implications for improving thermal comfort across European cities. For existing urban areas with limited space availability, the study recommends retrofitting historic buildings with improved insulation and reflective roofing materials. It also suggests utilizing the flat roofs of the modern buildings by implementing vertical greening strategies or replacing them with sloped roofs. Furthermore, the study emphasizes the importance of designing new urban developments with appropriate building heights,

orientations, and inter-building distances. Overall, this research provides a new perspective by encompassing a wide range of UMMs to study the surface temperature patterns, which are crucial for developing more effective urban heat mitigation strategies. The inclusion of relatively novel UMMs not extensively explored in existing literature underscores a significant gap in current knowledge, emphasizing the need for continued research. Further integration of these UMMs in future research will be essential to deepen our understanding of their complex relationships with urban thermal environments and to validate their broader applicability.

7.2 Future research

Integrating high-resolution thermal data, such as that obtained from the SDGSAT, can provide more detailed spatial and temporal insights into urban heat patterns. This high-resolution data will enable more precise identification of hotspots and the factors contributing to them. Moreover, to capture the joint effects of various factors influencing urban heat, it is advisable to employ more sophisticated techniques such as multivariate analysis, interaction plots, or advanced machine learning models (e.g., deep learning models). They might be better at capturing complex interactions between variables, potentially improving the accuracy and predictive performance of the model. However, the integration of such complex techniques brings additional challenges. Model design grows in complexity, requiring careful consideration of the architecture and parameters of advanced models. Computational requirements increase significantly, necessitating more powerful hardware and longer processing times.

Training the RFR model with the MTs layer, which provided information about the diversity within the buildings, could have been highly beneficial and may have improved the performance of the model. Notably, the UMMs used in this study are relatively new and have not been widely discussed in the existing literature. This highlights a significant gap in the current body of knowledge and underscores the necessity for further research. Conducting more studies like this one will facilitate a deeper understanding of these metrics and their influence on LST, thereby contributing to a more comprehensive body of research on urban heat patterns and mitigation strategies. Moreover, the current design strategies aimed at mitigating urban heat primarily target the challenges posed during hot summer months. For a more robust approach, comprehensive and evidence-based research across diverse regions characterized by different climatic zones and urban sizes, conducted at various times of day and seasons, is crucial. Such research is essential to grasp how these strategies perform under varying conditions. Further research should aim to develop adaptive urban heat mitigation strategies that are specifically tailored to the unique environmental and urban contexts of each city.

7.3 Ethical considerations, risks and contingencies

The data that support the findings of this study are available in ITC's repository. The authors, researchers, and all the other individuals who supported in the completion of this research were duly acknowledged. The information gathered from the expert interviews have been used for academic purposes and the responses will remain confidential and anonymous with the highest standard of research ethics, effectively addressing privacy and consent concerns. The findings of this study were entirely based on the empirical evidence gathered from the collected datasets. During the preparation of this work, the author used ChatGPT in order to grasp certain concepts, simplified explanations and paraphrase some sentences to refine the language and grammar. After using this tool/service, the author carefully examined and modified the output of this tool/service to guarantee its correctness and takes full responsibility for the content of the work.

List of references

Abdel-Rahman, E. M., Mutanga, O., Adam, E., & Ismail, R. (2014). Detecting Sirex noctilio grey-attacked and lightning-struck pine trees using airborne hyperspectral data, random forest and support vector machines classifiers. *ISPRS Journal of Photogrammetry and Remote Sensing*, *88*, 48–59. https://doi.org/10.1016/J.ISPRSJPRS.2013.11.013

AFP News. (2019, July 26). *Are Paris' beautiful Haussmann buildings stopping the city cooling down?* The Local. https://www.thelocal.fr/20190726/are-paris-beautiful-haussmann-buildings-stopping-the-city-cooling-down

Akpenpuun, T. D., Ogunlowo, Q. O., Na, W.-H., Rabiu, A., Adesanya, M. A., Dutta, P., Zakir, E., Ogundele, O. M., Kim, H.-T., & Lee, H.-W. (2023). Review of Temperature Management Strategies and Techniques in the Greenhouse Microenvironment. *Adeleke University Journal of Engineering and Technology*, *6*(2), 126–147. http://aujet.adelekeuniversity.edu.ng/index.php/aujet/article/view/338

Ayanlade, A. (2016). Variation in diurnal and seasonal urban land surface temperature: Landuse change impacts assessment over Lagos metropolitan city. *Modeling Earth Systems and Environment*, *2*(4), 1–8. https://doi.org/10.1007/s40808-016-0238-z

Baranka, G., Bozó, L., Ciglič, R., & Komac, B. (2016). Urban heat Island gold standard and urban heat Island atlas: Gold standard for UHI measurements and introduction of the Central-European urban heat Island atlas. *Counteracting Urban Heat Island Effects in a Global Climate Change Scenario*, 41–70. https://doi.org/10.1007/978-3-319-10425-6_2

Berger, C., Rosentreter, J., Voltersen, M., Baumgart, C., Schmullius, C., & Hese, S. (2017). Spatio-temporal analysis of the relationship between 2D/3D urban site characteristics and land surface temperature. *Remote Sensing of Environment*, *193*, 225–243. https://doi.org/10.1016/J.RSE.2017.02.020

Bhattacharya, B. K., Mallick, K., Desai, D., Bhat, G. S., Morrison, R., Clevery, J. R., Woodgate, W., Beringer, J., Cawse-Nicholson, K., Ma, S., Verfaillie, J., & Baldocchi, D. (2022). A coupled ground heat flux-surface energy balance model of evaporation using thermal remote sensing observations. *Biogeosciences*, *19*(23), 5521–5551. https://doi.org/10.5194/BG-19-5521-2022

Bhatti, S. S., Reis, J. P., & Silva, E. A. (2018). Spatial Metrics: The Static and Dynamic Perspectives. *Comprehensive Geographic Information Systems*, *3*, 181–196. https://doi.org/10.1016/B978-0-12-409548-9.09604-4

Breiman, L. (2001). Random forests. *Machine Learning*, *45*(1), 5–32. https://doi.org/10.1023/A:1010933404324

Burton, A. L. (2021). OLS (Linear) Regression. *The Encyclopedia of Research Methods in Criminology and Criminal Justice: Volume II: Parts 5-8*, 509–514. https://doi.org/10.1002/9781119111931.CH104

Caldas de Castro, M., & Singer, B. H. (2006). Controlling the False Discovery Rate: A New Application to Account for Multiple and Dependent Tests in Local Statistics of Spatial Association. *Geographical Analysis*, *38*(2), 180–208. https://doi.org/10.1111/J.0016-7363.2006.00682.X

Chamberlain, L., & Merritt, J. (2023, June 26). *Europe's schools and hospitals in urban heat islands and other cities news*. World Economic Forum. https://www.weforum.org/agenda/2023/06/europe-schools-hospitals-urban-heat-island-and-other-city-focused-stories/

Chen, H. C., Han, Q., & De Vries, B. (2020). Modeling the spatial relation between urban morphology, land surface temperature and urban energy demand. *Sustainable Cities and Society*, *60*, 102246. https://doi.org/10.1016/J.SCS.2020.102246

Chen, P. (2024). Inequality in heat: The role of spatial patterns of urban green infrastructure. *Urban Climate*, *53*, 101820. https://doi.org/10.1016/J.UCLIM.2024.101820

Cheung, J. O. P., & Liu, C. H. (2011). CFD simulations of natural ventilation behaviour in high-rise buildings in regular and staggered arrangements at various spacings. *Energy and Buildings*, *43*(5), 1149–1158. https://doi.org/10.1016/J.ENBUILD.2010.11.024

Chrysanthou, A., Van Der Schrier, G., Van Den Besselaar, E. J. M., Klein Tank, A. M. G., & Brandsma, T. (2014). The effects of urbanization on the rise of the European temperature since 1960. *Geophysical Research Letters*, *41*(21), 7716–7722. https://doi.org/10.1002/2014GL061154

de Winter, J. C. F., Gosling, S. D., & Potter, J. (2016). Comparing the pearson and spearman correlation coefficients across distributions and sample sizes: A tutorial using simulations and empirical data. *Psychological Methods*, *21*(3), 273–290. https://doi.org/10.1037/MET0000079

Derdouri, A., Wang, R., Murayama, Y., & Osaragi, T. (2021). Understanding the links between LULC changes and SUHI in cities: Insights from two-decadal studies (2001–2020). *Remote Sensing*, *13*(18), 3654. https://doi.org/10.3390/rs13183654

Dibble, J., Prelorendjos, A., Romice, O., Zanella, M., Strano, E., Pagel, M., & Porta, S. (2019). On the origin of spaces: Morphometric foundations of urban form evolution. *Environment and Planning B: Urban Analytics and City Science*, *46*(4), 707–730. https://doi.org/10.1177/2399808317725075

Du, S., Zhang, X., Jin, X., Zhou, X., & Shi, X. (2022). A review of multi-scale modelling, assessment, and improvement methods of the urban thermal and wind environment. *Building and Environment*, *213*, 108860. https://doi.org/10.1016/J.BUILDENV.2022.108860

Du, X. (2019). *Space Design for Thermal Comfort and Energy Efficiency in Summer*. [Thesis, TU Delft]. Architecture and the Built Environment. https://journals.open.tudelft.nl/abe/issue/view/727

Elmes, A., Rogan, J., Williams, C., Ratick, S., Nowak, D., & Martin, D. (2017). Effects of urban tree canopy loss on land surface temperature magnitude and timing. *ISPRS Journal of Photogrammetry and Remote Sensing*, *128*, 338–353. https://doi.org/10.1016/J.ISPRSJPRS.2017.04.011

Estoque, R. C., Murayama, Y., & Myint, S. W. (2017). Effects of landscape composition and pattern on land surface temperature: An urban heat island study in the megacities of Southeast Asia. *The Science of the Total Environment*, *577*, 349–359. https://doi.org/10.1016/J.SCITOTENV.2016.10.195

Estrada, F., Botzen, W. J. W., & Tol, R. S. J. (2017). A global economic assessment of city policies to reduce climate change impacts. *Nature Climate Change*, *7*(6), 403–406. https://doi.org/10.1038/nclimate3301

European Commission. (n.d.). *Consequences of climate change*. https://climate.ec.europa.eu/climate-change/consequences-climate-change_en

European Commission. (2019). *Main land-use patterns in the EU within 2015-2030*. https://joint-research-centre.ec.europa.eu/reports-and-technical-documentation/main-land-use-patterns-eu-within-2015-2030_en

European Commission, Joint Research Centre, Baranzelli, C., Siragusa, A., Aurambout, J. P., Alberti, V., Alonso Raposo, M., Attardo, C., Auteri, D., Ribeiro Barranco, R., Batista E Silva, F., Benczur, P., Bertoldi, P., Bono, F., Bussolari, I., Louro Caldeira, S., Carlsson, J., Christidis, P., Christodoulou, A., … Zulian, G. (2019). *The Future of Cities – Opportunities, challenges and the way forward* (C. Baranzelli, I. Vandecasteele, J. Aurambout, & A. Siragusa, Eds.). Publications Office of the European Union. https://doi.org/10.2760/364135

European Environment Agency. (2008). *Urban sprawl in Europe - The ignored challenge*. https://www.eea.europa.eu/publications/eea_report_2006_10/eea_report_10_2006.pdf/view

European Environment Agency. (2023, January 29). *The average summer season intensity of urban heat island (°C) and the projected number of extreme heatwaves in near future (2020-2052; RCP8.5)*. https://www.eea.europa.eu/data-and-maps/figures/the-average-summer-season-intensity

Feyisa, G. L., Meilby, H., Darrel Jenerette, G., & Pauliet, S. (2016). Locally optimized separability enhancement indices for urban land cover mapping: Exploring thermal environmental consequences of rapid urbanization in Addis Ababa, Ethiopia. *Remote Sensing of Environment*, *175*, 14–31. https://doi.org/10.1016/J.RSE.2015.12.026

Fleischmann, M. (2018). *Getting started — momepy 0.7.0 documentation*. https://docs.momepy.org/en/stable/user_guide/getting_started.html

Fleischmann, M. (2019). momepy: Urban Morphology Measuring Toolkit. *Journal of Open Source Software*, *4*(43), 1807. https://doi.org/10.21105/JOSS.01807

Fleischmann, M., Feliciotti, A., Romice, O., & Porta, S. (2020). Morphological tessellation as a way of partitioning space: Improving consistency in urban morphology at the plot scale. *Computers, Environment and Urban Systems*, *80*, 101441. https://doi.org/10.1016/J.COMPENVURBSYS.2019.101441

Fleischmann, M., Feliciotti, A., Romice, O., & Porta, S. (2021). Methodological Foundation of a Numerical Taxonomy of Urban Form. *Environment and Planning B: Urban Analytics and City Science*, *49*(4), 1283–1299. http://arxiv.org/abs/2104.14956

Fleischmann, M., Romice, O., & Porta, S. (2021). Measuring urban form: Overcoming terminological inconsistencies for a quantitative and comprehensive morphologic analysis of cities. *Environment and Planning B: Urban Analytics and City Science*, *48*(8), 2133–2150. https://doi.org/10.1177/2399808320910444

Fotheringham, A. S., & Brunsdon, C. (1999). Local Forms of Spatial Analysis. *Geographical Analysis*, *31*(4), 340–358. https://doi.org/10.1111/J.1538-4632.1999.TB00989.X

Friedman, J. H. (2001). Greedy function approximation: A gradient boosting machine. *The Annals of Statistics*, *29*(5), 1189–1232. https://doi.org/10.1214/AOS/1013203451

Futcher, J., Mills, G., Emmanuel, R., & Korolija, I. (2017). Creating sustainable cities one building at a time: Towards an integrated urban design framework. *Cities*, *66*, 63–71. https://doi.org/10.1016/J.CITIES.2017.03.009

Gabriel, K. M. A., & Endlicher, W. R. (2011). Urban and rural mortality rates during heat waves in Berlin and Brandenburg, Germany. *Environmental Pollution*, *159*(8–9), 2044–2050. https://doi.org/10.1016/J.ENVPOL.2011.01.016

Geletič, J., Lehnert, M., Savić, S., & Milošević, D. (2019). Inter-/intra-zonal seasonal variability of the surface urban heat island based on local climate zones in three central European cities. *Building and Environment*, *156*, 21–32. https://doi.org/10.1016/J.BUILDENV.2019.04.011

Givoni, Baruch. (1994). *Passive and low energy cooling of buildings*. 263. https://www.wiley.com/en-us/Passive+Low+Energy+Cooling+of+Buildings-p-9780471284734

Gonzales, J. J. (2023). Building-Level Comparison of Microsoft and Google Open Building Footprints Datasets (Short Paper). *In 12th International Conference on Geographic Information Science (GIScience 2023). Leibniz International Proceedings in Informatics (LIPIcs)*, *277*, 35:1-35:6. https://doi.org/10.4230/LIPICS.GISCIENCE.2023.35

Goodell, J. (2023, July 18). *Paris When It Sizzles: The City of Light Aims to Get Smart on Heat*. https://e360.yale.edu/features/paris-heat-waves-climate-change

Greenwell, B. M., Boehmke, B. C., & Mccarthy, A. J. (2018). *A Simple and Effective Model-Based Variable Importance Measure*. https://doi.org/10.48550/arXiv.1805.04755

Grigoraş, G., & Uriţescu, B. (2018). Spatial Hotspot Analysis of Bucharest's Urban Heat Island (UHI) Using Modis Data. *Annals of Valahia University of Targoviste, Geographical Series*, *18*(1), 14–22. https://doi.org/10.2478/AVUTGS-2018-0002

Groenendijk, E. M. C., & Dopheide, E. J. M. (2003). Planning and Management Tools. In *ITC Special Lecture Notes Series*. International Institute for Geo-Information Science and Earth Observation. https://research.utwente.nl/en/publications/planning-and-management-tools

Guan, Q., Yao, Y., Ma, T., Hong, Y., Bie, Y., & Lyu, J. (2021). Under the Dome: A 3D Urban Texture Model and Its Relationship with Urban Land Surface Temperature. *Annals of the American Association of Geographers*, *112*(5), 1369–1389. https://doi.org/10.1080/24694452.2021.1972790

Guerreiro, S. B., Dawson, R. J., Kilsby, C., Lewis, E., & Ford, A. (2018). Future heat-waves, droughts and floods in 571 European cities. *Environmental Research Letters*, *13*(3), 034009. https://doi.org/10.1088/1748-9326/AAAAD3

Guo, A., Yang, J., Sun, W., Xiao, X., Xia Cecilia, J., Jin, C., & Li, X. (2020). Impact of urban morphology and landscape characteristics on spatiotemporal heterogeneity of land surface temperature. *Sustainable Cities and Society*, *63*, 102443. https://doi.org/10.1016/J.SCS.2020.102443

Guo, A., Yue, W., Yang, J., He, T., Zhang, M., & Li, M. (2022). Divergent impact of urban 2D/3D morphology on thermal environment along urban gradients. *Urban Climate*, *45*, 101278. https://doi.org/10.1016/J.UCLIM.2022.101278

Guo, F., Hu, D., & Schlink, U. (2022). A new nonlinear method for downscaling land surface temperature by integrating guided and Gaussian filtering. *Remote Sensing of Environment*, *271*, 112915. https://doi.org/10.1016/J.RSE.2022.112915

Guo, G., Zhou, X., Wu, Z., Xiao, R., & Chen, Y. (2016). Characterizing the impact of urban morphology heterogeneity on land surface temperature in Guangzhou, China. *Environmental Modelling & Software*, *84*, 427–439. https://doi.org/10.1016/J.ENVSOFT.2016.06.021

Habibi, S. (2023). The effect of building orientation on energy efficiency. *Clean Technologies and Environmental Policy*, *26*(4), 1315–1330. https://doi.org/10.1007/S10098-023-02695-W

Halder, B., Bandyopadhyay, J., & Banik, P. (2021). Monitoring the effect of urban development on urban heat island based on remote sensing and geo-spatial approach in Kolkata and adjacent areas, India. *Sustainable Cities and Society*, *74*, 103186. https://doi.org/10.1016/J.SCS.2021.103186

Han, W. (2023). Analyzing the scale dependent effect of urban building morphology on land surface temperature using random forest algorithm. *Scientific Reports*, *13*(1), 1–10. https://doi.org/10.1038/s41598-023-46437-w

Hayward, B., Pelling, M., Castan Broto, V., Chow, W., Chu, E., Dawson, R., Khirfan, L., McPhearson, T., Prakash, A., Zheng, Y., Ziervogel, G., Pörtner, H., Roberts, D., Tignor, M., Poloczanska, E., Mintenbeck, K., Alegría, A., Craig, M., Langsdorf, S., … Rama, B. (2023). Cities, Settlements and Key Infrastructure. In H.-O. Pörtner, D. C. Roberts, M. Tignor, E. S. Poloczanska, K. Mintenbeck, A. Alegría, M. Craig, S. Langsdorf, S. Löschke, V. Möller, A. Okem, & B. Rama (Eds.), *Climate Change 2022: Impacts, Adaptation and Vulnerability. Contribution of Working Group II to the Sixth Assessment Report of the Intergovernmental Panel on Climate Change* (pp. 907–1040). Cambridge University Press. https://doi.org/10.1017/9781009325844.008

He, J., Kong, X., Jiao, L., Yan, J., Yin, C., An, Z., Mu, B., Wen, Q., Li, Y., Zhang, Y., Chen, W., Wang, L., & Song, Y. (2023). The Influence of Urban Form on Land Surface Temperature: A Comprehensive Investigation from 2D Urban Land Use and 3D Buildings. *Land*, *12*(9), 1802. https://doi.org/10.3390/LAND12091802

Heldens, W., Taubenböck, H., Esch, T., Heiden, U., & Wurm, M. (2013). Analysis of surface thermal patterns in relation to urban structure types: A case study for the city of Munich. *Remote Sensing and Digital Image Processing*, *17*, 475–493. https://doi.org/10.1007/978-94-007-6639-6_23

Heusinkveld, B. G., Steeneveld, G. J., Van Hove, L. W. A., Jacobs, C. M. J., & Holtslag, A. A. M. (2014). Spatial variability of the Rotterdam urban heat island as influenced by urban land use. *Journal of Geophysical Research: Atmospheres*, *119*(2), 677–692. https://doi.org/10.1002/2012JD019399

Hoeven, F. van der, & Wandl, A. (2015). Hotterdam: How space is making Rotterdam warmer, how this affects the health of its inhabitants, and what can be done about it. In *BookRxiv*. BookRxiv. https://doi.org/10.47982/BOOKRXIV.1

Hu, D., Meng, Q., Schlink, U., Hertel, D., Liu, W., Zhao, M., & Guo, F. (2022). How do urban morphological blocks shape spatial patterns of land surface temperature over different seasons? A multifactorial driving analysis of Beijing, China. *International Journal of Applied Earth Observation and Geoinformation*, *106*, 102648. https://doi.org/10.1016/J.JAG.2021.102648

Hu, L., & Brunsell, N. A. (2013). The impact of temporal aggregation of land surface temperature data for surface urban heat island (SUHI) monitoring. *Remote Sensing of Environment*, *134*, 162–174. https://doi.org/10.1016/J.RSE.2013.02.022

Hu, Y., Dai, Z., & Guldmann, J. M. (2020). Modeling the impact of 2D/3D urban indicators on the urban heat island over different seasons: A boosted regression tree approach. *Journal of Environmental Management*, *266*, 110424. https://doi.org/10.1016/J.JENVMAN.2020.110424

Hu, Y., Tang, R., Jiang, X., Li, Z. L., Jiang, Y., Liu, M., Gao, C., & Zhou, X. (2023). A physical method for downscaling land surface temperatures using surface energy balance theory. *Remote Sensing of Environment*, *286*, 113421. https://doi.org/10.1016/J.RSE.2022.113421

Huang, X., & Wang, Y. (2019). Investigating the effects of 3D urban morphology on the surface urban heat island effect in urban functional zones by using high-resolution remote sensing data: A case study of Wuhan, Central China. *ISPRS Journal of Photogrammetry and Remote Sensing*, *152*, 119–131. https://doi.org/10.1016/J.ISPRSJPRS.2019.04.010

Hulley, G. C., Ghent, D., Göttsche, F. M., Guillevic, P. C., Mildrexler, D. J., & Coll, C. (2019). Land Surface Temperature. *Taking the Temperature of the Earth: Steps towards Integrated Understanding of Variability and Change*, 57–127. https://doi.org/10.1016/B978-0-12-814458-9.00003-4

Hulley, G. C., Göttsche, F. M., Rivera, G., Hook, S. J., Freepartner, R. J., Martin, M. A., Cawse-Nicholson, K., & Johnson, W. R. (2022). Validation and Quality Assessment of the ECOSTRESS Level-2 Land Surface Temperature and Emissivity Product. *IEEE Transactions on Geoscience and Remote Sensing*, *60*. https://doi.org/10.1109/TGRS.2021.3079879

Hulley, G., & Hook, S. (2022). *ECOSTRESS Swath Land Surface Temperature and Emissivity Instantaneous L2 Global 70 m v002*. USGS. https://doi.org/10.5067/ECOSTRESS/ECO_L2_LSTE.002

IPCC. (2023). Summary for Policymakers. In *Climate Change 2022: Mitigation of Climate Change. Contribution of Working Group III to the Sixth Assessment Report of the Intergovernmental Panel on Climate Change* (pp. 3–48). Cambridge University Press. https://doi.org/10.1017/9781009157926.001

Irwan, S. S., Ahmed, A. Z., Zakaria, N. Z., & Ibrahim, N. (2010). Thermal and Energy Performance of Conditioned Building Due To Insulated Sloped Roof. *AIP Conference Proceedings*, *1250*, 476–479. https://doi.org/10.1063/1.3469712

Janssen, S. J. (2011). *Influences of urban morphology on the average temperature of Rotterdam city*. [Thesis, Eindhoven Technical University]. https://library.wur.nl/WebQuery/kvk/2093079

Jin, M., & Dickinson, R. E. (2010). Land surface skin temperature climatology: benefitting from the strengths of satellite observations. *Environmental Research Letters*, *5*(4), 044004. https://doi.org/10.1088/1748-9326/5/4/044004

Jollife, I. T., & Cadima, J. (2016). Principal component analysis: a review and recent developments. *Philosophical Transactions. Series A, Mathematical, Physical, and Engineering Sciences*, *374*(2065). https://doi.org/10.1098/RSTA.2015.0202

Jothimani, M., Gunalan, J., Duraisamy, R., & Abebe, A. (2021). Study the Relationship Between LULC, LST, NDVI, NDWI and NDBI in Greater Arba Minch Area, Rift Valley, Ethiopia. *Proceedings of the*

3rd International Conference on Integrated Intelligent Computing Communication & Security (ICIIC 2021), *4*, 183–193. https://doi.org/10.2991/AHIS.K.210913.023

Jung, Y., & Hu, J. (2015). A K-fold averaging cross-validation procedure. *Journal of Nonparametric Statistics*, *27*(2), 167–179. https://doi.org/10.1080/10485252.2015.1010532

Kabano, P., Lindley, S., & Harris, A. (2021). Evidence of urban heat island impacts on the vegetation growing season length in a tropical city. *Landscape and Urban Planning*, *206*, 103989. https://doi.org/10.1016/J.LANDURBPLAN.2020.103989

Kim, E.-S., Yun, S.-H., Park, C.-Y., Heo, H.-K., & Lee, D.-K. (2022). Estimation of Mean Radiant Temperature in Urban Canyons Using Google Street View: A Case Study on Seoul. *Remote Sensing*, *14*(2), 260. https://doi.org/10.3390/RS14020260

Kloog, I., Nordio, F., Coull, B. A., & Schwartz, J. (2014). Predicting spatiotemporal mean air temperature using MODIS satellite surface temperature measurements across the Northeastern USA. *Remote Sensing of Environment*, *150*, 132–139. https://doi.org/10.1016/J.RSE.2014.04.024

Kokkinidis, T. (2022, April 20). *Athens the Second Most Densely-Populated Area in Europe*. https://greekreporter.com/2022/04/20/athens-densely-populated-europe/

Kong, F., Chen, J., Middel, A., Yin, H., Li, M., Sun, T., Zhang, N., Huang, J., Liu, H., Zhou, K., & Ma, J. (2022). Impact of 3-D urban landscape patterns on the outdoor thermal environment: A modelling study with SOLWEIG. *Computers, Environment and Urban Systems*, *94*, 101773. https://doi.org/10.1016/J.COMPENVURBSYS.2022.101773

Kong, J., Zhao, Y., Carmeliet, J., & Lei, C. (2021). Urban heat island and its interaction with heatwaves: A review of studies on mesoscale. *Sustainability*, *13*(19), 10923. https://doi.org/10.3390/su131910923

Labetski, A., Vitalis, S., Biljecki, F., Arroyo Ohori, K., & Stoter, J. (2023). 3D building metrics for urban morphology. *International Journal of Geographical Information Science*, *37*(1), 36–67. https://doi.org/10.1080/13658816.2022.2103818

Li, H., Li, Y., Wang, T., Wang, Z., Gao, M., & Shen, H. (2021). Quantifying 3D building form effects on urban land surface temperature and modeling seasonal correlation patterns. *Building and Environment*, *204*, 108132. https://doi.org/10.1016/J.BUILDENV.2021.108132

Li, J., Song, C., Cao, L., Zhu, F., Meng, X., & Wu, J. (2011). Impacts of landscape structure on surface urban heat islands: A case study of Shanghai, China. *Remote Sensing of Environment*, *115*(12), 3249–3263. https://doi.org/10.1016/J.RSE.2011.07.008

Li, T., Cao, J., Xu, M., Wu, Q., & Yao, L. (2020). The influence of urban spatial pattern on land surface temperature for different functional zones. *Landscape and Ecological Engineering*, *16*(3), 249–262. https://doi.org/10.1007/s11355-020-00417-8

Li, X., Yang, Y., Mi, J., Bi, X., Zhao, Y., Huang, Z., Liu, C., Zong, L., & Li, W. (2021). Leveraging machine learning for quantitative precipitation estimation from Fengyun-4 geostationary observations and ground meteorological measurements. *Atmospheric Measurement Techniques*, *14*(11), 7007–7023. https://doi.org/10.5194/AMT-14-7007-2021

Li, Z. L., Wu, H., Duan, S. B., Zhao, W., Ren, H., Liu, X., Leng, P., Tang, R., Ye, X., Zhu, J., Sun, Y., Si, M., Liu, M., Li, J., Zhang, X., Shang, G., Tang, B. H., Yan, G., & Zhou, C. (2023). Satellite Remote Sensing of Global Land Surface Temperature: Definition, Methods, Products, and Applications. *Reviews of Geophysics*, *61*(1), e2022RG000777. https://doi.org/10.1029/2022RG000777

Liaw, A., & Wiener, M. (2002). Classification and Regression by randomForest. *R News*, *2*(3), 18–22. https://journal.r-project.org/articles/RN-2002-022/RN-2002-022.pdf

Liu, B., Guo, X., Jiang, J., Liu, B., Guo, X., & Jiang, J. (2023). How Urban Morphology Relates to the Urban Heat Island Effect: A Multi-Indicator Study. *Sustainability*, *15*(14), 10787. https://doi.org/10.3390/SU151410787

Liu, J., & Niyogi, D. (2020). Identification of linkages between urban heat Island magnitude and urban rainfall modification by use of causal discovery algorithms. *Urban Climate*, *33*, 100659. https://doi.org/10.1016/J.UCLIM.2020.100659

Logan, T. M., Zaitchik, B., Guikema, S., & Nisbet, A. (2020). Night and day: The influence and relative importance of urban characteristics on remotely sensed land surface temperature. *Remote Sensing of Environment*, *247*, 111861. https://doi.org/10.1016/J.RSE.2020.111861

Logan, T., & Smyth, M. (2019). *ECOSTRESS L1 User Guide D-57151 ECOsystem Spaceborne Thermal Radiometer Experiment on Space Station (ECOSTRESS) Mission Level 1 Product User Guide*. California. ECOSTRESS Algorithm Development Team, Jet Propulsion Laboratory, California Institute of Technology.

Martilli, A., Roth, M., Chow, W. T. L., Martilli, A., Roth, M., Demuzere, M., Lipson, M., Krayenhoff, E. S., Sailor, D., Nazarian, N., Voogt, J., Wouters, H., Middel, A., Stewart, I. D., Bechtel, B., Christen, A., & Hart, M. A. (2020). Summer average urban-rural surface temperature differences do not indicate the need for urban heat reduction. *Research Collection School of Social Sciences*, *573*, 1. https://doi.org/10.31219/osf.io/8gnbf

Matt Rees. (2020, July 8). *Cities find smart ways to adapt to climate change*. European Investment Bank. https://www.eib.org/en/stories/urban-climate-adaptation

McGlynn, T. P., Meineke, E. K., Bahlai, C. A., Li, E., Hartop, E. A., Adams, B. J., & Brown, B. V. (2019). Temperature accounts for the biodiversity of a hyperdiverse group of insects in urban Los Angeles. *Proceedings of the Royal Society B*, *286*(1912). https://doi.org/10.1098/RSPB.2019.1818

Milojevic-Dupont, N., Wagner, F., Nachtigall, F., Hu, J., Brüser, G. B., Zumwald, M., Biljecki, F., Heeren, N., Kaack, L. H., Pichler, P. P., & Creutzig, F. (2023). EUBUCCO v0.1: European building stock characteristics in a common and open database for 200+ million individual buildings. *Scientific Data*, *10*(1), 1–17. https://doi.org/10.1038/s41597-023-02040-2

Mo, Y., Xu, Y., Chen, H., & Zhu, S. (2021). A Review of Reconstructing Remotely Sensed Land Surface Temperature under Cloudy Conditions. *Remote Sensing*, *13*(14), 2838. https://doi.org/10.3390/RS13142838

Mohajerani, A., Bakaric, J., & Jeffrey-Bailey, T. (2017). The urban heat island effect, its causes, and mitigation, with reference to the thermal properties of asphalt concrete. *Journal of Environmental Management*, *197*, 522–538. https://doi.org/10.1016/J.JENVMAN.2017.03.095

Molina-Gómez, N. I., Varon-Bravo, L. M., Sierra-Parada, R., & López-Jiménez, P. A. (2022). Urban growth and heat islands: A case study in micro-territories for urban sustainability. *Urban Ecosystems*, *25*(5), 1379–1397. https://doi.org/10.1007/s11252-022-01232-9

Mujtaba, G., Shuib, L., Idris, N., Hoo, W. L., Raj, R. G., Khowaja, K., Shaikh, K., & Nweke, H. F. (2019). Clinical text classification research trends: Systematic literature review and open issues. *Expert Systems with Applications*, *116*, 494–520. https://doi.org/10.1016/J.ESWA.2018.09.034

Mukati, A. (2021). *Effect of Heatwaves on the Cooling Demand of Austrian Residential Buildings*. [Master's Thesis, KTH]. School of Industrial Engineering and Management. https://urn.kb.se/resolve?urn=urn:nbn:se:kth:diva-305826

Mutiibwa, D., Strachan, S., & Albright, T. (2015). Land Surface Temperature and Surface Air Temperature in Complex Terrain. *IEEE Journal of Selected Topics in Applied Earth Observations and Remote Sensing*, *8*(10), 4762–4774. https://doi.org/10.1109/JSTARS.2015.2468594

NASA. (n.d.). *AppEEARS*. https://appeears.earthdatacloud.nasa.gov/

National Disaster Management Authority. (2021). *Heatwave Action Alternate Roof Cooling Solutions*. https://ndma.gov.in/sites/default/files/PDF/Guidelines/Cool-Roof-Handbook.pdf

NL Times. (2023, July 14). *Heat wave causes 5 percent more deaths than expected in June*. https://nltimes.nl/2023/07/14/heat-wave-causes-5-percent-deaths-expected-june

NV5 Geospatial. (n.d.). *Hotspot Analysis*. https://www.nv5geospatialsoftware.com/docs/HotspotAnalysis.html

NYU & UN-Habitat. (2014). *Atlas of Urban Expansion*. http://atlasofurbanexpansion.org/cities/view/Paris

Ord, J. K., & Getis, A. (1995). Local Spatial Autocorrelation Statistics: Distributional Issues and an Application. *Geographical Analysis*, *27*(4), 286–306. https://doi.org/10.1111/J.1538-4632.1995.TB00912.X

Pal, R. K., Goyal, P., & Sehgal, S. (2020). Thermal performance of buildings with light colored exterior materials. *Materials Today: Proceedings*, *28*, 1307–1313. https://doi.org/10.1016/J.MATPR.2020.04.508

Peng, J., Dan, Y., Qiao, R., Liu, Y., Dong, J., & Wu, J. (2021). How to quantify the cooling effect of urban parks? Linking maximum and accumulation perspectives. *Remote Sensing of Environment*, *252*, 112135. https://doi.org/10.1016/J.RSE.2020.112135

Peng, Z., Jia, L., Li, L., Quan, S. J., & Yang, P. P. J. (2017). How the roofing morphology and housing form affect energy performance of Shanghai's workers' village in urban regeneration. *Energy Procedia*, *142*, 3075–3082. https://doi.org/10.1016/J.EGYPRO.2017.12.447

Portela, C. I., Massi, K. G., Rodrigues, T., & Alcântara, E. (2020). Impact of urban and industrial features on land surface temperature: Evidences from satellite thermal indices. *Sustainable Cities and Society*, *56*, 102100. https://doi.org/10.1016/J.SCS.2020.102100

Puche, M., Vavassori, A., & Brovelli, M. A. (2023). Insights into the Effect of Urban Morphology and Land Cover on Land Surface and Air Temperatures in the Metropolitan City of Milan (Italy) Using Satellite Imagery and In Situ Measurements. *Remote Sensing*, *15*(3), 733. https://doi.org/10.3390/RS15030733

Qin, Z., & Karnieli, A. (1999). Progress in the remote sensing of land surface temperature and ground emissivity using NOAA-AVHRR data. *International Journal of Remote Sensing*, *20*(12), 2367–2393. https://doi.org/10.1080/014311699212074

Quattrochi, D. A., & Luvall, J. C. (1999). Thermal infrared remote sensing for analysis of landscape ecological processes: Methods and applications. *Landscape Ecology*, *14*(6), 577–598. https://doi.org/10.1023/A:1008168910634

Rao, P. K. (1972). Remote Sensing of Urban Heat Islands from an Environmental Satellite. *Bulletin of the American Meteorological Society*, *53*, 647–648. https://www.scirp.org/reference/referencespapers?referenceid=2208155

Raschka, S. (2018). *Model Evaluation, Model Selection, and Algorithm Selection in Machine Learning*. https://doi.org/10.48550/arXiv.1811.12808

Reuters. (2023, August 25). *Milan records hottest day since 1763*. https://www.reuters.com/world/europe/milan-records-hottest-day-since-1763-2023-08-25/

Robitu, M., Groleau, D., & Musy, M. (2004). Energy balance study of water ponds and its influence on building energy consumption. *Building Services Engineering Research and Technology, 25*, 171–182. https://doi.org/10.1191/0143624404bt106oa

Robyn. (2020, September 4). *Advantages and Disadvantages Of A Flat Roof*. Buildworld. https://www.buildworld.co.uk/blog/archives/Advantages-and-Disadvantages-Of-A-Flat-Roof

Rokugawa, S., Matsunaga, T., Tonooka, H., Tsu, H., Kannari, Y., & Okada, K. (1999). Temperature and emissivity separation from ASTER on EOS AM-1 - preflight validation by ASTER airborne simulator -. *Advances in Space Research*, *23*(8), 1463–1469. https://doi.org/10.1016/S0273-1177(99)00299-9

Rotterdamse Dakendagen. (2020, December). *In conversation: How Rotterdam is using rooftops to create space for parks, solar and more*. C40. https://www.c40knowledgehub.org/s/article/In-conversation-How-Rotterdam-is-using-rooftops-to-create-space-for-parks-solar-and-more?language=en_US

Ru, C., Duan, S. B., Jiang, X. G., Li, Z. L., Huang, C., & Liu, M. (2023). An extended SW-TES algorithm for land surface temperature and emissivity retrieval from ECOSTRESS thermal infrared data over urban areas. *Remote Sensing of Environment*, *290*, 113544. https://doi.org/10.1016/J.RSE.2023.113544

Sabrin, S., Karimi, M., Fahad, M. G. R., & Nazari, R. (2020). Quantifying environmental and social vulnerability: Role of urban Heat Island and air quality, a case study of Camden, NJ. *Urban Climate*, *34*, 100699. https://doi.org/10.1016/J.UCLIM.2020.100699

Sandu, A. (2016, June 16). A comparative study of the urban morphology in Europe using GMES Urban Atlas: the post-socialist city vs. the capitalist city (Romania vs. France). *In 16th International Multidisciplinary Scientific GeoConference SGEM 2016*. https://doi.org/10.5593/SGEM2016/B23/S11.001

Santamouris, M., Cartalis, C., Synnefa, A., & Kolokotsa, D. (2015). On the impact of urban heat island and global warming on the power demand and electricity consumption of buildings—A review. *Energy and Buildings*, *98*, 119–124. https://doi.org/10.1016/J.ENBUILD.2014.09.052

Scarano, M., & Mancini, F. (2017). Assessing the relationship between sky view factor and land surface temperature to the spatial resolution. *International Journal of Remote Sensing*, *38*(23), 6910–6929. https://doi.org/10.1080/01431161.2017.1368099

Schober, P., & Schwarte, L. A. (2018). Correlation coefficients: Appropriate use and interpretation. *Anesthesia and Analgesia*, *126*(5), 1763–1768. https://doi.org/10.1213/ANE.0000000000002864

Senanayake, I. P., Welivitiya, W. D. D. P., & Nadeeka, P. M. (2013). Remote sensing based analysis of urban heat islands with vegetation cover in Colombo city, Sri Lanka using Landsat-7 ETM+ data. *Urban Climate*, *5*, 19–35. https://doi.org/10.1016/J.UCLIM.2013.07.004

Smid, M., Russo, S., Costa, A. C., Granell, C., & Pebesma, E. (2019). Ranking European capitals by exposure to heat waves and cold waves. *Urban Climate*, *27*, 388–402. https://doi.org/10.1016/J.UCLIM.2018.12.010

Sobrino, J. A., & Irakulis, I. (2020). A Methodology for Comparing the Surface Urban Heat Island in Selected Urban Agglomerations Around the World from Sentinel-3 SLSTR Data. *Remote Sensing*, *12*(12), 2052. https://doi.org/10.3390/RS12122052

Steininger, M. K. (1996). Tropical secondary forest regrowth in the Amazon: age, area and change estimation with Thematic Mapper data. *International Journal of Remote Sensing*, *17*(1), 9–27. https://doi.org/10.1080/01431169608948984

Stewart, I. D., & Oke, T. R. (2012). Local climate zones for urban temperature studies. *Bulletin of the American Meteorological Society*, *93*(12), 1879–1900. https://doi.org/10.1175/BAMS-D-11-00019.1

Sun, L., Nottrott, A., & Kleissl, J. (2012). Effect of hilly urban morphology on dispersion in the urban boundary layer. *Building and Environment*, *48*(1), 195–205. https://doi.org/10.1016/J.BUILDENV.2011.09.005

Tan, J., Zheng, Y., Tang, X., Guo, C., Li, L., Song, G., Zhen, X., Yuan, D., Kalkstein, A. J., Li, F., & Chen, H. (2010). The urban heat island and its impact on heat waves and human health in Shanghai. *International Journal of Biometeorology*, *54*(1), 75–84. https://doi.org/10.1007/s00484-009-0256-x

Telespazio. (2020, June 15). *In Milan, "heat islands" are fought by means of satellite data*. https://www.telespazio.com/en/news-and-stories-detail/-/detail/100620-milano-isole-di-calore

Thissen, J. (2013). Representing the Industrial City: Rotterdam, 1880-1970. In *Industrial Cities: History and Future*. Campus Verlag. https://dspace.library.uu.nl/handle/1874/293995

Tyson, J. (2021, February 9). *Milan: Italy's lost city of canals*. BBC. https://www.bbc.com/travel/article/20210208-milan-italys-lost-city-of-canals

Ulpiani, G. (2021). On the linkage between urban heat island and urban pollution island: Three-decade literature review towards a conceptual framework. *Science of The Total Environment*, *751*, 141727. https://doi.org/10.1016/J.SCITOTENV.2020.141727

Unal Cilek, M., & Cilek, A. (2021). Analyses of land surface temperature (LST) variability among local climate zones (LCZs) comparing Landsat-8 and ENVI-met model data. *Sustainable Cities and Society*, *69*, 102877. https://doi.org/10.1016/J.SCS.2021.102877

United Nations. (2018, May 16). *68% of the world population projected to live in urban areas by 2050*. United Nations. https://www.un.org/development/desa/en/news/population/2018-revision-of-world-urbanization-prospects.html

Visvanathan, G., Patil, K., Suryawanshi, Y., Meshram, V., & Jadhav, S. (2024). Mitigating urban heat island and enhancing indoor thermal comfort using terrace garden. *Scientific Reports*, *14*(1), 1–14. https://doi.org/10.1038/s41598-024-60546-0

Voogt, J. A., & Oke, T. R. (2003). Thermal remote sensing of urban climates. *Remote Sensing of Environment*, *86*(3), 370–384. https://doi.org/10.1016/S0034-4257(03)00079-8

Vox, G., Blanco, I., & Schettini, E. (2018). Green façades to control wall surface temperature in buildings. *Building and Environment*, *129*, 154–166. https://doi.org/10.1016/J.BUILDENV.2017.12.002

Wang, J., Georganos, S., Kuffer, M., Abascal, A., & Vanhuysse, S. (2022). On the knowledge gain of urban morphology from space. *Computers, Environment and Urban Systems*, *95*, 101831. https://doi.org/10.1016/J.COMPENVURBSYS.2022.101831

Wang, Q., Wang, X., Zhou, Y., Liu, D., & Wang, H. (2022). The dominant factors and influence of urban characteristics on land surface temperature using random forest algorithm. *Sustainable Cities and Society*, *79*, 103722. https://doi.org/10.1016/J.SCS.2022.103722

Wang, Y., Guo, Z., & Han, J. (2021). The relationship between urban heat island and air pollutants and them with influencing factors in the Yangtze River Delta, China. *Ecological Indicators*, *129*, 107976. https://doi.org/10.1016/J.ECOLIND.2021.107976

Ward, K., Lauf, S., Kleinschmit, B., & Endlicher, W. (2016). Heat waves and urban heat islands in Europe: A review of relevant drivers. *Science of The Total Environment*, *569–570*, 527–539. https://doi.org/10.1016/J.SCITOTENV.2016.06.119

Weng, Q. (2009). Thermal infrared remote sensing for urban climate and environmental studies: Methods, applications, and trends. *ISPRS Journal of Photogrammetry and Remote Sensing*, *64*(4), 335–344. https://doi.org/10.1016/J.ISPRSJPRS.2009.03.007

Weng, Q., Lu, D., & Schubring, J. (2004). Estimation of land surface temperature-vegetation abundance relationship for urban heat island studies. *Remote Sensing of Environment*, *89*(4), 467–483. https://doi.org/10.1016/j.rse.2003.11.005

Wheeler, D., & Tiefelsdorf, M. (2005). Multicollinearity and correlation among local regression coefficients in geographically weighted regression. *Journal of Geographical Systems*, *7*(2), 161–187. https://doi.org/10.1007/s10109-005-0155-6

Willsher, K. (2023, October 24). *From grey to green: the plan to turn Paris's zinc rooftops into gardens*. The Guardian. https://www.theguardian.com/environment/2023/oct/24/grey-to-green-plan-to-turn-paris-zinc-rooftops-into-gardens

World Health Organisation. (2021). Heat and health in the WHO European Region: updated evidence for effective prevention. In *:WHO Regional Office for Europe*. https://iris.who.int/handle/10665/339462

Wu, J., He, J., & Christakos, G. (2022). DIA models. *Quantitative Analysis and Modeling of Earth and Environmental Data*, 431–447. https://doi.org/10.1016/B978-0-12-816341-2.00011-3

Wu, Q., Li, Z., Yang, C., Li, H., Gong, L., & Guo, F. (2022). On the Scale Effect of Relationship Identification between Land Surface Temperature and 3D Landscape Pattern: The Application of Random Forest. *Remote Sensing*, *14*(2), 279. https://doi.org/10.3390/RS14020279

Xiao, J., Fisher, J. B., Hashimoto, H., Ichii, K., & Parazoo, N. C. (2021). Emerging satellite observations for diurnal cycling of ecosystem processes. *Nature Plants*, *7*(7), 877–887. https://doi.org/10.1038/s41477-021-00952-8

Yan, R., & Bai, J. (2020). A New Approach for Soil Moisture Downscaling in the Presence of Seasonal Difference. *Remote Sensing*, *12*(17), 2818. https://doi.org/10.3390/RS12172818

Yang, F., Lau, S. S. Y., & Qian, F. (2011). Urban design to lower summertime outdoor temperatures: An empirical study on high-rise housing in Shanghai. *Building and Environment*, *46*(3), 769–785. https://doi.org/10.1016/J.BUILDENV.2010.10.010

Yang, J., Jin, S., Xiao, X., Jin, C., Xia, J. (Cecilia), Li, X., & Wang, S. (2019). Local climate zone ventilation and urban land surface temperatures: Towards a performance-based and wind-sensitive planning proposal in megacities. *Sustainable Cities and Society*, *47*, 101487. https://doi.org/10.1016/J.SCS.2019.101487

Yang, J., Ren, J., Sun, D., Xiao, X., Xia, J. (Cecilia), Jin, C., & Li, X. (2021). Understanding land surface temperature impact factors based on local climate zones. *Sustainable Cities and Society*, *69*, 102818. https://doi.org/10.1016/J.SCS.2021.102818

Yang, J., Su, J., Xia, J. C., Jin, C., Li, X., & Ge, Q. (2018). The Impact of Spatial Form of Urban Architecture on the Urban Thermal Environment: A Case Study of the Zhongshan District, Dalian. *IEEE Journal of Selected Topics in Applied Earth Observations and Remote Sensing*, *11*(8), 2709–2716. https://doi.org/10.1109/JSTARS.2018.2808469

Yang, Q., Huang, X., & Li, J. (2017). Assessing the relationship between surface urban heat islands and landscape patterns across climatic zones in China. *Scientific Reports*, *7*(1), 1–11. https://doi.org/10.1038/s41598-017-09628-w

Yao, X., Zhu, Z., Zhou, X., Shen, Y., Shen, X., & Xu, Z. (2022). Investigating the effects of urban morphological factors on seasonal land surface temperature in a "Furnace city" from a block perspective. *Sustainable Cities and Society*, *86*, 104165. https://doi.org/10.1016/J.SCS.2022.104165

Yin, S., Liu, J., & Han, Z. (2022). Relationship between urban morphology and land surface temperature—A case study of Nanjing City. *PLOS ONE*, *17*(2), e0260205. https://doi.org/10.1371/JOURNAL.PONE.0260205

You, W., Shen, J., & Ding, W. (2017). Improving wind environment design based on assessing spatial distribution of ventilation efficiency in regional space. *Energy Procedia*, *142*, 2923–2929. https://doi.org/10.1016/J.EGYPRO.2017.12.418

Yuan, C., & Chen, L. (2011). Mitigating urban heat island effects in high-density cities based on sky view factor and urban morphological understanding: a study of Hong Kong. *Architectural Science Review*, *54*(4), 305–315. https://doi.org/10.1080/00038628.2011.613644

Zander, K. K., Cadag, J. R., Escarcha, J., & Garnett, S. T. (2018). Perceived heat stress increases with population density in urban Philippines. *Environmental Research Letters*, *13*(8), 084009. https://doi.org/10.1088/1748-9326/AAD2E5

Zhang, N., Zhang, J., Chen, W., & Su, J. (2022). Block-based variations in the impact of characteristics of urban functional zones on the urban heat island effect: A case study of Beijing. *Sustainable Cities and Society*, *76*, 103529. https://doi.org/10.1016/J.SCS.2021.103529

Zhang, Q., Xu, D., Zhou, D., Yang, Y., & Rogora, A. (2020). Associations between urban thermal environment and physical indicators based on meteorological data in Foshan City. *Sustainable Cities and Society*, *60*, 102288. https://doi.org/10.1016/J.SCS.2020.102288

Zhang, Y., Middel, A., & Turner, B. L. (2019). Evaluating the effect of 3D urban form on neighborhood land surface temperature using Google Street View and geographically weighted regression. *Landscape Ecology*, *34*(3), 681–697. https://doi.org/10.1007/s10980-019-00794-y

Zhang, Y., Wang, Y., Ding, N., & Yang, X. (2022). Spatial Pattern Impact of Impervious Surface Density on Urban Heat Island Effect: A Case Study in Xuzhou, China. *Land*, *11*(12). https://doi.org/10.3390/LAND11122135

Zheng, B., Bedra, K. B., Zheng, J., & Wang, G. (2018). Combination of Tree Configuration with Street Configuration for Thermal Comfort Optimization under Extreme Summer Conditions in the Urban Center of Shantou City, China. *Sustainability*, *10*(11), 4192. https://doi.org/10.3390/SU10114192

Zhou, D., Xiao, J., Bonafoni, S., Berger, C., Deilami, K., Zhou, Y., Frolking, S., Yao, R., Qiao, Z., & Sobrino, J. A. (2019). Satellite Remote Sensing of Surface Urban Heat Islands: Progress, Challenges, and Perspectives. *Remote Sensing*, *11*(1), 48. https://doi.org/10.3390/RS11010048

Zhou, Y., Zhao, H., Mao, S., Zhang, G., Jin, Y., Luo, Y., Huo, W., Pan, Z., An, P., & Lun, F. (2022). Exploring surface urban heat island (SUHI) intensity and its implications based on urban 3D neighborhood metrics: An investigation of 57 Chinese cities. *Science of The Total Environment*, *847*, 157662. https://doi.org/10.1016/J.SCITOTENV.2022.157662

Zhu, Z., Shen, Y., Fu, W., Zheng, D., Huang, P., Li, J., Lan, Y., Chen, Z., Liu, Q., Xu, X., & Yao, X. (2023). How does 2D and 3D of urban morphology affect the seasonal land surface temperature in Island City? A block-scale perspective. *Ecological Indicators*, *150*. https://doi.org/10.1016/J.ECOLIND.2023.110221

Annexures

Annexure I Summary of different datasets and methods used by various authors to analyse the impacts of urban morphology on LST (Source: Author, 2023)

PAPERS	AUTHORS	DATA USED	METHODS
Impacts of landscape structure on surface urban heat islands: A case study of Shanghai, China	Li et al., 2011	**LST, NDVI, ISA, Fv:** Landsat 7 ETM+ **LM:** LU Map (Aerial Photos) 2.5 m resolution	**Relation:** Statistical regression analysis & scatterplots
Analysis of Surface Thermal Patterns in Relation to Urban Structure Types: A Case Study for the City of Munich	Heldens et al., 2013	**LST:** Landsat (60 m resolution) & Daedalus (4 m resolution) **SVF:** DEM **USTs:** Munich Municipality	**Relation:** Multiple linear regression analysis
Effects of landscape composition and pattern on land surface temperature: An urban heat island study in the megacities of Southeast Asia	Estoque et al., 2017	**LST, MNDWI, LC, LMs:** Landsat-8 OLI/TIRS	Influence of mean LST, impervious surface & green space density calculated using: a) **Urban-rural gradient** analysis by creating multiple ring buffer zones with a distance interval of 300 m b) **Multiresolution grid-based** analysis **Relation:** Bivariate correlation analysis & scatter plot
Assessing the relationship between surface urban heat islands and landscape patterns across climatic zones in China	Yang et al., 2017	**LST, SUHI:** EOS-Aqua-MODIS 8-day composite product (version 5), SRTM DEM **LMs, SUHI:** LU/C Datasets (CLUDs) 30 m resolution	**Relation:** Spearman's rank correlation coefficient
Spatio-temporal analysis of the	Berger et al.,	**Urban LC:** VHR data	LC classification using

relationship between 2D/3D urban site characteristics and land surface temperature	2017	(UltraCamX & Ikonos-2) 1-4 m resolution **LST:** Landsat ETM+ **2D/3D UM:** nDSMs	**OBIA** **Relation:** Spearman's rank correlation coefficient
Assessing the relationship between sky view factor and land surface temperature to the spatial resolution	Scarano & Mancini, 2017	**LST:** Landsat 8, ASTER & TASI-600 **SVF Maps:** 3D building database (footprints & heights), LC Map (CLC), DSM	DSM created by adding building heights to a DTM **Relation:** Correlation analysis & scatter plot
Investigating the effects of 3D urban morphology on the surface urban heat island effect in urban functional zones by using high-resolution remote sensing data: A case study of Wuhan, Central China	Huang & Wang, 2019	**LC, UFZs, LMs:** ZiYuan-3 (ZY-3), 3D building data, OSM, & POI data **LST:** Landsat 8	**Relation:** ANOVA between LST & UFZs Pearson correlation analysis between LM & LST
Modeling the spatial relation between urban morphology, land surface temperature and urban energy demand	Chen et al., 2020	**2D/3D UM:** Top10NL-AHN2 (NL Database) **NDVI:** Landsat 8	**Relation:** Ordinary Least Squares Regression (OLS) & Geographically Mean Regression (GWR) Model
Impact of urban morphology and landscape characteristics on spatiotemporal heterogeneity of land surface temperature	Guo et al., 2020	**LST, NDVI/BI/SI:** Landsat OLI/TM **Night-Lighting:** NGDC, NOAA **DEM:** Geospatial Data Cloud **LU:** Dalian Land Resources	**Global/Local Moran's I Analysis** for LST spatial autocorrelation **Relation:** Ordinary Least Squares Regression (OLS) & Geographically Mean Regression (GWR) Model
The influence of urban spatial pattern on land surface temperature for different functional zones	Li et al., 2020	**LST, NDVI, NDBI:** Landsat 8 **LC, UFZs, LMs:** Ikonos, **2D/3D UM:** Building Engineering Administration & Real Estate Information Network	**Relation:** Zonal statistics, ANOVA & Spearman correlation between LST & LM within each UFZ
Night and day: The influence and relative importance of urban characteristics on remotely sensed land surface temperature	Logan et al., 2020	**LST, Albedo, ISA, NDVI/BI:** Landsat 8, LC **Tree canopy cover:** DEM, Landsat 5	**Relation:** Used **6 models**, Linear model, Multivariate Adaptive Regression Spline (MARS), Generalized Additive Model (GAM), Random Forest Regression (RFR), Gradient Boosted Regression Trees, Convolutional Neural Network (CNN)

Quantifying 3D building form effects on urban land surface temperature and modeling seasonal correlation patterns	Li et al., 2021	**LST:** Landsat 8, 7 **2D/3D UM:** Public data sharing platform, Wind Direction	**Relation:** Random Forest Regression (RFR) & Partial Dependence Plots (PDPs)
Analyses of land surface temperature (LST) variability among local climate zones (LCZs) comparing Landsat-8 and ENVI-met model data	Cilek & Cilek, 2021	**LST:** Landsat 8 **LCZ:** Building data, Google Earth Engine, Digital city maps **NDVI:** Sentinel 2 **LU:** Urban atlas	**Relation:** Zonal statistics, Boxplots, Kolmogorov-Smirnov tests, Q-Q plots, & histogram comparisons
Understanding land surface temperature impact factors based on local climate zones	Yang et al., 2021	**LST NDVI/MNDWI/ NDSI:** Landsat 8 OLI/TIRS **LCZ:** Building data from Baidumap, DEM	**Relation:** Correlation & Boxplots
Relationship between urban morphology and land surface temperature—A case study of Nanjing City	Yin et al., 2022	**LST, LU/C:** Landsat 8 **2D/3D UM:** 3D building database, STRM DEM, POI data, road network	**Relation:** Geographically Mean Regression (GWR) Model
Spatial Pattern Impact of Impervious Surface Density on Urban Heat Island Effect: A Case Study in Xuzhou, China	Zhang et al., 2022	**LST, ISA:** Landsat 8	**Relation:** Bivariate Global/Local Moran's I Analysis
Urban growth and heat islands: A case study in micro-territories for urban sustainability	Molina-Gómez et al., 2022	**LST, NDVI/BI/WI, NDISI:** Landsat 7 ETM+, 8 OLI/TIRS	**Relation:** Principal Component Analysis (PCA)
Investigating the effects of urban morphological factors on seasonal land surface temperature in a "Furnace city" from a block perspective	Yao et al., 2022	**LST:** Landsat 8 **2D/3D UM:** Block & Building data **Night-Lighting:** Luojia1–01	**Relation:** Distribution Index (DI), Random Forest Regression (RFR), ANOVA, Pearson correlation analysis
Insights into the Effect of Urban Morphology and Land Cover on Land Surface and Air Temperatures in the Metropolitan City of Milan (Italy) Using Satellite Imagery and In Situ Measurements	Puche et al., 2023	**LST, LCZ:** Landsat 8, building height/density data	**Random Forest (RF) Classification** used for LCZ mapping **Relation:** ANOVA & Box Plots
Analyzing the scale dependent effect of urban building morphology on land surface temperature using random forest algorithm	Han, 2023	**LST:** Landsat 8 OLI/TIRS **UM:** Building height from Baidu, Inc. (3 m resolution)	**Relation:** Random Forest Regression (RFR) Model
The Influence of Urban Form on Land Surface Temperature:	He et al., 2023	**LST:** Landsat 8 OLI/TIRS	**Relation:** Geographic Detector

A Comprehensive Investigation from 2D Urban Land Use and 3D Buildings		**3D UM:** Building data using API from Amap developer platform	
How does 2D and 3D of urban morphology affect the seasonal land surface temperature in Island City? A block-scale perspective	Zhu et al., 2023	**LST, NDVI/BI, MNDWI:** Landsat 8 OLI/TIRS **2D/3D UM:** Street boundary & building contour data	**Relation:** Random Forest Regression (RFR) Model

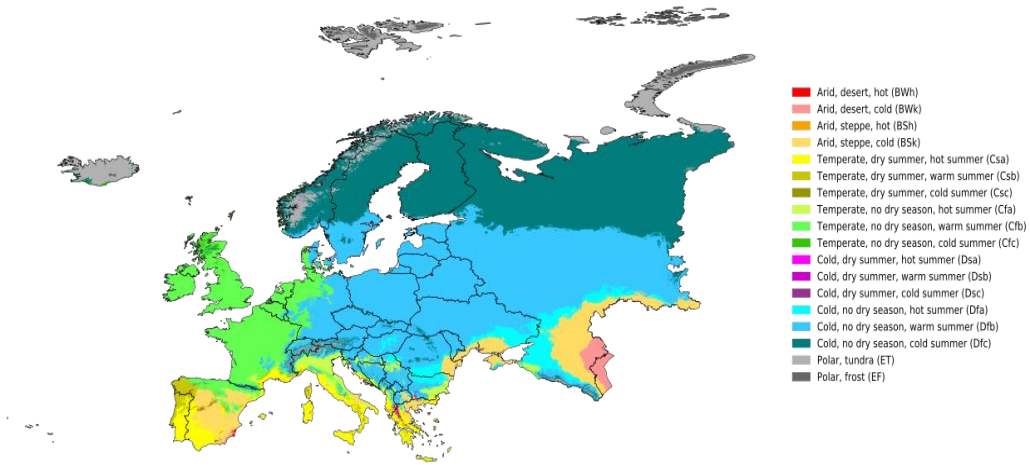

Annexure II Köppen-Geiger climate classification map for Europe (1980-2016)

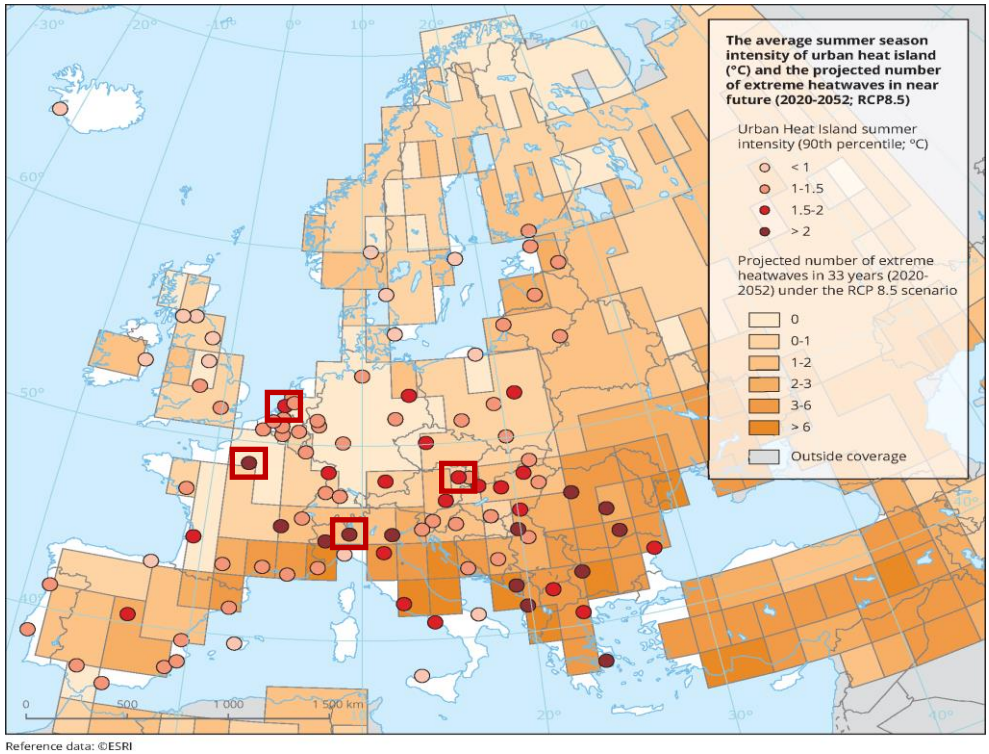

Annexure III Summer season intensity of urban heat islands (UHIs) (°C) and the projected number of extreme heatwaves in the near future (2020-2052) (Source: European Environment Agency, 2023). The red squares denote the cities selected for the study.

Annexure IV Description of UMMs computed using momepy

MORPHOMETRICS	DESCRIPTION
Area	Area of each building in a given GeoDataFrame.
FloorArea	Floor area of each building based on height and area.
LongestAxisLength (LAL)	Length of the longest axis of building.
Perimeter	Perimeter of each building in a given GeoDataFrame.
Volume	Volume of each building in a given GeoDataFrame based on its height and area.
CoveredArea	Total area covered by neighbours defined in spatial_weights and the building itself.
MeanHeight	Mean height of buildings within 100 meters of its neighbours.
CircularCompactness	Compactness index of each object in a given GeoDataFrame.
Convexity	Convexity index of each object in a given GeoDataFrame.
Elongation	Elongation of each object seen as elongation of its minimum bounding rectangle.
EquivalentRectangularIndex (ERI)	Equivalent rectangular index of each object in a given GeoDataFrame.
FormFactor	Form factor of each object in a given GeoDataFrame.
FractalDimension	Fractal dimension of each object in given GeoDataFrame.
Rectangularity	Rectangularity of each object in a given GeoDataFrame.
ShapeIndex	Shape index of each object in a given GeoDataFrame.
SquareCompactness	Compactness index of each object in a given GeoDataFrame.
Squareness	Squareness of each building in a given GeoDataFrame.
VolumeFacadeRatio (VFR)	Volume/façade ratio of each building in a given GeoDataFrame.
Orientation	Calculates the deviation of orientation of the longest axis of bounding rectangle of a building in range 0 – 45 from cardinal directions are captured.
SharedWalls	Length of shared walls of adjacent buildings.
Alignment	Mean deviation of solar orientation of buildings on adjacent cells from a building.
BuildingAdjacency	Tendency of the buildings to join into larger structures. It is calculated as a ratio of joined built-up structures and buildings within the extent defined in spatial_weights.
CellAlignment	Calculate the difference between cell orientation and the orientation of building.
NeighbourDistance	Mean distance to adjacent buildings (based on spatial_weights).
MeanInterbuildingDistance (MID)	Calculates the mean interbuilding distance between buildings on adjacent cells based on spatial_weights.
FloorAreaDensity	Gross density of the building.
Gini	Gini index of area of buildings within neighbours defined in spatial_weights.
Range	Range of areas of buildings within neighbours defined in spatial_weights
Shannon	Shannon areas of buildings within neighbours defined in spatial_weights.
Simpson	Simpson's diversity areas of buildings within neighbours defined in spatial_weights.